Diss. ETH Nr. 13490

Macroscopic parameters for two-phase flow

A dissertation submitted to the
Swiss Federal Institute of Technology Zürich

for the degree of
Doctor of Natural Sciences

presented by
Insa Neuweiler
Dipl.-Phys.
University of Heidelberg, Germany
born January, 1969
citizen of Germany

accepted on the recommendation of
Prof. Dr. Wolfgang Kinzelbach, examiner
Prof. Dr. Hannes Flühler, co-examiner

Zürich, 1999

Zusammenfassung

Das Ziel der vorliegenden Arbeit ist die Bestimmung effektiver Strömungsparameter für die Strömung zweier nicht mischbarer Fluide in einem heterogenen porösen Medium. Wegen ihrer Bedeutung für Gasdrucktests in Klüften wird als spezielle Konfiguration die radiale Verdrängung von Wasser durch Luft in einem zweidimensionalen Medium mit konstanter Zustromrate analysiert. Bei der Bestimmung effektiver Parameter wird das heterogene Medium auf einer räumlichen Skala, die sehr viel grösser ist als die Skala der Heterogenitäten, durch ein homogenes Medium beschrieben, dem die effektiven Parameter zugeordnet werden.

Anhand von Laborexperimenten in künstlichen heterogenen porösen Medien und der Analyse der Ergebnisse mit einem Invasionsperkolationsmodell wurde begründet, dass effektive Parameter für die Darstellung des Mediums ungeeignet sind, falls die Einflüsse des heterogen verteilten Kapillardrucks im Vergleich zu den viskosen Effekten gross sind. In kapillar dominiertem Fliessverhalten zerstört die fraktale Eigenschaft der Luftcluster die Analogie zu den gemittelten Grössen. Ein solches Verhalten wurde daher im weiteren ausgeschlossen.

Ein weiterer Teil der Arbeit bestand in der Untersuchung von numerisch berechneten Ensembles von Luftsättigungsfeldern. Zunächst wurden das Zeitverhalten von generischen Grössen wie der Rauhigkeit einer Isolinie in der Frontzone oder der Varianz der ensemblegemittelten Sättigung analysiert um ein qualitatives Verständnis des Strömungsprozesses zu entwickeln. Anschliessend wurden die gemittelten Sättigungsfelder auf entsprechenden homogenen Feldern reproduziert.

Effektive Strömungsparameter wurden analytisch in einer Störungstheorie zweiter Ordnung berechnet. Zunächst wurde das lineare Problem betrachtet, das dem des Schadstofftransports in einer radialen divergenten Strömung äquivalent ist. Es wurde gezeigt, dass in einem intermediären Zeitintervall zwei Effekte durch die Heterogenitäten verursacht werden. Der wichtigste ist ein Makrodispersionseffekt, der durch die Fluktuationen im advektiven Strömungsfeld entsteht und der proprortional zum Geschwindigkeitsfeld der Strömung ist. Da die Strömungsgeschwindigkeit im radialen Fall mit dem Radius abnimmt, wird nach einer gewissen Zeitspanne der Einfluss der Diffusion bemerkbar, der ein anderes Zeitverhalten der räumlichen Momente bewirkt. Als zweiter Effekt der Heterogenitäten entsteht eine Erhöhung der Diffusion um die Varianz des Zufallsfeldes.

Das voll nichtlineare Zweiphasenströmungsproblem unter Vernachlässigung der Kapillarkräfte wurde sowohl mit Störungstheorie zweiter Ordnung als auch mit Homogenisierungstheorie untersucht. Die Ergebnisse deuten auf einen ähnlichen Effekt wie im linearen Fall hin, einem Makrodispersionseffekt, der proportional zur Strömungsgeschwindigkeit der gesamten Strömung ist und der in nichtlinearer Weise von der Luftsättigung abhängt. Im Gegensatz zum Schadstofftransport hat die Darstellung der Auswirkungen der Heterogenitäten als ein Makrodispersionseffekt, der proportional zur Strömungsgschwindigkeit ist, in der Zweiphasenströmung kein Äquivalent im homogenen Modell. Die Ergebnisse werden durch die numerischen Simulationen qualitativ bestätigt.

Abstract

The purpose of this thesis is the determination of effective flow parameters for a flow process of two immiscible fluids in a heterogeneous porous medium. In particular the radial displacement of water by air in a two-dimensional medium with constant inflow rate was considered. This process is relevant for the performance of gas pressure tests in a fracture. In order to determine effective parameters, the heterogeneous medium is described as an equivalent homogeneous one on a scale which is much larger than the scale of the heterogeneities.

As a first step, laboratory experiments with artificial heterogeneous porous media were performed which were subsequently analysed with an invasion percolation model. It was shown that effective parameters do not capture the impact of the heterogeneities if heterogeneous capillary entry pressures dominate the flow behaviour. This is due to the fractal properties of the air clusters. In the following, flow conditions which lead to such a flow behaviour were therefore excluded.

Another part of this work is the study of numerically generated ensembles of air saturation fields. The time behaviour of generic properties such as the roughness of an gas saturation isoline in the vicinity of the front zone or the variance of the ensemble averaged gas saturation was calculated. The aim was to develop a qualitative understanding of the relevant processes. A reproduction of the averaged fields with a modified homogeneous model was also achieved.

Effective flow parameters were also determined analytically with a second order perturbation theory. As a first step the linear system was considered, which is equivalent to solute transport in a radially diverging flow field. It was shown that the heterogeneities cause two important effects in an intermediate time regime. First, a macrodispersion is obtained, which is caused by the fluctuations of the advective flow and which is proportional to the flow velocity. As the velocity decreases with $1/r$, after some time the influence of the diffusion becomes noticeable which leads to a different time behaviour. The second effect is an increase of the diffusion by the variance of the random field due to the heterogeneities.

The fully nonlinear system without capillarity effects was investigated with a second order perturbation theory and with homogenization theory. The results suggest an effect similar to that observed in the linear system. A macrodispersion is obtained, which is proportional to the total flow velocity and which depends on the saturation in a nonlinear way. As opposed to the solute transport case, the description of the influence of the heterogeneity as a macrodispersion which is proportional to the flow velocity has no counterpart in the homogeneous model in the two-phase flow equations.

The analytically calculated macroscopic effects were qualitatively confirmed by the numerical computations.

Contents

Chapter 1

Introduction

The study of flow processes in the subsurface is relevant for a number of different disciplines. Due to the complexity of these processes it is impossible to take into account all their different features which makes the task to describe "**the** flow process in the subsurface" unfeasible. Approaches which highlight different aspects are necessary in order to develop an understanding of the process as a whole. Flow processes in the subsurface are governed by processes taking place on a broad range of spatial and temporal scales. For example, the scale where a pore is resolved can be in the range of μm, whereas the scale of field applications can be in the range of km. The task in the characterization of flow in the subsurface makes simplifications necessary while still including all the important effects.

This work deals with the impact of heterogeneities of soil properties on flow processes. In nature, porous media are never homogeneous, although we assume homogeneity in the models we use. Heterogeneities can simplify the problems, e.g. if they are of regular structure and known. In general, however, we do not know the structure of the porous medium in a deterministic way. The problem arises already on the pore scale, as a porous medium consists of irregularly shaped pores. The knowledge we have about soil properties is generally on a small scale, e.g. on the scale of core samples. Practical applications, however, are usually on a much larger scale. We are therefore confronted with the problem, that it is not possible to resolve the small scale structure due to the lack of deterministic knowledge, and even if we knew it it would be infeasible to incorporate such complex structures into our calculations. The central issue is the incorporation of heterogeneities on the small scale into the description of the flow processes on the large scale in an efficient way. This procedure is known as *upscaling* and has been investigated intensively in the last decades.

If the scale of the heterogeneities is small compared to the scale of the application, it is possible that the flow in the heterogeneous medium is smooth on the large scale and the flow behaviour is similar to that of a homogeneous medium. We are then looking at the process on a scale, where the heterogeneities are already averaged out. Their averaged impact is captured by the large scale flow parameters we assign to an equivalent homogeneous medium. This procedure is sketched for the flow process

which is considered in this work, the radial displacement of water by air, in Fig. 1.1. The underlying assumption is, that the averaged impact of the heterogeneities does only lead to effects which have a counterpart in the homogeneous medium. The averaged large scale parameters are called effective parameters in the literature. The determination of effective flow parameters is an efficient way to account for the heterogeneities in the flow process.

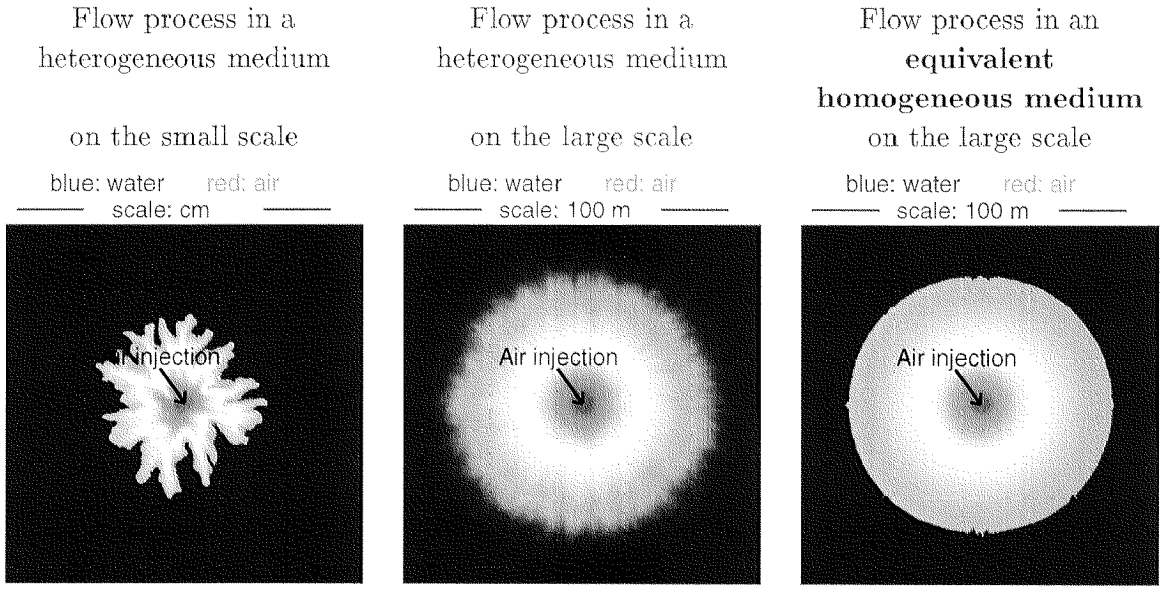

Figure 1.1: Description of a flow process (radial displacement of water by air) as one in an equivalent homogeneous medium

The random sample character of the knowledge we generally have about soil parameters has led to the socalled stochastic approach, which is based on the description of the porous medium as a random field. This approach allows the use of a number of powerful stochastic methods. Effective properties can be derived from quantities which are appropriately averaged over the random field. The average over the random field, which is denoted as ensemble average, is supposed to be equivalent to the spatial averaging over the heterogeneities. In this way we average out the scale of the fluctuations which we do not want to resolve. The inherent assumptions and principles are thoroughly discussed in a number of books and articles, see e.g. *Gelhar* [1993] or *Dagan* [1989]. As the stochastic approach is the basic method of this work, the most important definitions and basic ideas will be given at the end of the introduction.

Flow of one single phase in a heterogeneous porous medium has been investigated intensively and successfully. The heterogeneous permeability field can be represented by a homogeneous effective permeability, which depends on the geometrical dimensions of the flow problem (see e.g. *King* [1987] or *Gelhar* [1993]). For more complex problems like the flow of different immiscible phases the question of the existence and features of effective parameters is not so well answered. However, many field applications are concerned with the flow of more than one fluid. For instance in

the unsaturated soil zone we have to deal with the flow of two immiscible fluids, water and air. Also in the field of oil recovery or in remediation problems with non aquous phase liquids (NAPLs) the flow of at least two immiscible fluids, water and oil, has to be treated. The nonlinear behaviour of these flow processes makes the investigation of the heterogeneities very difficult. However, this is an important problem, as we have already learned from the linear flow processes that the impact of heterogeneities can be large and can in most cases not be neglected.

In this work the impact of heterogeneities on a two-phase flow process is investigated. We are treating the problem of a radial displacement of water by air with constant inflow rate Q in two dimensions. This special configuration was chosen, due to its relevance to some important applications. The most important one is gas pressure testing of fractures. In Switzerland some effort is made to test the properties of fractures in the context of the search for nuclear waste deposits in fractured rock. Pressure tests yield information on fracture conductivity. The flow of gas in saturated fractures has also to be investigated, as gas can be produced at the repository due to corrosion and may flow in a fracture system over long distances. The flow properties of fractures for a gas-water system are tested by injecting air at one point in the saturated fracture and monitoring at different observation boreholes. The fractures are often filled with fault gouge and can therefore be considered as 2-dimensional a porous medium. There are further applications, where the displacement of water by air is important, such as air sparging. An analogous process is water flooding in a reservoir where the water phase displaces the oil phase. As the injection mostly takes place at one point, it is reasonable to take into account a radial flow configuration.

The radial flow configuration has been investigated for linear phenomena such as single phase flow for some time now. *Shvidler* [1962] calculated effective conductivities for radial flow. *Neuman and Orr* [1993] calculated effective conductivity in a two-dimensional system numerically. *Indelman et al.* [1996] derived an equivalent transmissivity for converging flow analytically using a Lagrangian approach. *Fiori et al.* [1998] investigated the impact of a heterogeneous permeability field on the covariances of the flow parameters for radial flow. Also macrodispersion caused by advective solute transport in a heterogeneous radial flow configuration was recently derived by *Indelman and Dagan* [1999]. The method used for these analytical calculations is perturbation theory.

One of the main problems in the study of two-phase flow is the wide range of processes one has to deal with. This is illustrated in Figs. 1.2 through 1.4, where different two-phase flow experiments are illustrated. The nonlinear nature of this flow process leads to very different flow behaviour depending on the different flow conditions. It may be possible, but not in every case adequate to capture the influence of the heterogeneities by effective homogeneous flow parameters. Our aim in this work is therefore to investigate the impact of heterogeneities on the flow process from different points of view to decide on the justification of the effective parameter description.

The displacement of water by air is inherently unstable. Reviews on this issue are

given e.g. by *Homsy* [1987] or *Kueper and Frind* [1988]. On the one hand, the homogeneous process can already be subject to instabilities due to the different viscosities of water and air. On the other hand the nonlinear influence of the capillary pressure can force the flow of the air phase along preferential paths if the medium is heterogeneous. This phenomenon is known as channeling in the literature. The classification of the different stable and unstable flow types is characterized in *Lenormand et al.* [1988]. The channeling process originates on the pore scale. However, the nonlinearities lead to a transfer of the channeling behaviour to the large scale, where such phenomena have also been observed. The flow behaviour is definitely nonhomogeneous under these conditions. The existence and predictive power of effective parameters for the unstable case is questionable.

Channeling flow behaviour on the pore scale caused by capillary entry pressure effects has been investigated by *Furuberg et al.* [1996] or *Lenormand and Zarcone.* [1989]. In their work artificial porous media with a random, unknown structure were investigated and no correlation structure was assumed. In the analysis of their experiments the applicability of invasion percolation models, introduced by *Wilkinson and Willemsen* [1983] for flow in porous media, was confirmed. The application of percolation models to flow problems in porous media also on larger scales is reviewed by *Berkowitz and Ewing* [1998].

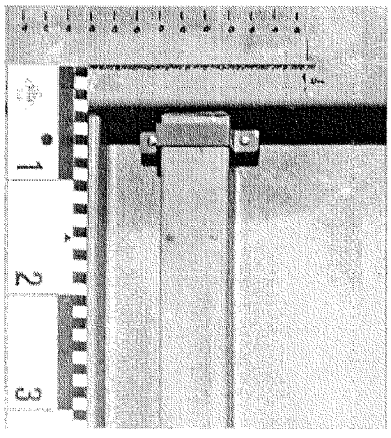

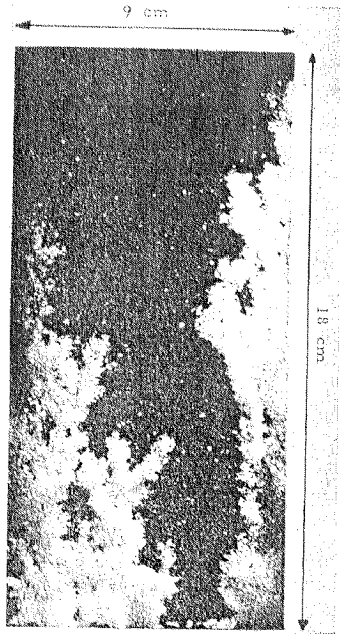

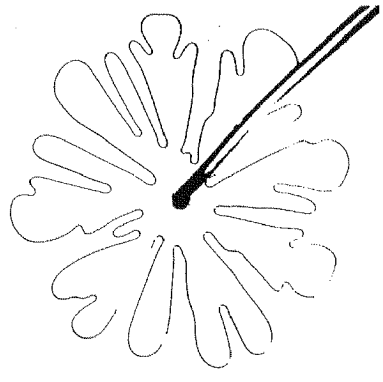

Left: Figure 1.2: Stable flow of water through soil at residual water saturation, dark regions: water, light regions: air, taken from *Stauffer* [1986]

Middle: Figure 1.3: Unstable displacement of oil by water in a porous medium, dark regions: oil, light regions: water, taken from *Chouke et al.* [1959]

Right: Figure 1.4: Unstable displacement of glycerine by air in a Hele Shaw cell, taken from *Paterson* [1981]

Chapter 2 of this work addresses the question of upscaling of two-phase flow under channeling conditions. Displacement of water by air in a correlated heterogeneous porous medium is investigated on the pore scale with laboratory experiments and

numerical simulations. The conditions are chosen in a way, that heterogeneities in the capillary effects determine the flow completely. The features of the flow process and the correspondence to the heterogeneities is investigated and we address the question whether or not ensemble averaged properties are meaningful to describe the flow process. The flow process is simulated numerically with an invasion percolation model. For channeling flow the results can be transferred to larger scales as well, if the pores are identified with lenses or correlated structures. The problem is modelled appropriately in pixelwise network formulation and not using the continuum scale equations.

Chapters 3 and 4 are devoted to the derivation of ensemble averaged quantities on the continuum scale, which implies that an average over a representative volume is possible. This is only the case if channeling phenomena can be excluded. In both chapters we make use of the stochastic approach and calculate ensemble averaged properties.

Effective parameters for two-phase flow on the continuum scale have been derived for some cases with numerical methods and also with analytical methods. There are quasi-analytical methods like renormalization techniques to obtain effective permeabilities on a grid (*King et al.*, [1993] or *Hansen et al.*, [1997]). The method of perturbation theory, which has been used for linear problems was also used for two-phase flow problems. In the work of *Mantoglou and Gelhar* [1987] and *Yeh et al.* [1985] it was used to derive effective parameters for flow in the unsaturated zone, where pressure gradients in the gas phase can be neglected. This is not the case in a displacement process. *Chang et al.* [1995] extended the mechanism to cases where pressure gradients in both phases occur. They investigated the influence of the heterogeneities on the convariances of the flow parameters. However, closed expressions were not obtained. Homogenization theory has also been applied to investigate effective flow parameters for two-phase flow, e.g. by *Amaziane et al.*, [1991] or *Bourgeat and Hidani* [1995]. The radial flow configuration was not taken into account there.

An analysis of mechanisms that are dominant in the homogeneous case and of their interaction with the heterogeneities is very complicated. It is therefore difficult to find solutions of the flow equations. They can be obtained by solving the equations numerically or, on the other hand, constructing approximate analytical solutions. The nonlinearities of the flow equations make analytical methods difficult to apply and make approximations and restrictions necessary. For this reason it is useful to take into account both approaches. Both of them have advantages and disadvantages for the treatment of the problem, which can complement each other. Numerical solutions are useful to develop an understanding of the impact of the different parameters of the flow equations and which are the important effects. All possible mechanisms can be included in the numerical simulations which therefore are good for a qualitative understanding. However, numerical solutions do not allow to determine general laws and formulae. Further, they are often subject to numerical artefacts. Analytical solutions are useful to gain insight into the causes of macroscopic effects. They tell us what to look for in otherwise time consuming

numerical calculations. However, analytical solutions for two-phase flow can only be found approximately and the flow equations have to be simplified. The disadvantage of analytical methods is the difficulty to assess whether or not the approximations made still lead to realistic scenarios. In this work both approaches are applied to investigate the problem of effective flow parameters for radial displacement of water by air, in heterogeneous media. In Chapter 3 of this work the question of effective flow properties for two-phase flow is treated with numerical methods. Based on the insight gained with the numerical methods analytical calculations are performed in Chapter 4 where a simplified form of the flow equations is considered. The method used to solve the flow equations analytically is perturbation theory.

Stochastic approach

In a stochastic approach the heterogeneous parameters, as for example the permeability of the medium, are considered to be random fields denoted by $\mathcal{Z}(\vec{x})$. That means at each location $\vec{x}$ the permeability would be represented by a random number $\mathcal{Z}$. Processes which are random in time are not considered here. The random fields are described by the probability distribution $P(\mathcal{Z}(\vec{x}))$ where $P(\mathcal{Z})d\mathcal{Z}$ denotes the probability that the property $\mathcal{Z}$ lies between $\mathcal{Z}$ and $\mathcal{Z} + d\mathcal{Z}$. The average over the probability distribution is equivalent to an average over the ensemble of all possible realizations of the parameter configuration $\mathcal{Z}(\vec{x})$. If we calculate effective quantities we average these quantities, which are in general functions of the random parameter. In the example of displacement of water by air, the random parameter would be the permeability and one function of it we are interested in would be the gas saturation. Functions $f(\mathcal{Z}, \vec{x})$ of $\mathcal{Z}$ which are averaged over the probability function

$$\int d\mathcal{Z}\, P(\mathcal{Z}) f(\mathcal{Z}) \equiv \overline{f}, \tag{1.1}$$

are denoted as ensemble averaged quantities.

The random field $f(\mathcal{Z})$ is a stationary random field if its autocovariance of two locations $\vec{x}$ and $\vec{x}'$ depends on the difference vector $\vec{x} - \vec{x}'$ only

$$C_{f\,f}(\vec{x}, \vec{x}') \equiv \int d\mathcal{Z} P(\mathcal{Z}) f(\mathcal{Z}, \vec{x}) f(\mathcal{Z}, \vec{x}') = C_{f\,f}(\vec{x} - \vec{x}'). \tag{1.2}$$

In the calculations performed in Chapters 3 and 4 we assume always stationarity for the random fields.

It is only adequate to represent a process in a single heterogeneous porous medium by an ensemble averaged process if the process has already sampled a representative part of the heterogeneous medium. We want to get spatially averaged parameters but due to the lack of knowledge about the spatial parameter distribution we calculate ensemble averaged parameters. The averaging processes are equivalent to each other if the random field is ergodic. This means that the stochastic properties of the ensemble have to be captured in the single realization already. The spatial average of one realization of the random field $\mathcal{Z}(\vec{x})$ is then equivalent to the ensemble

average over the parameter $\mathcal{Z}$ at one location

$$\langle \mathcal{Z}(\vec{x}) \rangle \equiv \lim_{V \to \infty} \int_V d^d x \mathcal{Z}(\vec{x}) = \overline{\mathcal{Z}(x)}. \tag{1.3}$$

As the single realization is not of infinite spatial extent, this property has to be investigated with respect to the length scales of the system. A derivation for this is given e.g. in *Dagan* [1989]. It turns out that ergodicity can only be fulfilled if the length scale of fluctuations on the large scale is much larger than the averaging volume. Another criterion for the ergodicity of a random field is, that the averaging volume is much larger than the correlation length of the field l_0. These criteria are intuitively reasonable. The stochastics of the ensemble can only be captured by one realization if many correlation lengths are included. The average over space does not depend on the location $\vec{x}$. For this reason the ensemble average has to be independent of the location $\vec{x}$ where it is performed. This cannot be fulfilled if the field has a trend.

We can now consider a heterogeneously distributed parameter, like e.g. permeability, which can be represented by an ergodic random field. If we want to assign effective parameters to the medium on a large scale, the fluctuations of quantities which depend on this parameter have to be averaged out. We assume that their values on this averaged scale are equivalent to their ensemble mean. The procedure to calculate effective properties is therefore the following. An expression for the large scale quantity we want to calculate has to be derived. This expression will depend on the small scale heterogeneities, for example on the permeability. Effective parameter are derived from appropriately ensemble averaged large scale quantities. They are dependent on the stochastic properties of the heterogeneous field, like variance and correlation length. The ensemble averages can be calculated if appropriate assumptions for the probability distribution $P(\mathcal{Z})$ are made.

Chapter 2

Pore scale processes - Capillary dominated flow

The focus of this part of the thesis is to look at a flow situation where capillary entry pressure effects control essentially the flow behaviour. In this case the flow is subject to strong channeling effects and the concept of effective parameters is questionable. Those channeling phenomena arise on the smallest scale in the system, the pore scale. Our investigations were therefore concentrated on this scale, assuming that our observations can essentially be transferred to larger scale flow with channeling behaviour caused by heterogeneously distributed capillary entry pressure effects. The flow behaviour was first investigated in laboratory experiments which is described in Section 2.1. In Section 2.2 the results are reproduced with numerical simulations using an invasion persoclation model. The question of effective parameters and upscaling of medium properties is addressed in the latter part of this section.

2.1 Experiments with 2d plexiglass media

Laboratory experiments of displacement of water by air were performed in artificial two-dimensional porous media with a given correlation structure. Although the quantity of interest is the radial flow configuration, the laboratory experiments were performed with linear sources and a uniform average flow configuration. The reason is that the experimental models were taken from another experiment performed earlier, which had a uniform flow configuration (see *Su and Kinzelbach* [1999]). The setup of these models is very time-consuming due to the high resolution of the pixels. It was therefore decided to use the uniform flow configuration in the experiment to analyze the flow behaviour qualitatively. In the numerical simulations with invasion percolation the radial configuration was considered in addition to the uniform one.

2.1.1 Artificial porous media

The two-dimensional porous media were implemented by two plexiglass plates, one of them having a rough surface. They were taken from the work of *Su and Kinzelbach* [1999] and the detailed description of the setup is given there. The rough surface was milled pixelwise into the plexiglass, each pixel representing a square shaped pore. The space between the two plates forms a 2d porous medium. The model differs from previously investigated artifical pore scale porous media like e.g. in *Lenormand and Zarcone.* [1989] or *Furuberg et al.* [1996], where the models consist of pores and connecting throats between the pores. However, for flow dominated by capillary entry pressure, this does not result in major differences in the flow behaviour. In the models cited above the entry pressure is assigned to a throat whereas the pore volume is assigned to the pore. In the model used in this work, both quantities are assigned to the pore. If the models are considered as networks, the differences concern only connectivity of the grid, which has no principal influence on the flow. The porous media have a dimension of 0.4 m x 0.4 m containing 513 x 513 pores, $7.8 \cdot 10^{-4}$ m x $7.8 \cdot 10^{-4}$ m each. The thickness of the pores is randomly distributed.

Distribution of the pore sizes

The models used in this work differ from the models cited above in the properties of the pore distribution. In the earlier models, the pore volumes and capillary pressures are modeled by uncorrelated random numbers. Here two different distributions for the parameters are used, both of them having a spatial correlation structure. The first distribution has an exponential variogram with a finite correlation length, the second one has a fractal variogram and therefore no defined correlation length, but correlation structure on all scales. Hence the influence of correlation on flow dominated by capillary entry pressure can be investigated, which was considered to be important for the problem of upscaling.

All the pores have the same lengths in x- and in y-direction, but the apertures in z-direction are randomly distributed. The capillary entry pressure of a pore can be assigned by the Laplace-Young equation

$$P_c = \sigma \left(\frac{1}{r_1} + \frac{1}{r_2} \right).$$

σ is the surface tension between the two fluids and r_1 and r_2 are the radii of curvature. The in-plane radius is much bigger than the radius resulting from the aperture radius and the corresponding term is neglected for this reason. This is an approximation which is valid if the fluid-fluid interface is not branched on the single pore scale. The capillary entry pressure is then determined by the relationship

$$P_c = 2\sigma \frac{1}{b},$$

where b is the aperture at the interface. Also a permeability can be assigned via the

relation

$$K_{\text{abs}} = \frac{b^2}{12},$$

assuming that the flow in a pore can be considered as laminar flow between parallel plates (*Witherspoon et al.* [1980]).

The aperture distributions were generated with the code fgen, which was developed by *Robin et al.* [1993], for the exponential variogram and with a fractional brownian motion code for the fractal variogram. Further details about the codes can be found in *Su and Kinzelbach* [1999]. Histograms of the generated distribtions are shown in Figs. (2.1) and (2.2). The generated fields are shown in Figs. (2.3) and (2.4). The large column at aperture zero in the histograms are due to the fact that the apertures were generated with a normal distribution, which is not restricted to positive values. As apertures smaller than zero are unphysical they are all set to zero.

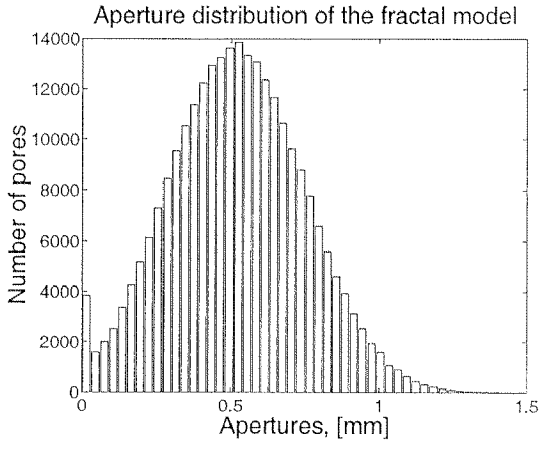

Figure 2.1

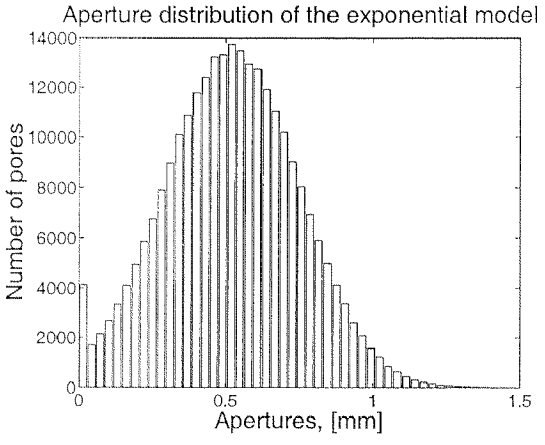

Figure 2.2

Histograms of the generated aperture fields

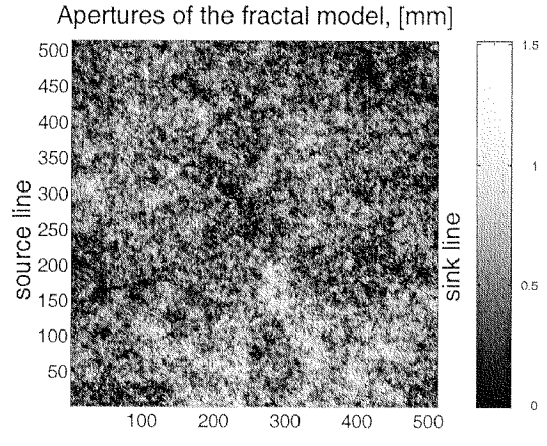

Figure 2.3

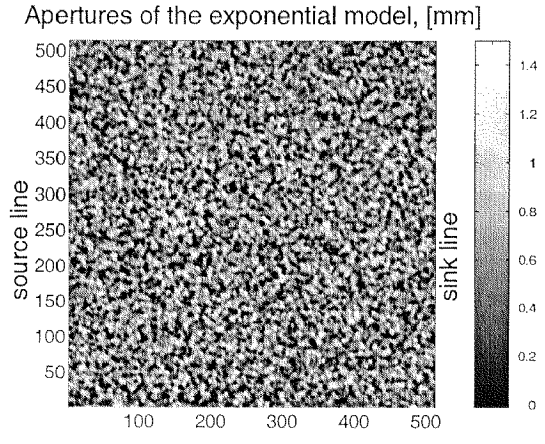

Figure 2.4

Generated aperture fields

During the use of the plexiglass boxes in former experiments, the plexiglass had been subject to deformations, so that at the time the experiments for this work

were performed, the distributions were not exactly the same as the generated ones. Therefore the real distributions were redetermined in the work of *Sorensen* [1999]. A light transmission technique was applied and from the measured light intensity at a pixel the aperture could be calculated by the law of Lambert-Beer. The procedure is described in *Sorensen* [1999]. The recalculated aperture distribution fields and the variograms are shown in Figs. (2.5) through (2.8).

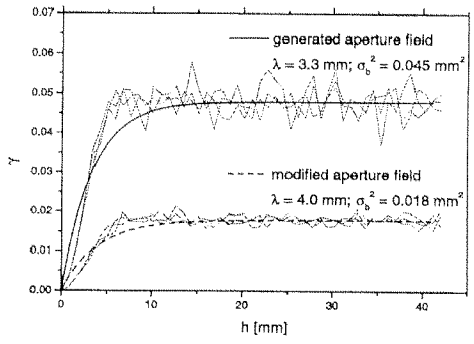

Figure 2.5

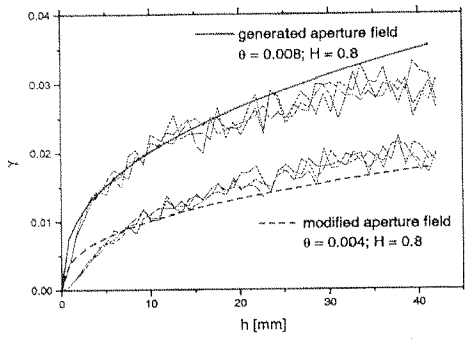

Figure 2.6

Variograms of the generated and remeasured fields, taken from *Sorensen* [1999]

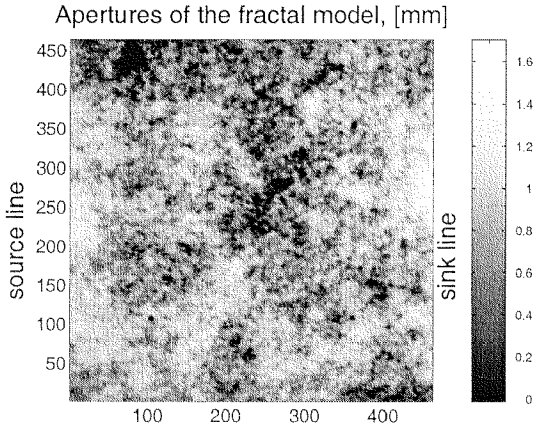

Figure 2.7

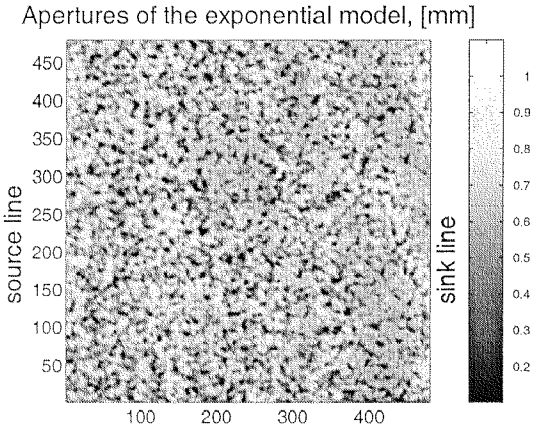

Figure 2.8

Recalculated aperture fields

It can be observed that the regions at the source and the sink line are deformed in such a way that the apertures tend to be larger than when they were generated. This effect is bigger in the model with fractal variogram. The source is in this case no longer a straight line, but can rather be considered as bent. The differences in the variances in the variograms are due to the fact, that the measured fields had a coarser resolution than the generated fields. It was not possible to get a pixelwise picture. One measured pixel therefore contains averaged information about more than one real pixel, which reduces the variance of the measured distribution. However, it can be noted that also in the recalculated variograms no additional trend can be observed. From this we conclude that the deformations have no severe

impact on the correlation structure. For the analysis of the data, the distributions of *Sorensen* [1999] were used. The mean aperture of the exponential model are then $\bar{b} = 5.8 \cdot 10^{-4} m$ and for the fractal model $\bar{b} = 6.6 \cdot 10^{-4} m$ and the correlation length in the exponential model is $l_0 = 4.0 \cdot 10^{-3} m$ where 100 x 100 correlation lengths are contained in the whole medium. The Hurst coefficient in the fractal model is $H = 0.8$ which is the same as the Hurst coefficient of the theoretically generated field.

2.1.2 Experimental setup

The experimental setup is sketched in Fig. (2.9).

The porous medium, consisting of the two plexiglass plates, is connected to reservoirs at its open sides. The reservoir at the source line is open, so that at this line the pressure in the air phase is atmospheric pressure. The sink line is connected to a sealed reservoir which is filled with water. When the air is entering the sealed reservoir at breakthrough it is moving to the top of the reservoir driven by buoyancy forces. Therefore the pressure in the water phase at this line is given by the hydrostatic pressure even over some time after breakthrough. At the bottom of the sealed reservoir a pump is connected, so water can be pumped out at constant flow rate. This configuration was chosen instead of pumping air into the model, in order to avoid the effect of a blowing up deformation of the model which would be expected in a plexiglass box. The model is placed on a plane cold light source, providing a uniform illumination from below. The part of the light source which is not used for the illumination of the model is covered by a wooden frame.

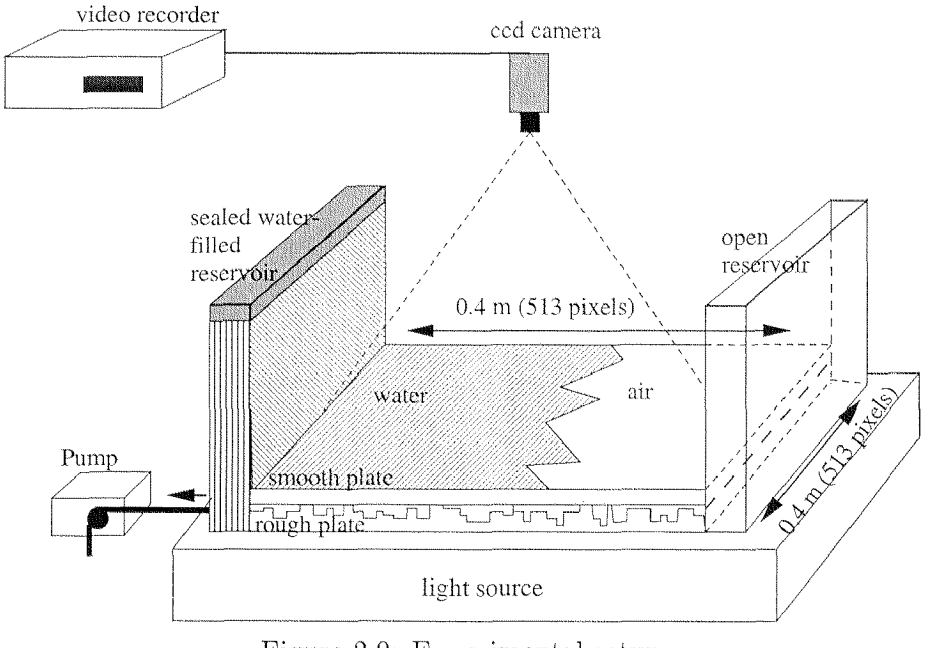

Figure 2.9: Experimental setup

Water saturation of the model was achieved by flooding the dried model in the

beginning with CO_2, using a volume of about 100 times the pore space. Then degassed water is pumped into the vertically tilted model from the sink line which is at the bottom. Water is flowing from bottom to top so that the water front is stabilized. Trapped amounts of CO_2 are dissolving quickly in the degassed water and are thus removed from the system. A very good degree of saturation could be obtained with this procedure, leaving only few (< 20) single pores filled with gas. After saturating the models with water, the water is pumped out of the horizontally tilted model with constant pumping rate.

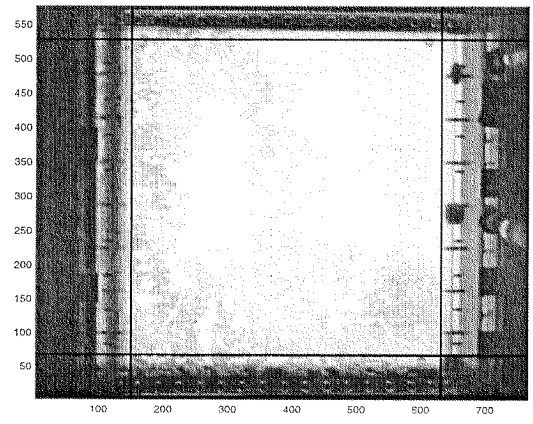

Figure 2.10:
Digitized picture at breakthrough

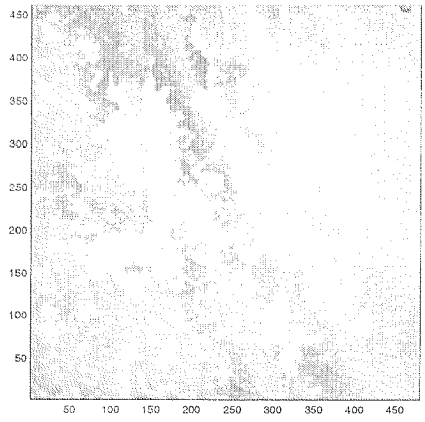

Figure 2.11:
Digitized picture after cutting the edges

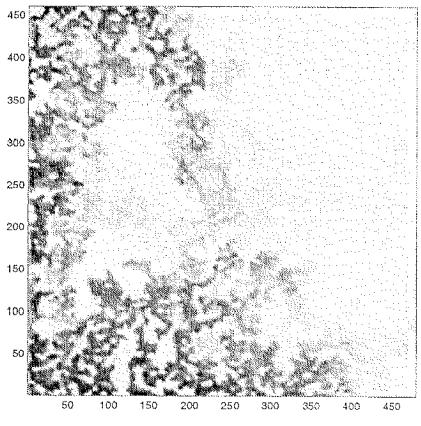

Figure 2.12: Difference picture

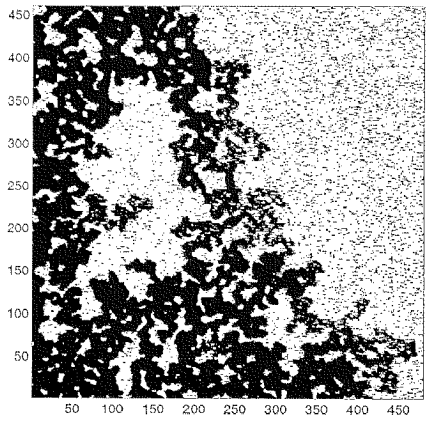

Figure 2.13: Binary picture

This process is filmed by a CCD camera, placed about 1m above the model. The pictures are stored on a video tape and digitized afterwards by a PC containing a grabber card. The resolution of the digitized pictures is 576 x 768 pixels. Gray values on a scale of 0 to 255 are assigned to the pixels. After cutting the edges of the picture that do not belong to the model, the resolution of the model is between 460 to 490 pixels per side. The contrast of the pictures between water phase and air phase is low, so before the beginning of the experiment, a picture of the water filled model was taken and subtracted from the pictures taken during the experiment. A cutoff gray value has then to be assigned to get a binary picture. This procedure is illustrated in Figs. (2.10) through (2.13). The different gray levels for the pixels in

the air phase, visible in Fig. (2.12), are due to a residual amount of water in the pixels, that evaporates after some time.

2.1.3 Flow parameters of the experiments

The flow process was supposed to be dominated by the capillary entry pressure effects. For this reason the flow rates were chosen to be small. As an orientation the phase diagram proposed by *Lenormand et al.* [1988] was used (see Fig. (2.14)).

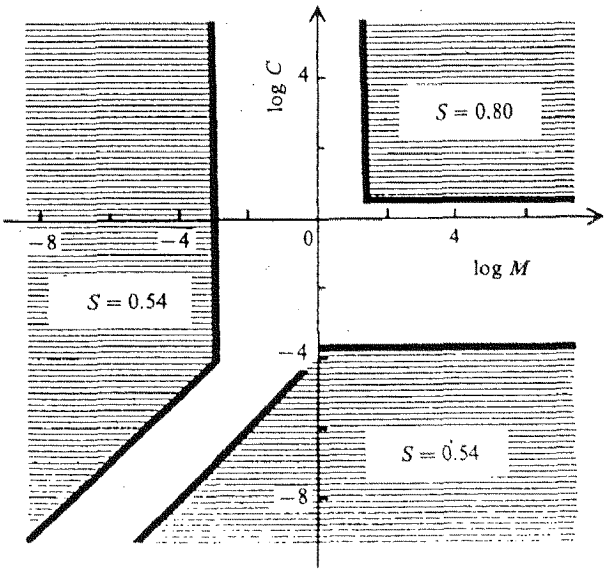

Figure 2.14 Phase diagram for two-phase immiscible displacement, characterizing the different flow types. Taken from *Lenormand et al.* [1988]

The diagram divides two-phase immiscible displacement processes into three domains, stable displacement, viscous fingering and capillary fingering, depending on two dimensionless numbers: the viscosity ratio

$$\mathcal{M} = \frac{\mu_1}{\mu_2} \tag{2.1}$$

and the capillary number

$$N_{\mathrm{Ca}} = \frac{u\mu_1}{\sigma},$$

σ being the surface tension between the fluids, u being the pore velocity and μ_i being the viscosity in phase i, where phase 1 displaces phase 2. The conditions where the flow is governed by capillary forces only were determined by *Lenormand et al.* as described by the parameter region in the lower right part of their diagram. The left part represents the conditions where flow is determined by the viscous forces in phase 2 (viscous fingering dominated) and the upper right part presents conditions where flow is determined by viscous forces in phase 1 (stable displacement).

In the experiment described here the viscosity ratio is given by

$$\mathcal{M} = \frac{\mu_{\text{air}}}{\mu_{\text{water}}} = 0.018 \rightarrow \log(\mathcal{M}) = -1.7.$$

The volumetric flow rate was chosen as $Q = 8.33 \cdot 10^{-9} \frac{m^3}{s}$, which leads to a capillary number of

$$N_{\text{Ca}} = 8.852 \cdot 10^{-9} \rightarrow \log(N_{\text{Ca}}) = -8.05$$

for the exponential model and

$$N_{\text{Ca}} = 7.792 \cdot 10^{-9} \rightarrow \log(N_{\text{Ca}}) = -8.11$$

for the fractal model. These numbers are in the region of capillary dominated flow.

In a second set of experiments a constant head gradient type of boundary conditions was used to test the sensitivity to the boundary conditions. The pump was decoupled from the setup sketched in Fig. (2.9) and the outlet tube was fixed in a position 1 cm below the plane of the model. The capillary number can now only be estimated by taking the mean velocity over the whole experiment. The time difference between inlet and breakthrough was 39 minutes for the exponential model and 33 minutes for the fractal model, leading to the capillary numbers $N_{\text{Ca}} = 4.21 \cdot 10^{-8}$ and $N_{\text{Ca}} = 4.99 \cdot 10^{-8}$ or $\log(N_{\text{Ca}}) = -7.4$ and $\log(N_{\text{Ca}}) = -7.3$ which are both still in the capillary dominated regime. The differences between the resulting gas saturation fields and the fields obtained with constant inflow were small. The flow process in the capillary dominated regime was not sensitive to the applied boundary conditions in our experiments.

2.1.4 Results of the measurements

The pictures of the gas saturation at breakthrough are shown in Figs. (2.15) through (2.17). The flow process itself did not take place in a steady way, but rather stepwise. The air body was not moving for a while, after that a whole cluster of pixels was filled rapidly, and then the cluster was immobile again. This phenomenon was also observed in similar experiments (compare e.g. *Shaw* [1986]) and is known as "moving in Haines jumps". It is a confirmation of the flow being controlled by capillary effects. The air body does not move until the pressure in the gas phase exceeds the smallest capillary entry pressure at the water-air boundary, necessary to invade the next pore. It is likely that there are several pores with small entry pressure connected to the invaded pore which are then invaded quickly.

In the pictures of the air body at breakthrough some artefacts can be observed. In the fractal model the large connected cluster at the source line is certainly due to the deformation of the plexiglass plates in this area. In the exponential model there is a path at the lower boundary filled with air. It is likely that this is a boundary effect and the plates do not stick to each other tightly enough along this line.

The difference between the correlation structures of the two different models can be seen in the pictures at breakthrough. The exponential model has a finite correlation length and the air cluster seems to be composed of small clusters of the size of the correlation length (compare Fig. (2.16)). The fractal model has no finite correlation length and is therefore composed of single pixels. The air body appears denser than that in the exponential model. However, in both models the clusters composed of either subclusters of the size of the correlation length or of pixel size appear on different length scales. The exponential model does not lead to a continuum type of flow. This phenomenon will be discussed in the next section.

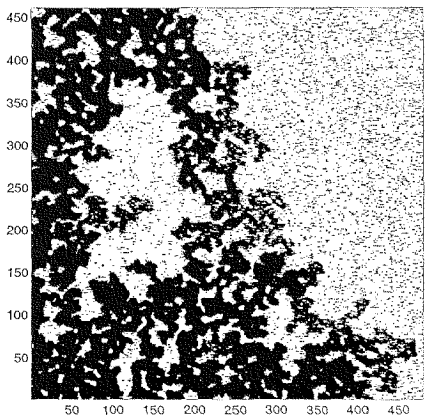

Figure 2.15: Gas saturation in the exponential model

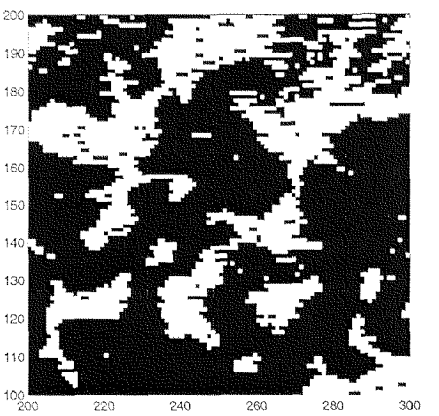

Figure 2.16: Part of the exponential model, 100 X 100 pixels

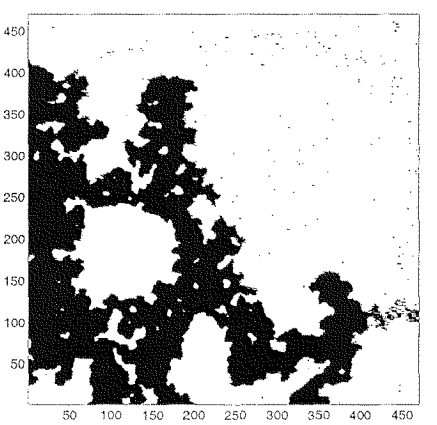

Figure 2.17: Gas saturation in the fractal model

2.2 Numerical simulation of the experiments with invasion percolation

2.2.1 The model of invasion percolation

Besides numerical models based on a continuum description of two-phase flow, a number of approaches for numerical network models is often used to describe small scale processes. On the pore scale Lattice Boltzmann models are used to model the

exact solution for the Navier Stokes equation in the pore space (see e.g. *Rothman* [1988]). For the simulation of unstable two-phase flow, where viscous forces are dominant, the model of diffusion limited aggregation, introduced by *Witten and Sander* [1983], is used (see e.g. *Trantham and Durnford* [1999], *Flury and Fluehler* [1995]). For capillary dominated flow the invasion percolation model is often appropriate.

In order to model capillary entry pressure determined flow an invasion percolation code with trapping was used. The model of invasion percolation (in the following denoted by IP) was established by *Wilkinson and Willemsen* [1983] for the description of fluid displacement in porous media and was extended to the invasion percolation with trapping by *Dias and Wilkinson* [1986]. By comparison with laboratory experiments it could be shown in a number of studies that IP is a model that describes the displacement of one fluid by another immiscible one very well, if capillary forces determine the flow, see e.g. *Lenormand and Zarcone* [1989], *Furuberg et al.* [1996] or *Glass and Yarrington* [1996]. The IP describes the flow process on the pore scale.

The principle of percolation theory and invasion percolation are explained in a number of books and reviews, see e.g. *Stauffer* [1992]. It has been applied to a variety of physical problems in many fields, e.g. solid state physics. Also in the field of flow in porous media percolation models, including IP, have been used and analyzed. Detailed review articles can be found in e.g. *Berkowitz and Ewing* [1998] or *Golden* [1997]. Nevertheless, in the following the basic concepts and mechanisms will be explained briefly.

Percolation is a process defined on a grid consisting of sites and bonds connecting the sites. Random numbers are assigned either to the bonds or to the sites so that we speak of bond and site percolation respectively. Most of the IP processes cited above are bond-percolation processes. The experiments described in these papers were constructed in a way, that the pore throats, or bonds respectively, are the objects that are assigned to a capillary entry pressure and which are random. The experiments described in Section 2.1 are constructed in a different way and the entry pressures should rather be assigned to the pores, or grid sites respectively. The IP model used here is therefore a site percolation model. The differences between site percolation and bond percolation are minor and lie mainly in the connectivity of the random numbers (*Stauffer* [1992]).

In a site oriented invasion percolation process each site of a lattice has a probability that this site can be invaded. This probability is interpreted as inverse resistance of the pore and for two-phase immiscible displacement is proportional to the capillary entry pressure. In general the probability is randomly distributed. There are two different states for the sites, one is 'occupied by the displaced fluid', denoted with $\mathcal{D}$ and the other one is 'occupied by the invading fluid', denoted with $\mathcal{I}$. At the beginning of the percolation process all sites of the lattice are in the state $\mathcal{D}$. Some sites are connected to a 'source'. Usually these are the sites at one of the boundaries. As the percolation begins, the site with the highest probability out of the set of sites that are connected to the source is occupied and changes its state from $\mathcal{D}$ to $\mathcal{I}$. Its neighbouring sites now become connected to the source. This procedure is repeated until one site gets connected to the 'sink', usually the boundary opposite to the

'source', when changing its state from $\mathcal{D}$ to $\mathcal{I}$. The cluster of the invaded sites is called percolation cluster. In general the criterium for a pore to be accessible for invasion is that it must be connected to the source.

In an invasion percolation process with trapping, site clusters which are in the $\mathcal{D}$-state and are surrounded by invaded sites or invaded sites and the boundary (excluding the 'sink'-boundary) are 'trapped' and can no longer be invaded. This mechanism reflects the incompressibility of the displaced fluid as it cannot be moved if there is no connection to the 'sink' where it can be removed from the grid. An inherent assumption is, that the pressure gradients never get high enough to move a whole cluster of trapped fluid.

The algorithm for IP with trapping is in principle built in the following way. The steps are explained on the left hand side. On the right hand side the steps are performed for the example of a 6x6 grid. The site probabilities are written on the sites.

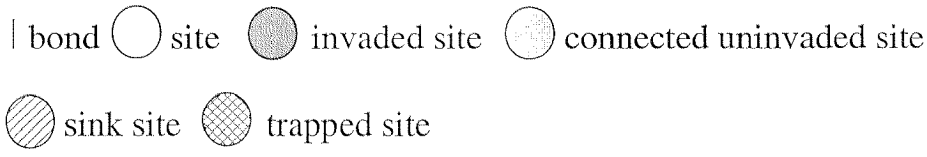

1. Definition of a grid, assignment of probabilities to the sites, definition of the source and the sink, definition of the sites that are connected to the source

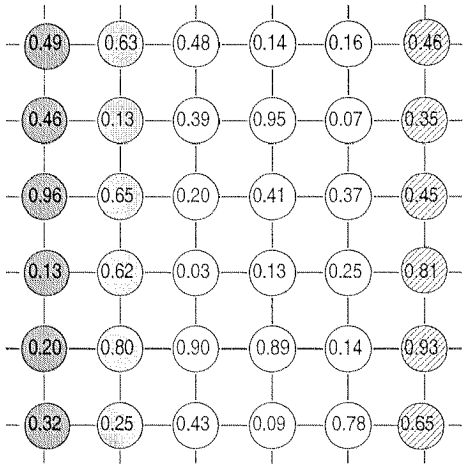

2. Looking through the connected untrapped sites for the site with the highest probability for invasion (corresponding to the largest pore), changing the state of the site to 'invaded' $\mathcal{I}$, definition of the nearest neighbours of the site as connected

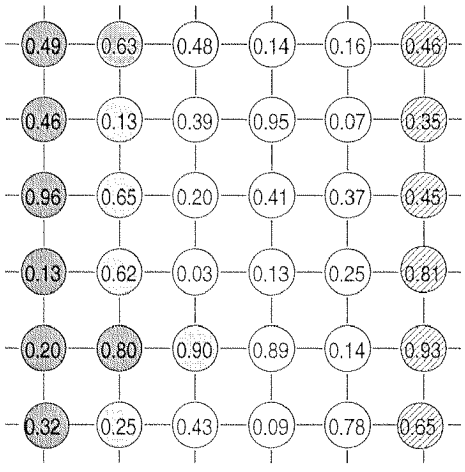

3. Looking through the grid for trapped displaced fluid clusters, definition of these clusters as trapped

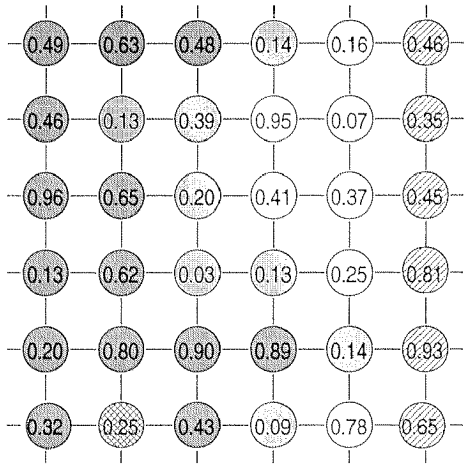

4. Repeating 2. through 3. until breakthrough

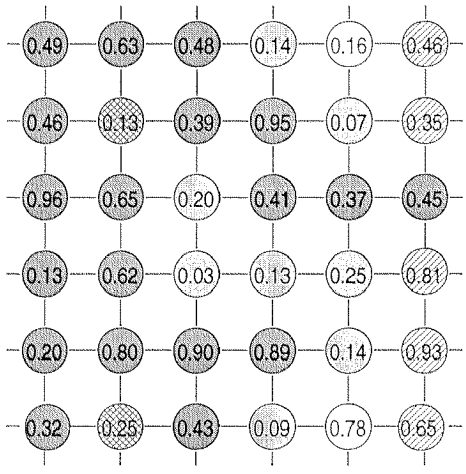

The trapping routine slows down the process as in each step the whole invaded domain has to be checked for trapped clusters (compare *Wilkinson and Willemsen* [1983]). Nevertheless the IP simulation is still much faster in terms of computer time as the simulation of a two-phase immiscible displacement process described by the dynamical differential flow equations on the pore scale.

2.2.2 Applicability of the IP model

Comparisons with experiments show that an IP simulation reproduces the invaded fluid clusters and therefore describes the mechanism that dominates the flow process. However IP is an enormous simplification of the flow as it includes only the main mechanism in a rough sketch. The applicability of IP is therefore confined to special cases and the inherent approximations should be discussed to specify the quality of the simulation.

The main flow mechanism can be described as follows. The pressure increases in the invading phase with a rate which is slow enough to guarantee a spatially evenly distributed pressure. The pressure increases until it exceeds the smallest capillary entry pressure of the pores at the fluid-fluid interface and the pore is invaded. The pressure in the invading phase is then relaxed and builds up again until the next

pore can be invaded. It is evident that this is analogous to IP.

In the original IP process no quantitative dynamics is included. The IP 'sees' only the range of pores which are invaded, but there is no pressure variable. Therefore it does not reproduce the pressure increase and the time development of the displacement process. *Furuberg et al.* [1996] included pressure in the IP and could then describe also the dynamical behaviour of the flow and the pressure distribution. If a flow process with constant inflow rate is considered, it is possible to assign a time to a state of the cluster from the flow rate and the displaced volume.

IP can only describe flow that is driven by capillary forces. Other forces have to be negligible compared to them. The inherent assumption is therefore always that there are no spatial pressure gradients in the invading fluid, which is only reasonable for flow processes with very small flow rates and for invading fluids with a small viscosity. To quantify these limitations *Lenormand et al.* [1988] have proposed a diagram for the application of different model types, IP being among them, dependent on mobility ratio (here: viscosity in phase 1 over viscosity in phase 2) and capillary number, which is determined by the flow rate. *Meakin et al.* [1992] included a trend in the threshold distributon and could so reproduce also flow processes with additional buoyancy forces.

IP also makes the assumption that an increase of the pressure leads to the same overpressure at all pores at the front, suggesting that the pressure gradients are the same, independent of the distance from the pore to the 'sink' boundary. This means that viscous forces have to be negligible compared to the capillary forces. As the 'sink' boundary is at constant pressure this is only valid if the fluid-fluid interface is far away from the boundary.

IP is a binary process, a site is filled with either the displaced fluid or with the invading fluid. It is therefore not able to represent phenomena that include the presence of both fluid phases at one site like for example film flow. It is therefore also impossible to describe phenomena that take place at a scale that is larger than the pore scale, as saturation can only be 0 or 1. *Yortsos et al.* [1993] extended IP to a model, where a number between 0 and 1 is assigned to the sites and the random number that represents the capillary pressure is also dependent on the saturation. It is then necessary to recalculate the random numbers iteratively after each step.

As there are only bonds and sites in the IP model it is not possible to represent physical properties of the porous medium like tortuosity or wettability properties. It is also not possible to descibe fluid properties like density, compressibility or viscosity. Still, much effort has been made to extend IP to include physical properties.

The trapping process obviously is another approximation of the real process. In IP trapping is binary. A cluster of the displaced fluid is totally accessible for the invading fluid until the last pore at its boundary is invaded. In reality, trapping is rather a continuous process. If there are only a few pores that connect a cluster of fluid to the sink, it is already shielded and the accessibility for the invading fluid is already reduced. If one site of a cluster of displaced fluid is invaded, the volume that has been occupied has to be removed from the grid over the 'sink' boundary. IP with trapping neglects the fact, that this is easier if there are many connecting

paths to the sink and the conductivity for the displaced fluid is higher.

IP is a reasonable model for immiscible fluid displacement of a more viscous fluid by a less viscous one which is determined by capillary forces and that takes place at slow flow rates at the pore scale. It also requires knowledge about the pore size distribution. If these criteria are not fulfilled other kinds of models would be more appropriate.

2.2.3 Fractal behaviour of the clusters

A very important property of invasion percolation clusters is that these clusters are fractals. This can be explained in the following way. In a general percolation, a random number is assigned to each site of a grid. If the number is higher than a certain probability p, the site is 'occupied', if it is lower the site is empty. Certain characteristic properties of the field depend on the probability p. If p is lower than a critical probability p_c, there will be no cluster of occupied sites, that span over one side of the grid to the other. If p is higher than p_c, there will be at least one cluster that spans over the grid. The critical probability p_c depends only on the geometrical properties of the grid. At the critical point the grid gets conductive. It has been shown (see e.g. *Stauffer* [1992]) that for each probability p there is a typical length $\zeta(p)$ below which the occupied sites in a domain of this scale are fractals and above which they behave like Euclidean clusters. This length scale diverges at the critical probability p_c. As IP is constructed in a way, that the grid is exactly at the sate of breakthrough, it is always at the percolation threshold. The percolation cluster in an IP is therefore a fractal. For invasion percolation on a two-dimensional grid the fractal dimension D_{frac} has been determined by *Furuberg et al.* [1988] or *Lenormand and Zarcone* [1985] as 1.82. Consequently, the concept of an representative elementary volume (REV), which is explaned e.g. in *Bear* [1972] is not applicable for such flow processes, as has already been stated by *Lenormand and Zarcone* [1989]. The REV concept is based on the requirement that a variable, like porosity or in this case the fluid saturation, which has been averaged over a spatial volume, turns out to be constant and independent of the averaging volume if the averaging volume is larger than the REV. However, fractal structures are inherently nonstationary and the space A they fill out in a volume of radius r is given by

$$A \propto r^{D_{\text{frac}}},$$

with D_{frac} being the fractal dimension. Fractal clusters also have the property to include inner clusters of all sizes smaller than the total cluster size.

In the articles cited above the field of the probability numbers is uncorrelated, as the fractal models they are compared to have been investigated and defined for uncorrelated random fields. The purpose of many investigations of general percolation models (not IP) is to get information about the behaviour near the critical threshold probability p_c. The behaviour of several physical quantities Z, like conductivity, near the critical probability was a focus of interest. Theoretical analysis allows us

to get expressions for the behaviour near the critical threshold probability. This behaviour can usually be described by a power law

$$Z \propto (p - p_c)^{\epsilon},$$

if the length scale of the grid is larger than ζ. ϵ is an exponent that does no longer depend on the geometrical properties of the grid, but just on the Euclidean dimension. These laws cannot be applied to IP, as it is always at the critical percolation threshold. However, the behaviour of these properties at the threshold, where it scale with the length of the grid, can often be written as

$$Z \propto L^{-\nu}$$

where ν is the critical exponent and L is the length of the scale of consideration.

2.2.4 Results of the simulations

In our case, most of the investigations about general percolation clusters are not of large importance, despite of their fractal properties. The main purpose here is rather to use the IP as a model that describes immiscible displacement under the conditions described above, as these were the conditions in the laboratory experiments described in Section 2.1. We are interested in the possibility to upscale capillary entry pressure dominated flow processes, and the numerical simulations were used to investigate this question.

In order to obtain the site probabilities the apertures of the artificial fractures were rescaled to numbers between 0 and 1 and assigned to the grid sites. The largest aperture was assigned a probability 1, the smallest aperture a probability 0, as the large pores have a smaller entry pressure for the nonwetting fluid. Both aperture distributions, the distribution with exponential variogram and the distribution with the fractal variogram were used. Figs. (2.18) through (2.20) show the results of the simulations. Comparing them to Figs. (2.15) and (2.17) we note, that the IP reproduces the saturation distribution in the fractal model very well, whereas the match for the exponential model is only qualitatively good. Some large features in the cluster, like the large trapped area of water in the middle can be recovered, but not the small features, like e.g. the point of breakthrough or parts at the lower boundary. In order to take into account the boundary flow effect at the lower boundary in the exponential model, as mentioned in Section 2.1, a second IP simulation was performed, where a part of the lower boundary was added to the source. The cluster responded to this change and some features are reproduced much better with this adapted simulation, but nevertheless the agreement is still only qualitative. The reason for the difference of the small scale features in experiment and simulation is the lack of knowledge of the exact aperture distribution. As explained in Section 2.1 the aperture distribution was not available pixel by pixel, but redistributed from the 513x513 to a 460x460 resolution. This redistribution has a large effect on the grid with finite correlation length, which can be seen when a

small random change of the original grid is performed. The outcome of a simulation on a grid with the exponential aperture distribution, each aperture changed by a random number between 0 and 0.1, is given in Fig. (2.21). It can be seen, that the large scale features of the cluster are preserved, but the small scale features like the point of breakthrough are changed. The fractal aperture distribution is less sensitive to changes as can be seen in Fig. (2.22). The patterns and clusters of the invaded fluid on the one hand are caused by the fractal properties of the cluster as explained above. If there is a correlation structure in the field, patterns and clusters and their sizes are also determined by the correlation length. However, whether a correlation induced subcluster is invaded can be determined by one or two single sites. When there are many small clusters, the sensitivity to variations in the probability distribution is therefore larger than when there are a few larger clusters, where the probability to reach the clusters is larger.

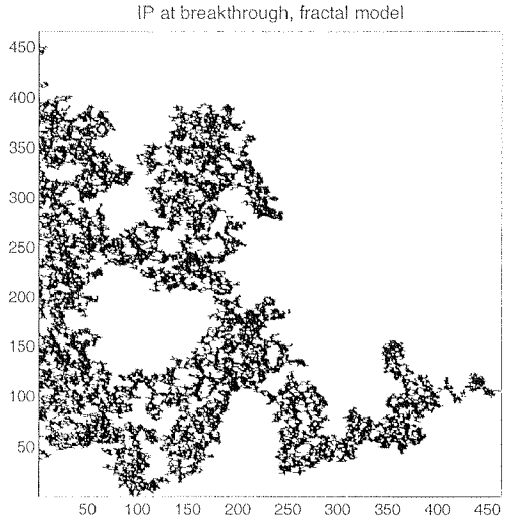

Figure 2.18

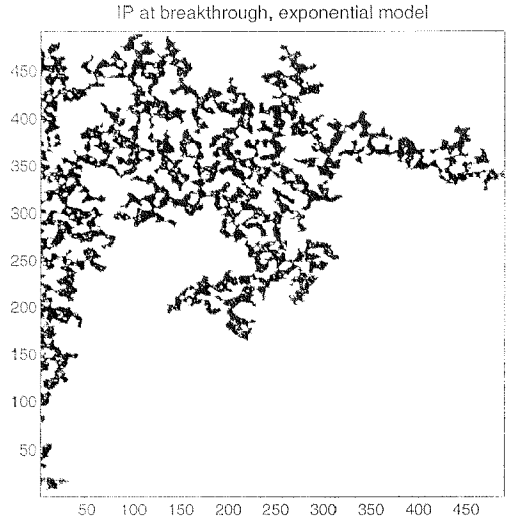

Figure 2.19

IP simulation using the fields of the experiments

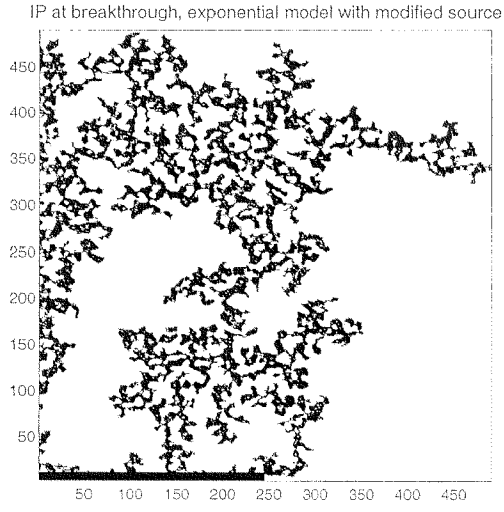

Figure 2.20: IP simulation using the fields of the experiments

In both cases, in the simulation of the fractal model and in the simulation of the

exponential model, we note, that the simulation gives a less compact cluster than the ones obtained experimentally. The simulated clusters have a much more detailed structure. The reason is, that the flow in the experiment was not really pixelwise, but rather areas of pixels were invaded at one step. But differently from the Haines-jump mechanism, not only the pores in the neighbourhood of the next invaded pore with sufficiently small entry pressure were invaded, but the whole neighbourhood. This is an artefact stemming from the construction of the models. The plane plate is on the top side, the rough plate at the bottom. Buoyancy forces drive the air to the top of the pore, so is does not invade the whole pore and does not "see" the whole roughness of the bottom plate. The roughness effect is therefore smeared out.

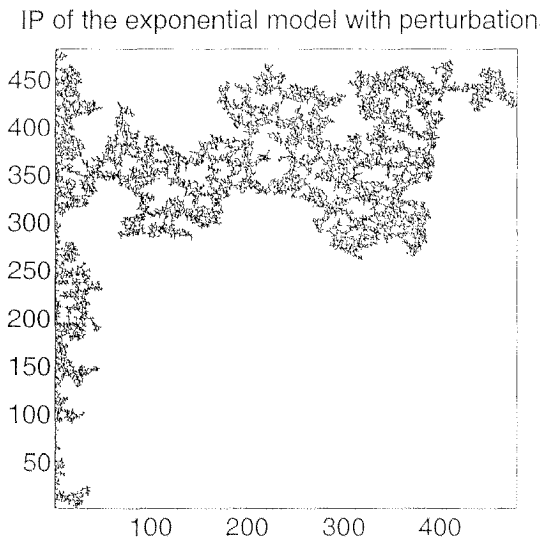

Figure 2.21

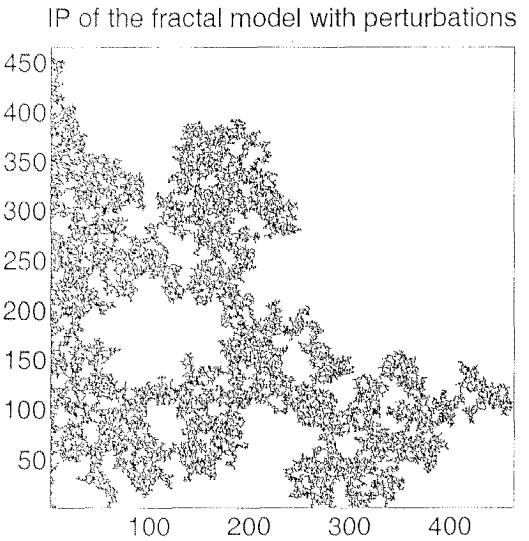

Figure 2.22

IP simulation using the fields of the experiments with added small perturbations

Due to the high cost of the models it was decided to proceed with the models the way they were constructed. Keeping the explanation of the artefacts in mind it can be concluded, that for the experiments described in Section 2.1 IP is a reasonable method to simulate the displacement processes.

2.2.5 Upscaling by spatial averaging

The problems with spatial averaging of IP clusters have already been discussed in Section 2.2.3. The fractal properties are in contradiction to the REV concept. It is therefore questionable if it is reasonable to describe two-phase immiscible displacements under conditions where IP is a good model on a larger scale by assigning continuum approach parameters to it. This would imply the average over an REV. The non-smooth, fractal behaviour is initiated at the very beginning, on the pore scale, and is therefore important on all scales.

This can be seen very well in the experimental results from Section 2.1. The outcome of the measurements can be averaged pixelwise. The results are shown in Figs. (2.23)

through (2.24) for an average of 8x8, 16x16, 32x32 pixels and an average of 116x116 pixels, leading to a 4x4 cell picture. Taking into account that for the model with exponential variogram one correlation length is equivalent to 5 pixels at least in the last picture a homogeneous saturation distribution would be expected. However, the large scale patterns remain in all cases, due to the fractal behaviour of the flow process. With the increase of the averaged pixels it gets more difficult to distinguish between the model with the fractal and the model with the exponential variogram.

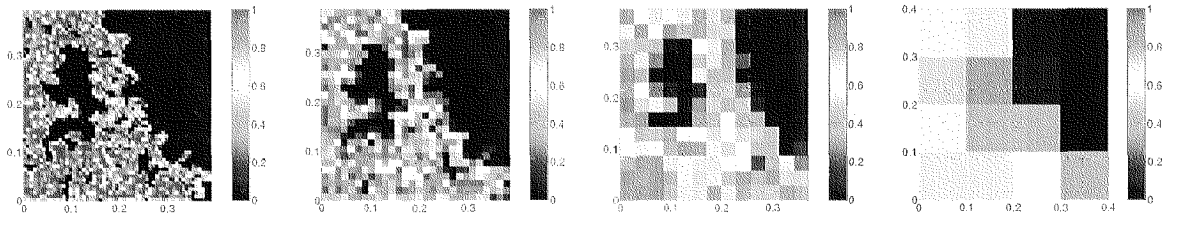

Figure 2.23: Average over 8x8, 16x16, 32x32 and 116x116 pixels, exponential model

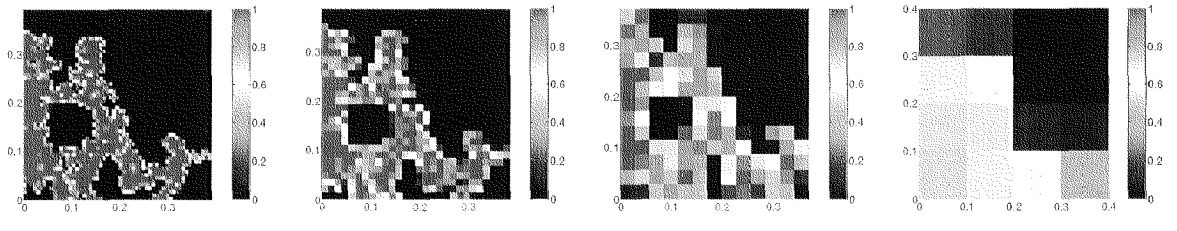

Figure 2.24: Average over 8x8, 16x16, 32x32 and 116x116 pixels, fractal model

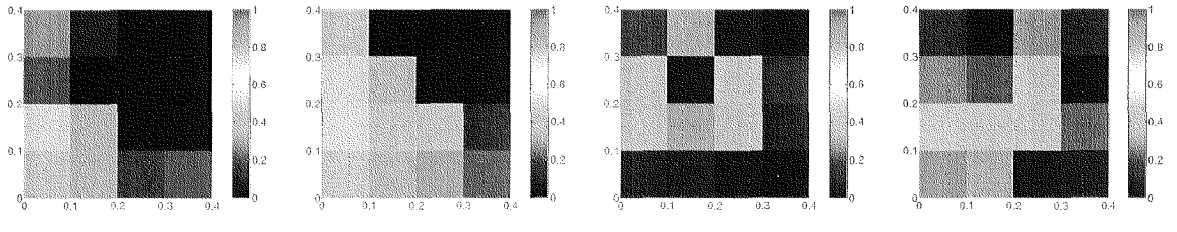

Figure 2.25: Average over 125x125 pixels of 4 different IP simulations with 500x500 sites

Pixelwise averages of saturation distributions produced with IP simulations show the same behaviour. This can be seen in Fig. (2.25). The random fields of the IP have the same stochastic properties as the field with exponential variogram in the laboratory experiment. There are also large scale patterns that remain after averaging over many correlation lengths. On the one hand that confirms that the large scale patterns in the experiments are not produced by artefacts of the experiment and that two-phase immiscible displacement on the pore scale is really well described by IP. On the other hand this is a confirmation that all volume averaging approaches like the REV concept are no reasonable concepts for these processes.

Another spatial averaging approach is averaging over one spatial dimension to obtain a smooth distribution in the remaining dimensions. This has been performed

by *Sorensen* [1999]. He averaged the experimentally obtained saturation distribution over the y-axis, which is the axis parallel to the line source. He also tried to reproduce the one-dimensional saturation distribution with the code TOUGH2, which is a model based on the continuum approach. The averaged distributions and the numerically produced saturations are shown in Fig. (2.26). It is evident that the averaged saturation distribution can hardly be considered as an outcome of a flow process in a homogeneous medium. Although the average over the y-axis was performed over 100 correlation lengths, the variation of the distribution is as high as its mean. This can already be understood by looking at the two-dimensional pictures in Fig. (2.15) and (2.17). At some locations x there are only few pores filled with gas over the y-line, but at one of the next x-locations there are many. The sparsely populated y-lines are like bottlenecks which the gas has to pass in order to reach better accessible pores. The reason for this is the same as in the twodimensional averaging approach, the occurence of large scale patterns due to the fractal properties of the gas cluster.

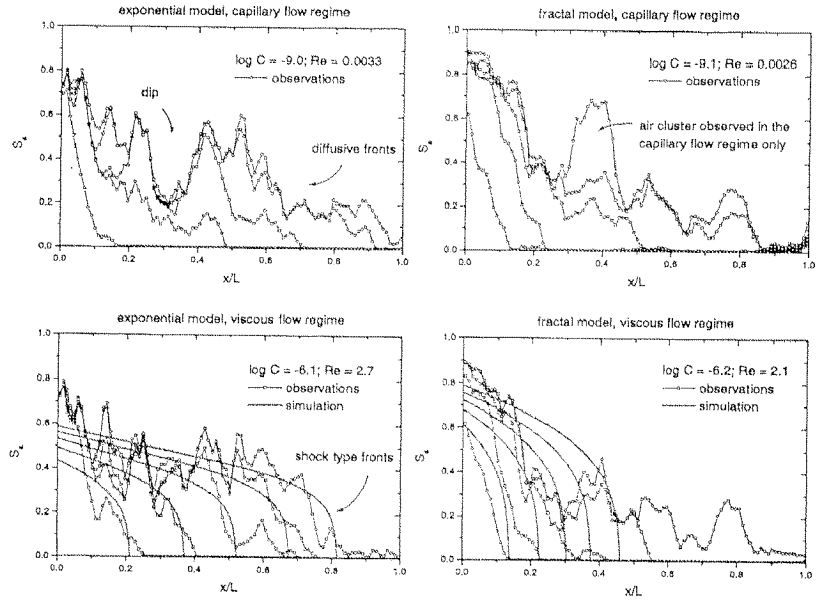

Figure 2.26: Spatial averaging over one dimension, taken from *Sorensen* [1999]

The discussion of the pore scale flow process can be transferred to the larger scale in the continuum approach, for heterogeneous media, where capillary entry pressures are high and heterogeneously distributed and flow rates of the displacement process are very small. The pore size distribution is translated into the distribution of permeabilities or entry pressures, respectively. Permeability and entry pressure are related to each other via e.g. a Leverett scaling. In this case the same mechanisms that lead to the channeling behaviour on the pore scale is dominating the flow on a large scale. It can be assumed that the large scale immiscible displacement can then be described by an IP as well. It is of course difficult to confirm this assumption by field measurment observations, as field experiments cannot be performed under

controlled conditions and the spatial distribution of permeability and entry pressures is in general not known. It is also difficult to get a detailed saturation distribution in a field measurement. However, in intermediate scale experiments like VEGAS (see *Kobus* [1996] or *Bastian and Helmig* [1999]) these channeling behaviour has been observed also on the large scale. On the large scale the saturation will not be a binary distribution like in the pore scale flow, however regarding the saturation as binary by inserting a threshold will lead to more or less the same result, as the binary pressure jump structures will overrule the continous features. To the same reasons as in the case of pore scale flow the approach to perform volume averaging and assign effective parameters to a larger soil domain is not applicable. Although the parameter field can fulfil the requirements of ergodicity, the flow process cannot become ergodic due to the fractal features of the saturation clusters.

2.2.6 Upscaling by ensemble averaging

The stochastic approach is a method applied extensively for upscaling. A detailed discussion of this approach is postponed to Chapter 3. The basic idea is to describe one existing realization of the field of random paramters as an ensemble of media with the same stochastic properties. Under certain assumptions the volume averaging is equivalent to the average over the ensemble. From the ensemble averaged quantities effective parameters can be deduced. However, in the immiscible displacement described here, the assumptions for the equivalence of ensemble and spatial averaging are not fulfilled, as ergodicity cannot be reached. The effective parameter concept applied to this kind of displacement is not reasonable for describing the single realization behaviour. However, the ensemble averaged quantities have predictive power for risk assessment analysis. The averaged saturation at the sink boundary is not a quantity that will be measured at anyone place in an experiment in the single realization. The measured saturation will be 1 or 0. But the averaged saturation can be considered as a probability distribution for the binary result. The ensemble averaged saturation at one point is the probability to measure saturation 1 at this point. Considering the ensemble averaged fields in this way, the aim to obtain effective parameters for a homogeneous continuum model from the ensemble averaged heterogeneous field is reasonable. Continuum models on a larger scale can be based on these effective parameters. Again the resulting saturation fields have to be interpreted as probability distributions.

An ensemble of IP simulations was performed and the outcome was averaged. To have stationary parameter fields the ensemble was produced with an aperture distribution with a Gaussian variogram. Mean, variance and correlation length were chosen as in the experiment. The random fields were generated using the model fgen (*Robin et al.* [1993]), which is based on the fast Fourier transform method. The method is briefly described in Chapter 3. An ensemble of 100 realizations of 500x500 pixel fields was produced and the saturation clusters produced on these fields were averaged.

The averaged steady state saturation fields after breakthrough are shown in Fig.

(2.27). We observe that the IP clusters are subject to boundary effects. This is due to the inherent trapping mechanism. Sites at the boundary line can only be invaded from one direction and sites in the neighbourhood of the boundary line have a lower probablitiy to be invaded from the direction of the boundary. The density of invaded sites is therefore lower in the region of the boundaries. This is of course an artefact of the model as the ideal model would be infinitely extended in the y-direction. In IP simulations the boundary effects are avoided by applying periodic boundary conditions at the edges which does not match the physical boundary conditions in the experimental model. Here the boundary effects are avoided by excluding the boundaries. They are marked by lines in Fig. (2.27). Fig. (2.28) shows the plot of a cut in x-direction at the middle of the y-axis and a reproduction by a numerical continuum approach model. The parameters for a Brooks-Corey parametrization are given in Table 2.1. The Brooks-Corey parametrization is discussed in Chapter 3.

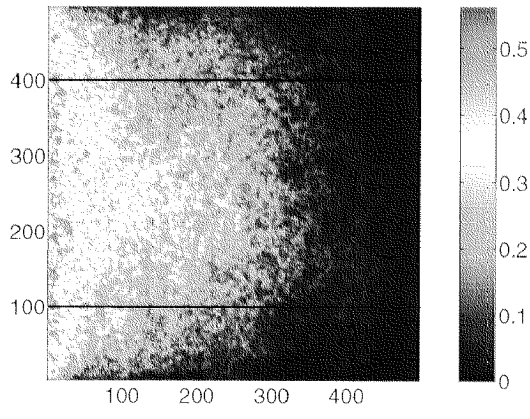

Figure 2.27: Averaged IP fields

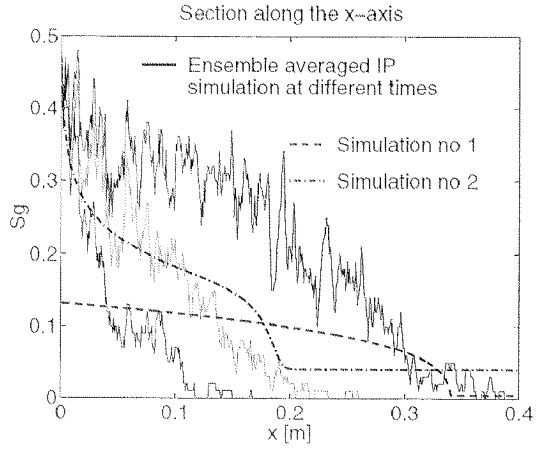

Figure 2.28: Section along the x-axis

	Parameters for a Brooks-Corey parametrization				
	porosity ϕ	permeability K_{abs}	initial saturation S_{init}	entry pressure $P_{\text{c entr}}$	λ
1: Estimated from parameter distribution	1	$2 \cdot 10^{-8} m^2$	0.004	190 Pa	4.0
2: Fitted to the results	1	$2 \cdot 10^{-14} m^2$	0.04	1 Pa	0.9

Table 2.1 Parameter table for the uniform flow simulation

One can see that for the ensemble averaged fields a continuum approach simulation can be performed. The first fit is performed with parameters estimated from the aperture distribution. The permeability was set as $K_{\text{abs}} = b_g^2/12$ where b_g is the geometric mean of the apertures, and the parameters for the capillary pressure and relative permeability were also determined from the aperture distribution, using the

relation $P_c = 2\sigma/b$. The parameters were calculated by *Sorensen* [1999]. For the second fit the parameters were chosen by trial and error to obtain a more reasonable fit. By comparing the parameters one can see that there are differences between them. The ensemble averaged fields can be reproduced by a continuum model fairly well, however parameters cannot be estimated from the aperture distribution. The fluctuations of the saturation curve are still very high considering that the average was performed over 100 realizations. The continuum type flow is of diffusive type. The gas saturation is not subject to selfsharpening effects and no gas front is established.

2.2.7 Radial flow configuration

The actual flow configuration of interest is radial. For this reason another ensemble of IP clusters was calculated for a radial configuration, assuming that IP describes the flow process in a manner as reasonable as in the uniform flow configuration. In this case the 'source' boundary is one site in the middle of the grid and the 'sink' boundary is on a circle around this site. The grid and the outcome of one simulation are shown in Figs. (2.29) and (2.30).

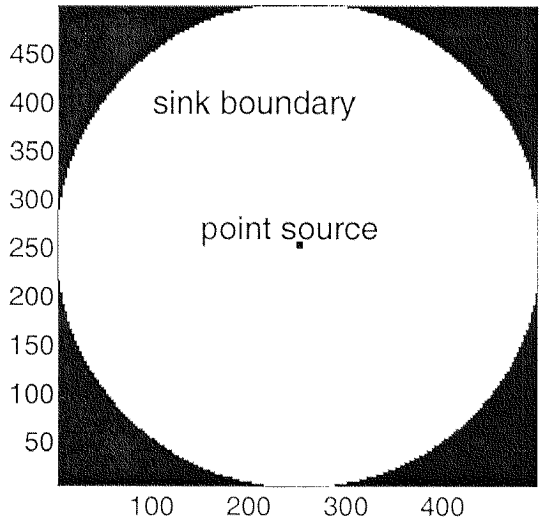

Figure 2.29: Radial IP simulations: grid

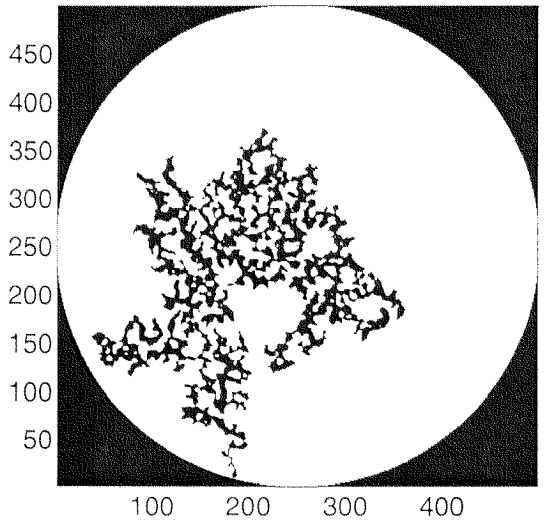

Figure 2.30: Outcome of one simulation

It is obvious that in the radial case the concept of spatial averaging would also not be reasonable. This can be concluded from the outcome of different single realization simulations shown in Appendix A. The plot of a radial section of the averaged saturation field and saturation obtained with a numerical simulation in a homogeneous medium is shown in Fig. (2.32). One plot is again obtained with parameters from the aperture distribution and one is obtained using parameters to get a good fit. The parameters are shown in Table 2.2.

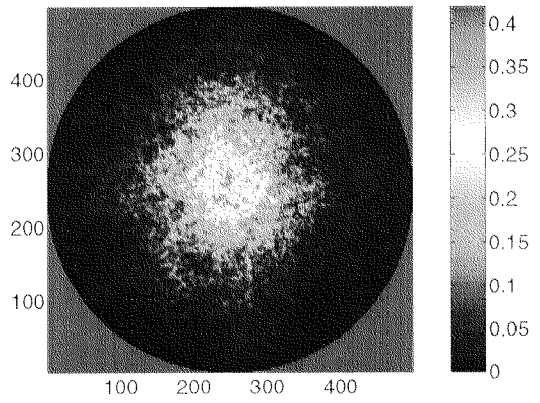

Figure 2.31: Averaged gas clusters with radial configuration

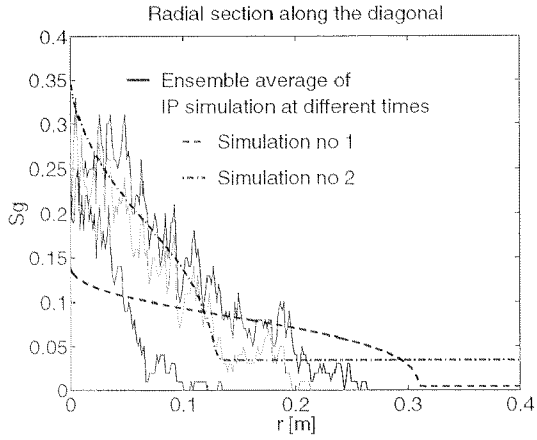

Figure 2.32: Radial section of the gas saturation field

	Parameters for a Brooks-Corey parametrization				
	porosity ϕ	permeability K_{abs}	initial saturation S_{init}	entry pressure $P_{\text{c entr}}$	λ
1: Estimated from parameter distribution	1	$2 \cdot 10^{-8} m^2$	0.004	190 Pa	4.0
2: Fitted to the results	1	$4 \cdot 10^{-9} m^2$	0.03	1 Pa	0.9

Table 2.2 Parameter table for the radial flow simulation

2.2.8 Estimation of breakthrough times

It is not reasonable to apply continuum approach concepts to the single realization nor to upscale the continuum flow equations for this kind of flow. Therefore different questions have to be asked for the single realization. An effective permeability of the medium would be of no use for predicting the flow, as the gas will flow along a few highly permeable paths and will not explore the whole medium. A question that cannot be answered without detailed knowledge of the medium is therefore at which point the air will break through. However, for many applications the question of breakthrough time at a certain distance is also very important. Also the distance from a source where one has to reckon with occurence of gas saturation at a certain time might be of interest. These quantities can be estimated from the basic knowledge of fractal structures. Considering an uncorrelated field, the number of sites that are invaded in an area of size L x L is given by

$$N(L) \propto L^{D_{\text{frac}}} \tag{2.2}$$

D_{frac} being the fractal dimension. This relation also leads directly to an estimation of the residual saturation for a medium of the length scale L. It would also be proportional to $L^{D_{\text{frac}}}$.

For a given pumping rate Q the time of a given state can be assigned to pixel number N via the mean aperture $\bar{b}$,

$$V = N \cdot \bar{b} \cdot \Delta x \cdot \Delta y = Q \cdot t \rightarrow N = \frac{Qt}{\bar{b}\Delta x \Delta y}.$$

From this a typical cluster length can be defined and a radius of the gas body can be estimated as

$$L \propto N^{1/D_{\text{frac}}} = \frac{(Qt)^{1/D_{\text{frac}}}}{\bar{b}\Delta x \Delta y}.$$

With the same reasoning a breakthrough time can be estimated for a given distance from the source as

$$t \propto \frac{L^{D_{\text{frac}}} \bar{b} \Delta x \Delta y}{Q}.$$

The usage of the mean aperture is an approximation which introduces error. In the IP process mainly the large pores are invaded, so that the mean aperture of the invaded cluster will be larger than the mean aperture of the whole field. However, results from the simulations yielded an underestimation of the mean aperture by 20 per cent which is not too big.

One has to keep in mind, that these are only rough estimates and only represent the main characteristics. Breakthrough times will certainly be earlier, as the relation (2.2) is only valid at large disctances from the boundaries. At the sink boundary the cluster is sparser than in the middle, as the cluster growth is stopped as soon as a pixel of the sink is reached. The pixels in the region around these sites can therefore not be invaded. For the same reason the radius of an invaded area will be larger than that obtained from the above estimation.

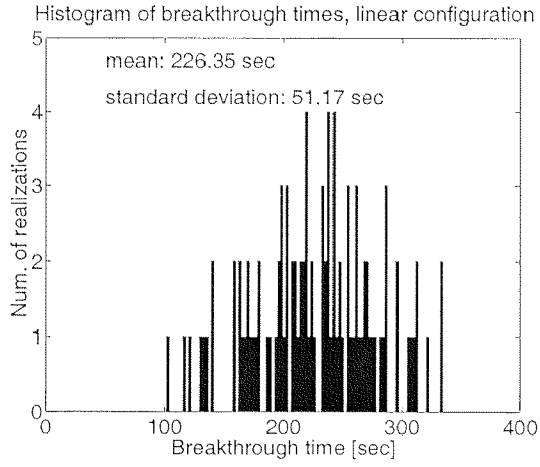

Figure 2.33: Linear configuration

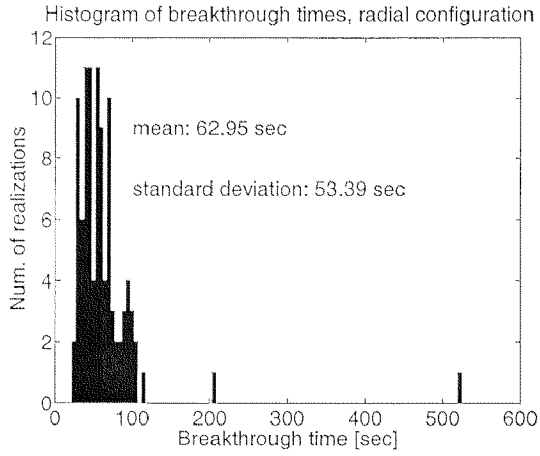

Figure 2.34: Radial configuration

It has also to be considered, that estimations like these only describe the behaviour in an averaged sense. The fractal behaviour of the process makes single realization to

single realization fluctuations very large. In Fig. (2.33) and Fig. (2.34) histograms of the breakthrough times for the ensemble of 100 IP simulations are shown. The distribution is still broad and the single realization can deviate a lot from the mean. Reliable estimations for a real flow process in a porous medium that is dominated by capillary effects are therefore very difficult to make if there are no known large scale structures in the medium.

2.3 Conclusions of experiments and simulations

We conclude that the real saturation distribution in a two-phase immiscible displacement experiment in the single realization where the more mobile phase displaces the less mobile one and capillary entry pressures dominate the flow behaviour cannot be reproduced with the continuum approach. The reason is that the REV concept, or a volume averaging concept for the larger scale, are not appropriate for this kind of flow. However, ensemble averaged gas saturation fields of media with parameter distribution with finite correlation length can be reproduced by continuum approaches. We have to interpret the saturation in these cases not as a real saturation but rather a probability distribution of outcomes of experiments. If we interpret the saturation in this way, it is reasonable to upscale the continuum equations to larger scales.

For the simulation of flow in the single realization, invasion percolation is a reasonable approach. If there are correlation structures on the scale of the experiment, and these structures are known, the flow pattern can be very well predicted with these methods. However, if the correlation length of the medium is small, detailed knowledge of the distribution would be necessary to predict the flow pattern exactly. Knowing the fractal nature of the cluster and its fractal dimension, averaged quantities like breakthrough times or cluster radii can be estimated for flow processes with constant flow rate. However, the single realization can deviate a lot from the mean which makes reliable predictions difficult.

Chapter 3

Numerical multi-realization calculations

Many field applications of two-phase flow take place on a large scale where the pore scale can not be resolved. The flow equations are described on a continuum scale where the pore space is averaged over an REV. Large scale heterogeneities influence the flow behaviour also on the large scale. One method to take them into account is to describe the heterogeneous porous medium as an effectively homogeneous one in an averaged sense, as outlined in the introduction (Chapter 1). Effective parameters capture the impact of the heterogeneities. To get a better understanding of the averaged behaviour on the large scale, numerical simulations of the twodimensional flow process were performed using the code TOUGH2 (*Pruess* [1991b]). As the flow equations which are described in more detail in Section 3.1, contain a lot of arbitrariness in the parametrization of the saturation dependent parameters, a sensitivity analysis with respect to the features of these parametrizations is performed in Section 3.2. In Section 3.3 the averaged saturation fields, averaged over an ensemble of heterogeneous media, and the deduced effective properties are discussed. Finally it is investigated in Section 3.4 whether the single realization behaviour converges to that of the average field at large scale and how this can be quantified.

3.1 Description of the problem

In this section, the flow equations for the problem of interest and their special features are discussed.

3.1.1 Flow equations

The flow of two immiscible fluids which we call phase 1 and phase 2, is described by the continuity of mass equations

$$\partial_t(\rho_i \phi S_i(\vec{x},t)) + \vec{\nabla} \cdot \vec{F}_i = s_{M\,i} \tag{3.1}$$

where i stands as index for the phase, S is the saturation (volumetric percentage of the phase), s_M stands for all source and sink terms, ρ is the density, ϕ is the porosity and $\vec{F}$ is the mass flux of the phase. It is assumed, that one phase consists of one component only, the gas phase of air and the liquid phase of water. The mass flux is described by a modified form of Darcy's law,

$$\vec{F}_i = -\frac{K_{\text{abs}} k_{r\,i}(S_i)\rho_i}{\mu_i}\vec{\nabla}P_i = -K_{\text{abs}} m_i(S_i)\vec{\nabla}P_i, \tag{3.2}$$

with K_{abs} being the absolut saturated permeability, μ the viscosity and P_i the partial pressure in phase i. $k_{r\,i}$ is the relative permeability of phase i. The ratio of the relative permeability and the viscosity, is called the mobility of phase i m_i. It is a function of the saturation. The form (3.2) of Darcy's law has not been derived from the pore scale flow equations via an upscaling procedure but is an empirical relation. It is discussed in the literature, whether this is a too simplified form of Darcy's law since it neglects the dependency of the flow in one phase on the pressure gradient in the other phase. However, this is not taken into account here, as these effects are supposed to be of minor importance.

Buoyancy forces are neglected in Eq. (3.2), as their influence is beyond the scope of this work. We are dealing with a two-dimensional horizontal configuration.

There are two more relations, which together with Eqs. (3.2) and (3.1) add up to a set of six coupled equations for six variables. One is the obvious relation

$$S_1 + S_2 = 1, \tag{3.3}$$

as we are dealing with non-deformable porous media. The other one relates the pressure difference in both phases to the capillary pressure P_c.

$$P_c(S_i) = P_1 - P_2. \tag{3.4}$$

The concept of a capillary pressure is analogous to the microscale phenomenon of capillary pressure in a capillary tube. The pressure difference in both phases in this case is related to the geometrical dimensions of the tube. The macroscopic capillary pressure is an empirically obtained function of saturation. The assumption, that the capillary pressure is only dependent on the saturation is an approximation. It has been observed, that it is subject to hysteresis (e.g. *Lehmann* [1998]). However, as we considere a pure drainage process here, this is not taken into account.

The Eqns. (3.1) through (3.4) are written for a scale where an average over the REV has already been performed. The pore scale processes are very complicated and the impact of all the properties that determine the small scale processes, such as wettability of the medium, have to be captured by the empirically obtained functions for the capillary pressure and the relative permeability.

The configuration of the problem of interest here is a two-dimensional radial displacement of water by air, air being pumped into the medium at a single point with a constant mass inflow rate Q_M. The domain is considered to be unbounded. This leads to the source term

$$s_{\text{air}} = Q_M\, \delta^2(\vec{x}), \qquad s_{\text{water}} = 0 \tag{3.5}$$

and the boundary conditions are

$$S_{\text{air}}(|\vec{x}| \to \infty, t) \to 0, \qquad S_{\text{water}}(|\vec{x}| \to \infty, t) \to 1. \tag{3.6}$$

3.1.2 Numerical code

Apart from some special cases, there are no analytical solutions for Eqns. (3.1) through (3.4). One approach is therefore to solve the equations numerically. Lots of codes have been produced in the last decades and as the focus is less on the numerical solution method in principle but rather the qualitative analysis of the flow process, the ready made code TOUGH2 (*Pruess* [1987]) was selected. The code has been upgraded and improved over many years and its reliability has been tested in a number of cases. A further advantage is that the source code itself is available, which makes it possible for the user to perform changes in the code.

TOUGH2 solves the flow equations of two immiscible phases of two fluids. The flow equations are discretized using an integral finite difference scheme. A thorough discussion on discretization schemes and numerical methods to solve two-phase flow equations can be found e.g. in *Helmig* [1997]. The scheme and principles used in TOUGH2 are briefly explained here, a more detailed description of the code is given in *Pruess* [1987] and *Pruess* [1991b].

Discretization of the flow equations

Although for the discretization in the numerical calculations a nine-point scheme was used, the principles of a five-point scheme discretization are explained in the following, to simplify matters. The discretization scheme is based on the integration of the mass conservation equation for phase i in Eq. (3.1) over a cell volume V_n. In TOUGH2 one phase is supposed to consist of more than one component, the gas phase of air and steam and the liquid phase of water and air which is dissolved in the water. The distribution of the fluid in phase i is approximated as a homogeneous one in one cell. The volume integral over the mass density M of component κ can then be written as

$$\int_{V_n} M^\kappa(\vec{x}) d^d x = M_n^\kappa V_n, \qquad M_n^\kappa = \phi \sum_{\text{i=gas, liquid}} S_i \rho_i X_i^\kappa \tag{3.7}$$

The dimension d can be 1, 2 or 3. X_i^κ stands for the mass fraction of phase i of the component κ. For the mass flux in cell n the same consideration can be made. Making the approximation that the mass flux of component κ, $\vec{F}^\kappa$, over one interface of the cell is homogeneously distributed, the volume integral over the divergence of the flux can be written as

$$\int_{V_n} \vec{\nabla} \cdot \vec{F}^\kappa = \int_{\Omega_n} \vec{F}^\kappa d\vec{A} = \sum_m A_{nm} F_{nm}^\kappa \tag{3.8}$$

where Ω_n stands for the surface of the volume V_n and A_{nm} are the interfaces of the cell with the neighbouring cells m. The time is discretized implicitly, which leads to the integrated continuity equation for the mass of one component κ over one cell n

$$M_n^\kappa(t+\Delta t) - M_n^\kappa(t) - \frac{\Delta t}{V_n}\left(\sum_m A_{nm} F_{nm}^\kappa(t+\Delta t) + V_n s_n^\kappa(t+\Delta t)\right) \equiv Res_n^\kappa(t+\Delta t) = 0 \tag{3.9}$$

Res_n is the residual of the equation and s_n stands for the source and sink terms in this cell. One advantage of the integral formulation is, that the only grid information needed is the volume of the cells, the distance to the neighbouring cells and the area of the interfaces. In principle this allows any irregular grid. The flux over the cell boundaries is calculated from the pressure difference in the two cells which the interface connects via Darcy's law. The pressure is approximated by its values in the center of the cells, and the flux of one component κ is written as

$$F_{nm}^\kappa = \sum_{\text{i=gas, liquid}} -\frac{K_{(\text{abs m,n})} k_{(\text{rel;i; m,n})} \rho_{(i;\, m,n)} X^\kappa_{(i;\, m,n)}}{\mu_{(i;\, m,n)}} \frac{P_{(i;\, n)} - P_{(i;\, m)}}{x_n - x_m}, \tag{3.10}$$

where x is the location of the cell center. For the parameters $K_{\text{abs}}, k_{\text{rel}}$, ρ, X^κ and μ, appropriate averages of cell properties along the connecting line of cell n and m have to be chosen. The mass balance equations (3.9) for N nodes leads to an equation system of $2 \cdot N$ equations. The equations are coupled and they are nonlinear in saturation S due to the nonlinear material properties such as relative permeability and capillary pressure. The nonlinearities are treated by Newton-Raphson iteration. TOUGH2 provides four different solvers for the linearized equations. In the calculations performed here a bi-conjugate gradient squared method (BCGS) solver was used. The time stepping can be treated by adjusting the time steps using convergence criteria. In the calculations performed here this was done in the following way: If the Newton Raphson steps required to fulfil the convergence criteria were more than eight, the time step was reduced by a factor of 1/4. If less than four steps were required, the time step was doubled. This time stepping is very convenient especially for radial flow, as the grid Peclet number, which compares advective effects with diffusive ones, is changing with space due to the decreasing of the velocity with $1/r$.

To model radial flow configurations in a cartesian grid causes problems due to the grid orientation, as the preferential directions are aligned with the grid orientation. For this reason a nine-point scheme was used for the discretization (code provided by Dr. Karsten Pruess, LBNL Berkeley). In a nine point scheme the flux in one cell (i,j) is not only calculated from the neighbouring cells $(i+1,j; i-1,j; i,j+1; i,j-1)$ but also from the cells in the diagonal $(i+1,j+1; i-1,j+1; i+1,j-1; i-1,j-1)$, where the interfaces of the neighbouring cells are weighted with a factor 2/3 and the cells in the diagonal with a factor 1/6 (compare Fig. (3.1)). The application of a nine point scheme reduces the grid orientation effects (see e.g. *Pruess* [1991a]) as the Laplace operator Δ occuring in Eq. (3.2) is approximated to higher order in the cell distance.

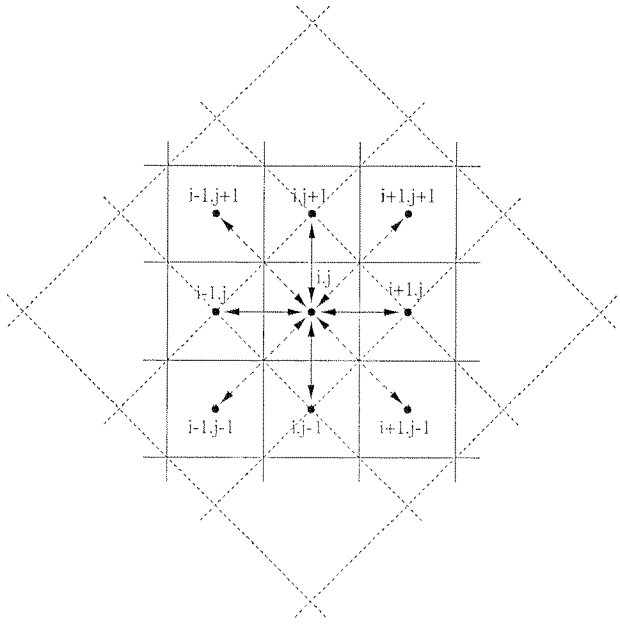

Figure 3.1: Five- and nine-point finite difference approximations, reproduced from *Pruess* [1991a]

Flow parameters

Depending on the specific kinds of fluids, one has to focus on different kinds of problems. For this reason the equations of state that specify the types of fluids are in TOUGH2 provided in a number of modules. Here we use the module EOS3, describing an air-water system. The dissolution of air in the liquid phase is described by Henry's law. Water can be evaporated in the gas phase (and condensed from the gas to the water phase). The properties of air are derived from the ideal gas equations. The temperature was set low, to 10 degrees Celsius (283 K), to avoid the effects of water evaporation. Also the Henry constant was artificially set very high ($10^{30}Pa$) to avoid the effects of air being dissolved in the water. These effects were considered not to be of importance and were excluded in order to avoid unnecessary complexity of the flow processes. It has to be mentioned that the code TOUGH2 also includes gravity effects and as a main part, effects from temperature gradients leading to heat flux. These effects are not taken into account in the Eqns. (3.1) through (3.4) as in the calculations performed here the temperature was set constant and the flow process was considered to take place in the horizontal plane.

A remark is in order considering the averaging of the permeabilities over the connection line between the cell centers. The physically most reasonable way to average them would be to use a harmonic weighting of the product of absolute and relative permeability using the distances to the interfaces as weighting factors. However, for a displacement process, this weighting scheme causes numerical problems, as the harmonic averaging procedure gives more weight to smaller numbers. If the porous medium is almost saturated with water behind the front zone, the product of relative and absolute permeability is almost zero, which leads to a very small harmonic

mean. This leads to oscillations and slow convergence of the Newton Raphson iterations. To achieve stability without reducing the time step to infeasibly small values, it is recommended to use a full upstream weighting of the product of relative and absolute permeability. In the weighting of the total permeabilities which has been performed in our calculations an upstream weighting scheme was used for this reason.

Sinks and sources in TOUGH2 are treated as wells with defined flow rates of the specified fluid phase. The constant inflow was modeled as an air injection well. The formulation of the problem implies boundaries at infinity. These were approximated in the simulations with Dirichlet boundary conditions for all unknowns at the boundaries of the modeled domain. In TOUGH2 such boundary conditions are realized by assigning a volume which is much larger than the volume of the inner grid cells to the corresponding cells.

Air is a compressible gas. It is treated in TOUGH2 as an ideal gas. The compressibility affects the flow Eqns. (3.1) through (3.4) via the density. In general density effects have to be expected in most applications and will have an impact on the flow behaviour. However, in order to focus on the flow behaviour due to the nonlinear soil properties, it was made sure in the calculations that density effects do not become important. The relative gradient of the density can be estimated using the ideal gas approximation for air,

$$\rho_{\text{air}} = \frac{P_{\text{air}} m}{RT} \qquad \rightarrow \qquad \frac{\vec{\nabla}\rho}{\rho} = \frac{\vec{\nabla}P}{P}, \tag{3.11}$$

where R is the gas constant and m is the molecular weight. By estimating the pressure gradient with Darcy's law and choosing appropriate parameters for permeability, inflow rate and initial gas pressure, it was made sure that the relative density gradient was held at a value of a few percent. In one case where the inflow rate was enhanced and this requirement was no longer fulfilled, the density for gas was set artificially constant to exclude compressibility effects. This case will be commented on in the text.

3.1.3 Heterogeneous fields

Heterogneities of the parameters

To consider heterogeneities in Eqns. (3.1) through (3.4), in principle all parameters can vary in space. If one considers the porous medium as being composed of different soil types, each having a different pore structure and a different permeability, the soil types will also have different characterizations via the relative permeability functions and the capillary pressure. All the parameters that enter the functions for relative permeability and capillary pressure can be random fields. Considering the fields in this way, the flow process which is already very complicated in homogeneous porous media, is influenced by so many effects, that it becomes by far too complex to take into account all the different mechanisms. For this reason, only

the most important features, permeability and magnitude of capillary pressure, are considered to be heterogeneous. Moreover, they are the quantities that have been investigated the most thoroughly in laboratory and field experiments. In contrast to that very little is known about the role of heterogeneities in relative permeabilities, although relationships between the parametrizations of relative permeability and capillary pressure, based on their dependence on the soil properties, exist (e.g. *Brooks and Corey* [1966]). Very often a Leverett coupling of capillary pressure and permeability is assumed (see e.g. *Marle* [1981]). It has its counterpart on the pore scale. Permeability is proportional to the square of the pore radius whereas the capillary pressure for one pore is proportional to the reciprocal value of the radius. Assuming the absolute permeability can be modelled as

$$K_{\text{abs}}(\vec{x}) = \overline{K}_{\text{abs}} \cdot \mathcal{Z}(\vec{x}) \tag{3.12}$$

where $\mathcal{Z}(\vec{x})$ is a random field with mean 1, the capillary pressure is modelled as

$$P_c(\vec{x}) = \overline{P}_c \cdot \sqrt{(\mathcal{Z}(\vec{x}))^{-1}}. \tag{3.13}$$

This kind of scaling was realized in the numerical simulations using the SEED option in TOUGH2 which provides the spatial variance of absolute permeability and capillary pressure in the way described by Eqns. (3.12) and (3.13) with a random field $\mathcal{Z}(\vec{x})$ which can be read externally.

Random field generator

The random fields were generated with the code FGEN (*Robin et al.* [1993]). It uses a fast Fourier method to generate correlated stationary random fields with given mean, variance, correlation length and distribution type. The principal methods will be explained here, a detailed discussion can be found in *Robin et al.* [1993].

The method takes advantage of the fact, that the Fourier transform of the autocovariance of a stationary random field $\mathcal{Z}$,

$$C(\vec{x}) = \int d^d x' \mathcal{Z}(\vec{x}')\mathcal{Z}(\vec{x}' + \vec{x}) \tag{3.14}$$

can be written as

$$\hat{C}(\vec{k}) = \hat{\mathcal{Z}}(\vec{k}) \cdot \hat{\mathcal{Z}}(\vec{k}). \tag{3.15}$$

The Fourier transformation $\hat{f}(\vec{k})$ of a function $f(\vec{x})$ is defined as

$$\hat{f}(\vec{k}) = \int d^d x f(\vec{x}) \exp\left(-2\pi i \vec{x}\vec{k}\right) \tag{3.16}$$

and the inverse transformation as

$$f(\vec{x}) = \int d^d k \hat{f}(\vec{k}) \exp\left(2\pi i \vec{x}\vec{k}\right). \tag{3.17}$$

The identity (3.15) is a consequence from the stationarity of the random field. If we have a autocovariance function $C(\vec{x})$, we can calculate its Fourier transform $\hat{C}(\vec{k})$. An *uncorrelated* random field in Fourier domain, $\hat{\mathcal{Z}}(\vec{k})$, which has a mean of 0 at each value of $\vec{k}$ and a variance equal to the corresponding Fourier transform of the given covariance $\hat{C}(\vec{k})$ at the value $\vec{k}$, corresponds to an inverse transformation to the coordinate space, $\mathcal{Z}(\vec{x})$, which has a mean of 0, a variance of 1 and the autocovariance function $C(\vec{x})$. This is shown in *Schwarz* [1999]. By assigning *uncorrelated* random numbers with the corresponding properties (mean 0 and variance $\hat{C}(\vec{k})$) to each Fourier mode k, a correlated random field can be constructed in coordinate space which has the autocovariance function $C(\vec{x})$. This construction is performed on a finite grid in Fourier space which is periodically repeated, yielding a random field on a grid in coordinate space. The random field is then extended to the full space domain by interpolating between the grid values. Variance and mean are adjusted by normalizing the field to the corresponding values. Possible errors in this method are due to the discretization on a grid and are discussed in *Robin et al.* [1993]. The method performs well if the whole field which is calculated is large compared to the correlation structure and if the size of the grid cells is small compared to the correlation structure.

In the calculations performed here, random fields were constructed using a Gaussian autocovariance function. The fields were transformed to log-normally distributed fields to represent realistic distributions of absolute permeabilities.

3.1.4 Setup of the numerical model

In order to save CPU time, only a quarter of the flow field was modeled, which was supposed to be reasonable due to symmetry of the system under consideration. As the correlation structure is not properly represented at the boundaries of the quarter field, the gas saturation field was only analyzed in a restricted domain within lines through the origin which are 10 degrees apart from the boundaries. The numerical simulations were performed on a Cartesian 96 x 96 cell grid. The horizontal cell dimensions were 0.1 m x 0.1 m, the height of the model was assumed as 0.01 m. The flow parameters are given in Table 3.1.

Porosity Φ $[-]$	0.2
Absolute permeability K_{abs} $[m^2]$ (isotropic)	$4 \cdot 10^{-11}$
Brooks Corey coefficient λ for (3.20) and (3.20) $[-]$	1.4, 2.0
Capillary scaling pressure $P_{c\,0}$ for (3.26) $[Pa]$	different values
Initial gas pressure P_{air} $[Pa]$	$1.02 \cdot 10^5$
Initial gas saturation S_g $[-]$	0.01
Mass inflow rate Q_M $[kg/s]$	$4 \cdot 10^{-6}$
Temperature T $[K]$	283

Table 3.1 : Parameters for the numerical simulations

The air injection well was placed in the bottom left corner. The left and bottom boundaries imposed are no-flow boundary conditions, whereas the right and top boundaries obey Dirichlet boundary conditions for the equation variables, realized with 4 rows of very large cells with increasing size (0.5 m, 1 m, 5 m, 10 m). A sketch of the setup of the numerical model is given in Fig. (3.2).

The initial saturation could not be set to 0 due to numerical problems. If the cell has a saturation of 0 for one phase, the system is in a single phase state. For this fluid to get into the cell, it has to evolve via condensation or vaporization first. This causes problems in the numerical simulations. For this reason the initial gas saturation was set to $S_g = 0.01$. In the heterogeneous media, there are pressure gradients if the initial saturation is uniformly distributed, and during the first time steps the system gets to capillary equilibrium, which means the initial saturation is distributed in a way that the pressure gradients due to the heterogeneous capillary pressure are equalized.

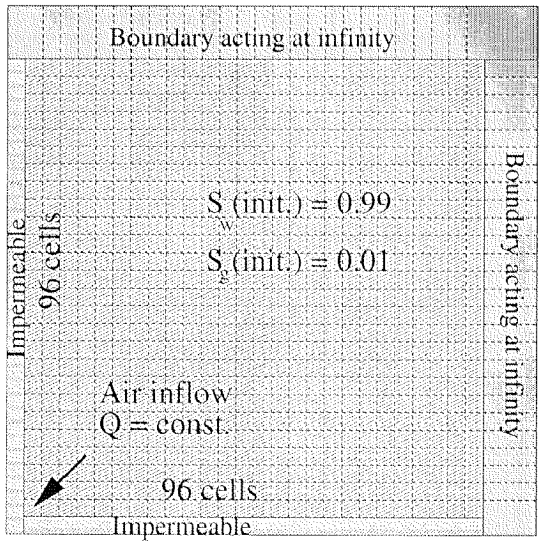

Figure 3.2: Setup of the numerical model

3.2 Sensitivity of the flow behaviour to the parametrizations

As there is some arbitrariness in the flow equations (3.1) through (3.4) it is necessary to perform a sensitivity analysis with respect to the different features of the parameters and decide how to chose them for the problem of interest. There is a wide range of parametrizations discussed in the literature. It is more important to get an understanding of the typical features of the functions and of their impact on the flow process than to take a decision for a given formulation of parametrization.

3.2.1 Relative permeability

The essentail concept of relative permeability is based on the idea that the two immiscible phases flow in different sections of the porous medium. The higher the saturation of one phase is in a part of the porous medium, the bigger is the part of the medium that is "available" for flow of that phase and the higher is its relative permeability. The relative permeability of one phase is therefore a monotonically increasing function of the phase saturation. The assumption, that both phases do not interfere with each other, leads to the equation

$$k_{r\,\mathrm{gas}} + k_{r\,\mathrm{water}} = 1. \tag{3.18}$$

The monotonically increasing behaviour has been confirmed in a large number of laboratory experiments (e.g. *Stauffer and Dracos* [1986], *Fischer* [1995]), however, behaviour different from that described by (3.18) has also been observed in many cases.

The relative permeability functions capture a further phenomenon, the residual saturation. In drainage and wetting experiments there is always a residual amount of water or air, which cannot be removed from the system. These are clusters of water or air that are trapped and cannot be moved or water that is very strongly bound to the pore surfaces due to dielectric forces. The water saturation or gas saturation can therefore not drop below these residual saturations and the relative permeability below the residual saturation is zero. Although the values of the residual saturations can be quite high (see e.g *Fischer* [1995]), we will neglect these effects for simplicity, as it does not change the principal mechanisms but just scales down the range of values for the saturation. By rescaling of the saturations the residual saturations can be taken into account at any time.

Two parametrizations are very common, the parametrization of Brooks and Corey (*Brooks and Corey* [1966]) and the parametrization of van Genuchten (*van Genuchten* [1980]). For the relative permeabilities there are no essential differences and the formulations can more or less be transferred to each other (*Helmig* [1997]). Neglecting residual saturations, we get for the Brooks-Corey parametrization

$$k_{r\,\mathrm{water}}(S_w) = (S_w)^{(2+3\lambda_1)/\lambda_1} \tag{3.19}$$

$$k_{r\,\mathrm{gas}}(S_g) = S_g^2 \cdot (1 - (1 - S_g)^{(1+2/\lambda_1)}) \tag{3.20}$$

and for the van Genuchten parametrization

$$k_{r\,\mathrm{water}}(S_w) = \sqrt{S_w} \cdot (1 - (1 - S_w^{(1/\lambda_2)})^{\lambda_2})^2 \tag{3.21}$$

$$k_{r\,\mathrm{gas}}(S_g) = \sqrt{S_g} \cdot (1 - (1 - S_g)^{(1/\lambda_2)})^{2\lambda_2}. \tag{3.22}$$

λ_1 and λ_2 are related to the soil properties. There are also applications where water phase relative permeabilities as in Eqns. (3.20) or (3.22) are used and the gas phase relative permeability is defined as $k_{r\,\mathrm{gas}} = 1 - k_{r\,\mathrm{water}}$ according to Eqn. (3.18). An example for relative permeability functions (Brooks-Corey with $\lambda_1 = 2$) is given in Fig. (3.3).

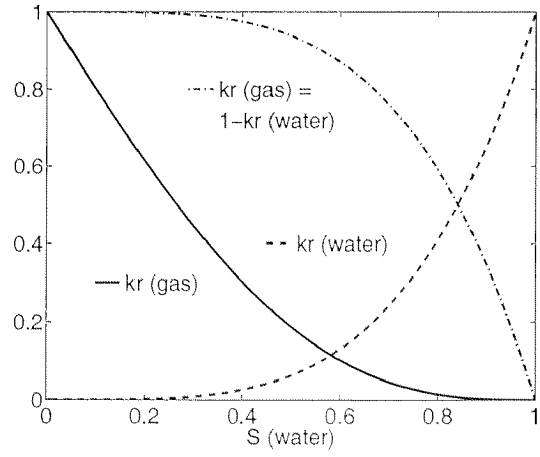

Figure 3.3: Example for relative permeabilities, using Brooks Corey formulation

The relative permeabilities can lead to selfsharpening effects of a front of one phase. This becomes clear if we consider the advective term in the mass conservation equation (3.1),

$$\vec{\nabla}\left(K_{\text{abs}}\frac{k_r}{\mu}\vec{\nabla}P\right) = K_{\text{abs}}\frac{1}{\mu}\frac{dk_r}{dS}\vec{\nabla}S\vec{\nabla}P + K_{\text{abs}}\frac{k_r}{\mu}\Delta P. \tag{3.23}$$

The first term on the right-hand side of Eq. (3.23) is equivalent to a term that describes advective transport with a velocity $K_{\text{abs}}(dk_r/dS)(1/\mu)\nabla P$. If the derivative of the relative permeability with respect to saturation is monotonically increasing, smaller saturations will have a smaller "velocity" and the front of a displacement process is selfsharpening. The opposite is true if the derivative is decreasing. In this case, the front will smear out and the flow process is more of a diffusive kind.

$d^2k_{r\,\text{gas}}/dS^2_{\text{gas}}$ depending on the parameter λ for different values of S_{gas}, values > 0: convex, values < 0: concave

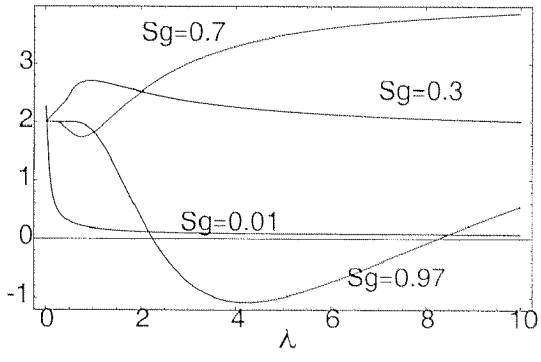

Figure 3.4: Brooks Corey

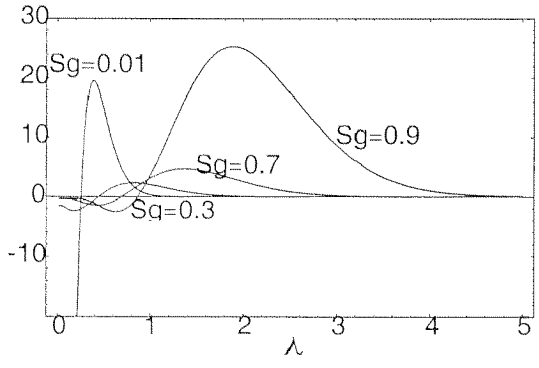

Figure 3.5: van Genuchten

Except for the gas relative permeability at very large gas saturation the Brooks-Corey parametrization is always convex (cf. Fig. (3.4)). For the van Genuchten parametrization there are some regions where the relative permeability curve be-

comes concave (cf. Fig. (3.5)). In the flow scenario considered here we are interested in the situation at small gas saturation and large water saturation. In this case for both types of parametrization the functions are convex, except for a van Genuchten parametrization with very small λ_2. The relation given by Eq. (3.18) would in that case lead to a concave relative permeability for gas and therefore to a flow type different from that with Eqns. (3.20) or (3.22) as relative permeability function.

Fig. (3.6) shows the result of numerical simulations of radial displacement of water by air with three different parametrizations for $k_{r\,\mathrm{gas}}$, (3.20) with $\lambda_1 = 2$ ($\rightarrow$ convex), (3.22) with $\lambda_2 = 0.2$ ($\rightarrow$ concave) and (k_r (gas) = 1-(3.20)) with $\lambda_1 = 2$ ($\rightarrow$ concave). This figure illustrates that the behaviour of the derivative of the relative permeability with respect to saturation at the initial saturation is a decisive quantity for displacement flow processes.

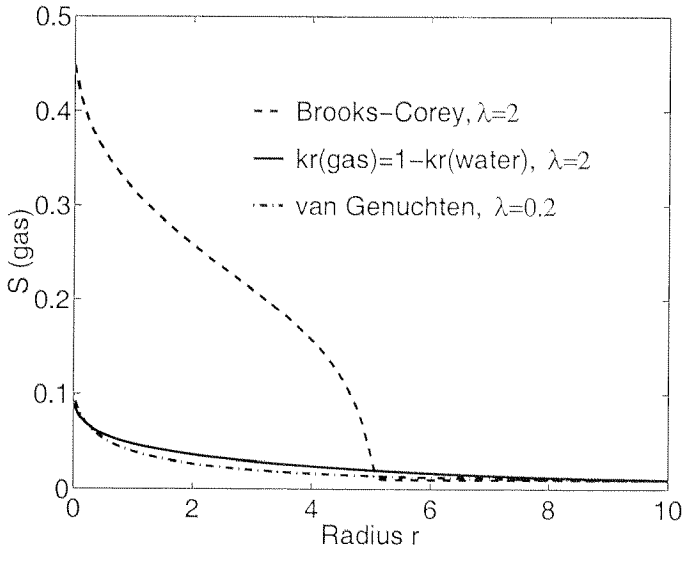

Figure 3.6: Radial section of the gas saturation field, using convex and concave relative permeability functions

It is difficult to determine which behaviour is realistic for water displacement by air. It has been observed in experiments of displacement of a wetting fluid by a nonwetting one in porous media, that the fluid interface remains sharp during the flow process and the displacing fluid develops a front that moves through the medium (e.g. *Chouke et al.* [1959]).

The same effect has been observed in laboratory experiments that have been performed during the preparatory work for the experiments treated in Chapter 2. Air was injected into a water saturated, quasi homogeneously packed flat sand box. The flow configuration was a quarter five spot pattern, injection of air at one corner with an outlet at the opposite corner. The flow process has been analyzed with the same setup as described in Fig. (2.9), except for the fact that the illumination was from above instead of from below. The experiments were not satisfactory, as the flow was not homogeneous due to the sensitivity of the flow process to heterogeneities on the smallest scale. However, the results could be analyzed with respect to the

selfsharpening behaviour. Fig. (3.7) shows the difference pictures of two consecutive pictures. The darker regions are zones of increase of air. These zones are sharply bounded at the front zone. We can therefore conclude, that the air is moving as a compact body and the displacement is modeled best with a convex relative permeability function. In the following, the Brooks-Corey formulation - (3.20) and (3.22) - is used.

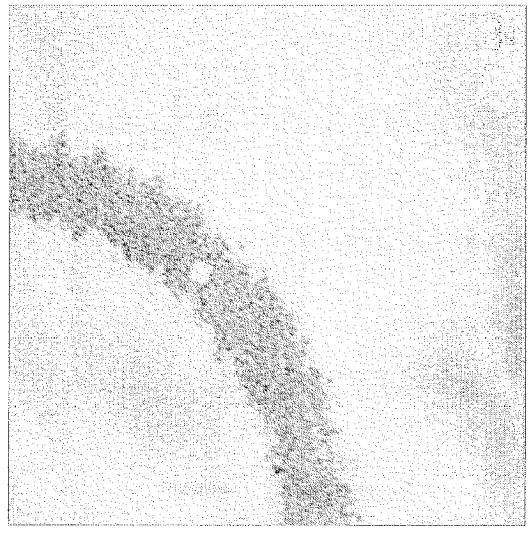

Figure 3.7: Difference picture of two consecutive pictures

3.2.2 Capillary pressure

The capillary pressure is the difference between the pressure in the nonwetting phase and the pressure in the wetting phase. It describes the large scale impact of the capillary pressure phenomena on the small scale. It reflects the fact that in a water wetting porous medium more energy is needed to have a pore filled with air than to have it filled with water due to the wettability properties of the medium. A larger force, and therefore a higher pressure gradient, is needed for pressing air into a pore than for water. In equilibrium, the pressure in the air phase has to be larger than in the water phase, in order to counteract the capillary forces. The capillary pressure in the continuum equation describes the impact of the capillary effect of a large number of pores. Its quantity is therefore dependent on the saturation. It needs less pressure gradient to fill the large pores than the small ones, as the surface to volume ratio is smaller in the large pores. Therefore the large pores are filled first and the capillary pressure is small at small gas saturation. Then the smaller pores are filled and the capillary pressure gets larger. Therefore the capillary pressure is a function that increases monotonically with gas saturation. If the pore distribution is peaked, the gradient is small, if it is broad the gradient is large.

If the soil is saturated at the beginning there is a certain pressure gradient necessary to start the inflow of air into the medium, as the capillary force due to the largest pores has to be surmounted. The importance of this capillary entry pressure is

discussed in the literature. In measurements it is difficult to decide whether there is a steep slope at the end point or whether there is a discontinous step to 0. However, many experiments indicate the existence of a capillary entry pressure (*Stauffer* [1999] or *Ustohal et al.* [1998]).

There is a large number of possible parametrizations for the capillary pressure. The most common ones are once again the parametrizations of Brooks and Corey

$$P_c(S) = P_{c\,\mathrm{entr}} \cdot \left(\frac{1}{S_w}\right)^{1/\lambda_1} \tag{3.24}$$

and van Genuchten

$$P_c(S) = P_{c\,0}\left((S_w)^{(-1/\lambda_2)} - 1\right)^{(1-\lambda_2)} \tag{3.25}$$

Eqns. (3.24) and (3.25) differ with regard to the existence of an entry pressure. In formulation (3.24) there is an entry pressure $P_{c\,\mathrm{entr}}$, whereas in (3.25) the capillary pressure decreases continuously to 0 if the water saturation goes to 1. This difference has an impact on the flow behaviour. Fig. (3.8) illustrates both parametrizations. To be consistent with the relative permeability parametrization, the capillary pressure is modeled with a Brooks-Corey parametrization, however in a slightly different form than Eq. (3.24) . The formulation that has been used here for the capillary pressure is one of the capillary pressure functions implemented in the TOUGH2 code and it is equivalent to the Brooks-Corey formulation. The capillary entry pressure in this formulation is combined additively with the capillary pressure function,

$$P_c(S) = P_{c\,\mathrm{entr.}} + P_{c\,0} \cdot \left(\frac{1}{S_w} - 1\right)^{1/\lambda_1}. \tag{3.26}$$

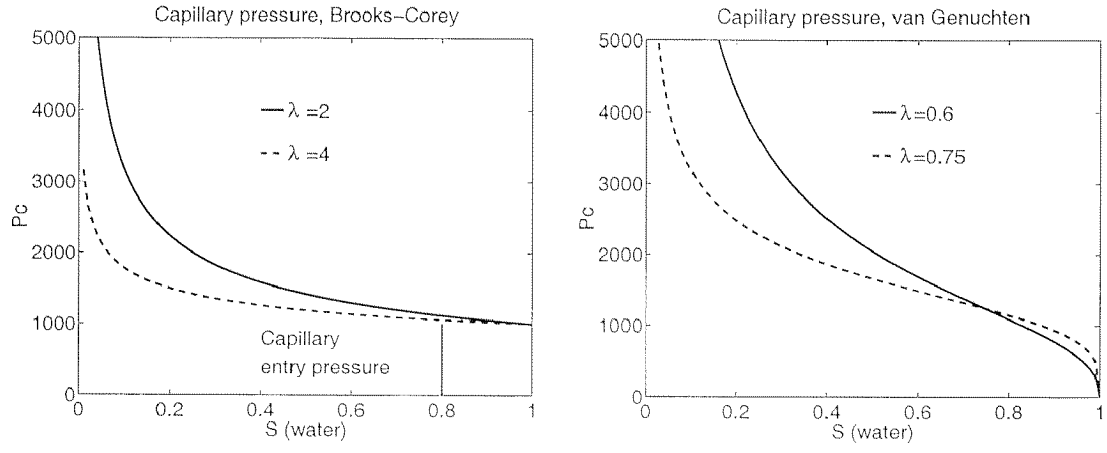

Figure 3.8: Typical capillary pressure functions

Features of the capillary pressure

In Eqn. (3.26) there are two parameters that determine the properties of the capillary pressure function. The entry pressure $P_{c\,\mathrm{entr.}}$ is not taken into account as will

be explained later. On the one hand there is the factor $P_{c\,0}$ which affects the magnitude of the capillary pressure. On the other hand there is the parameter λ_1 which affects the slope of the capillary pressure curve. The capillary pressure curves for three examples of $P_{c\,0}$ and three examples of λ_1 together with radial sections of the corresponding gas saturation fields are shown in Figs. (3.9) through (3.12).

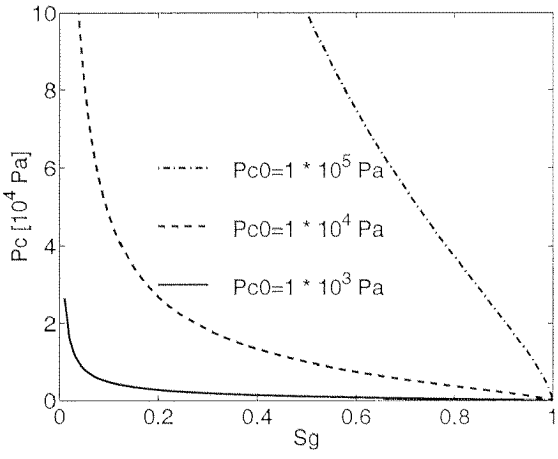

Figure 3.9: Capillary pressure for different $P_{c\,0}$.

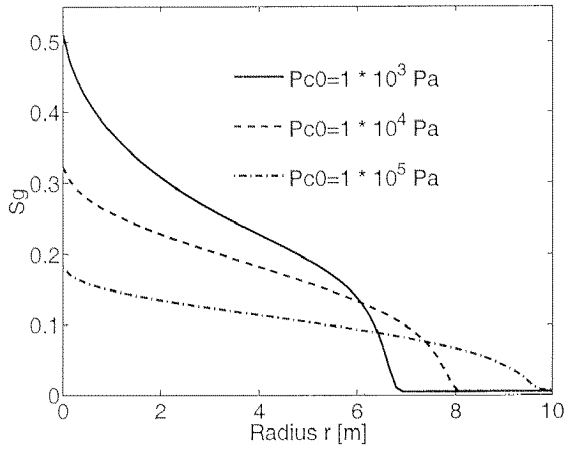

Figure 3.10: Radial section of S_g for the corresponding values of $P_{c\,0}$

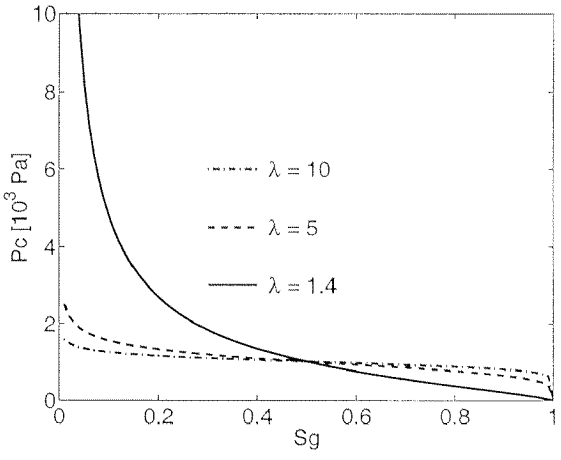

Figure 3.11: Capillary pressure for different λ

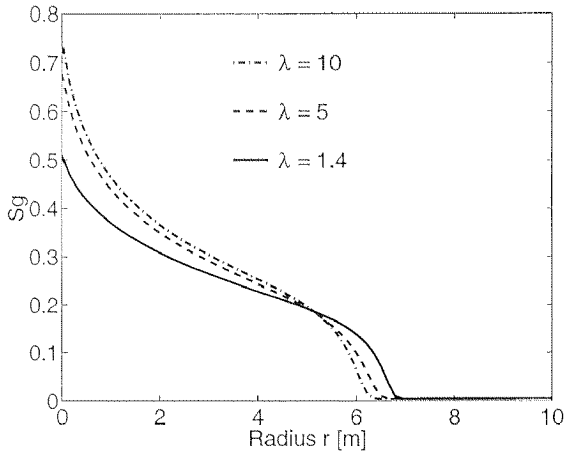

Figure 3.12: Radial section of S_g for the corresponding values of λ

A higher capillary pressure corresponds to a smaller gas saturation. $P_{c\,0}$ has an impact on the gas saturation profile at all values of gas saturation and therefore influences the behaviour at the injection point as well as the behaviour at the front. A higher value of $P_{c\,0}$ reduces the gas saturation in both parts of the profile. The slope of the capillary pressure curve has an impact mainly at high values of gas saturation. The impact at small gas saturation is less important, however it has different impact in both parts. A flatter slope leads to smaller values of the capillary

pressure and higher values of gas saturation at the injection, however it leads to higher values for capillary pressure and smaller values of gas saturation at the front. The impact at the front is smaller than at the injection point. The range of the impact of λ_1 is limited, as a value of $\lambda_1 = 5$ already leads to a very flat capillary pressure curve, a further increase of λ_1 has not much more impact.

Heterogeneous capillary pressure

If the capillary pressure field is heterogeneous and modeled as described in Eqs. (3.12) and (3.13), the Leverett scaling leads to an enhancement of the effects of the heterogeneities. The cells with lower permeability have a higher capillary pressure function, both effects make them less accessible for the inflowing air. The opposite would be true if a dry porous medium would be invaded with water. This is illustrated in Fig. (3.13), where an isoline of the gas saturation is shown for three different cases. Two media with heterogeneous permeability field and constant capillary pressure, one with high variance of log conductivity σ_f^2 and the other one with low σ_f^2, are compared to a medium with low variance σ_f^2 where both permeability and capillary pressure are heterogeneous. The deviations of the front grow with σ_f^2. They also grow if the capillary pressure is heterogeneously distributed. The coupling acts like an enhancement of the variance of log permeability if the behaviour of the front is considered.

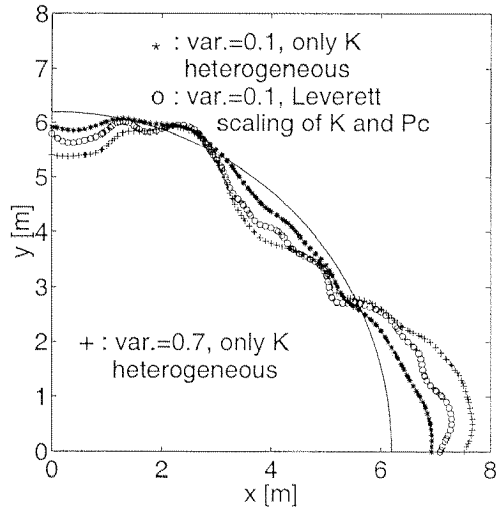

Figure 3.13: Isolines of gas saturation for $S_g = 0.1$

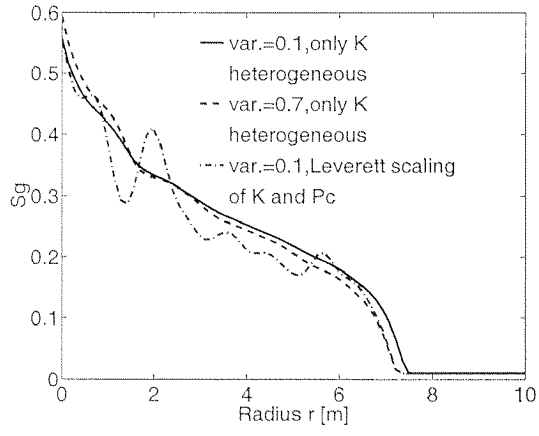

Figure 3.14: Radial sections of the gas saturation field at 45^o

However, there is a qualitative difference in the flow behaviour with capillary pressure and permeability both heterogeneously distributed on the one hand, and the flow behaviour when just the permeability is heterogeneous on the other hand. The equilibrium gas saturation state of the saturation behind the front is very heterogeneous if the capillary pressure is heterogeneous. It is smooth if the capillary pressure is constant. This is illustrated in Fig. (3.14), where a radial section of the gas saturation field is plotted for the three cases. The different values of σ_f^2 have no

impact, whereas the fluctuations of the gas saturation behind the front get large if the capillary pressure is heterogeneous.

An important feature of the capillary pressure for flow in heterogeneous porous media is the existence of the entry pressure. The Leverett scaling yields a field of heterogeneous entry pressures. If there is a heterogeneous entry pressure field in an initially saturated porous medium, there are cells that will not be invaded as the pressure gradients in the neighbouring cells will not get large enough to exceed the entry pressure. This leads to channeling effects and is the large scale analogon to the channeling patterns on the pore scale system as described in Chapter 2. If there is no entry pressure the effect is smeared out, as each saturated location has capillary pressure zero and just the slope of the increase is heterogeneously distributed. The impact of entry pressure effects is illustrated in Fig. (3.15) and (3.16).

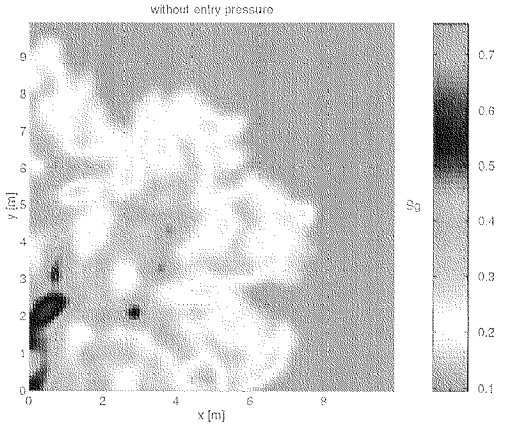

Figure 3.15: S_g field without entry pressure

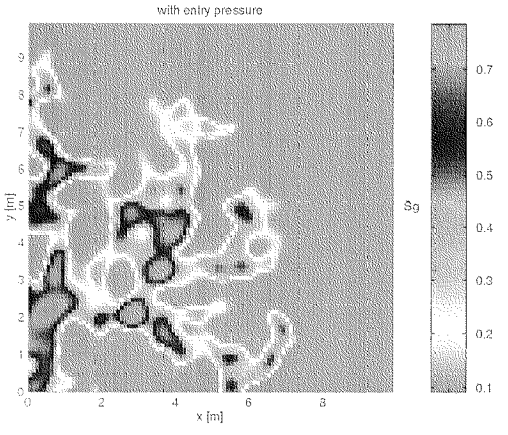

Figure 3.16: S_g field with entry pressure

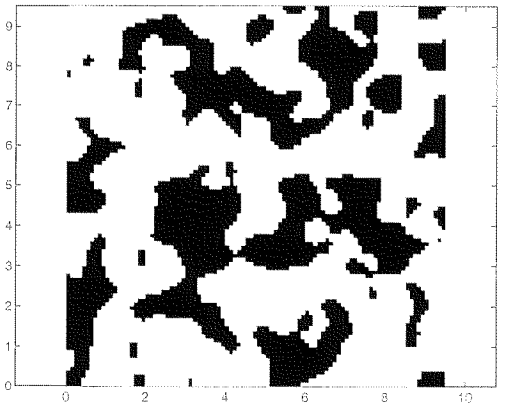

Figure 3.17: Binary entry pressure field

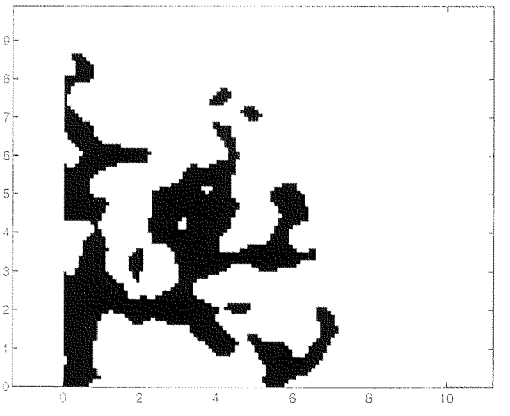

Figure 3.18: Binary gas saturation field

The gas saturation fields of two numerical simulations are shown, one with entry pressure effects, the other one without. Figs. (3.17) and (3.18) show binary pictures of the entry pressure field for the simulation including entry pressure with a threshold of $P_c = 1500Pa$ and of the saturation field with a threshold of $S_{\text{gas}} = 0.25$. It can be observed that the gas saturation field almost duplicates the entry pressure field which supports to the interpretation as a channeling flow process which is modeled

best with invasion percolation.

Channeling is a realistic scenario which has been observed in field and laboratory experiments many times. However, as discussed in Chapter 2, it is not reasonable to try to describe a flow scenario with strong channeling effects by an analogous homogeneous continuum. The differences between "reality" (single realization) and "model" (ensemble average) are large and remain large over time. Ensemble averaged quantities are not very meaningful to describe the actual realization in these cases and can only be used for risk analysis questions. In the following we limit ourselves therefore to scenarios without channeling effects. The entry pressure $P_{\text{c entr.}}$ in Eq. (3.26) was therefore set to 0 in all the following calculations.

3.3 Ensemble averages - effective behaviour

Following the line of the stochastic approach, flow parameters would be assigned to each realization, afterwards they are averaged over the ensemble. These averaged parameters would be the effective parameters of the system. A procedure which is less demanding and under certain assumptions yields the same result would be to derive effective parameters from the ensemble averaged saturation fields. An ensemble of heterogeneous fields can be produced, the gas saturation can be calculated numerically and averaged over the ensemble.

Such a procedure is possible in principle, but not entirely justified for a number of reasons. On the one hand we do not have parameters of the medium, but rather parameter functions for the capillary pressure and relative permeability. It is not clear how these functions can be obtained from the gas saturation. This point will be analysed in more detail in the next chapter. A more important problem is, that the condition for the ensemble averaging approach to be reasonable is, that the flow behaviour in the single heterogeneous realization does not deviate very much from the flow behaviour in the corresponding homogeneous medium. This can only be valid after a certain time, when the gas has "sampled" already a lot of the heterogeneities, which means the gas front must have passed many correlation lengths. The fields therefore have to be very large. The number of realizations that are necessary to be able to make a quantitative analysis can also be very large. To reach this point in numerical simulations is already very difficult in linear flow processes like in solute transport (private communication from H. Kinzelbach and M. Dentz). The nonlinear flow equations for two-phase flow are even more demanding in terms of computer time. With the setup described in Section 3.1.4, it would not be feasible to derive effective parameters quantitatively.

The task here was to get a qualitative understanding of the impact of the heterogeneities on the flow process with the help of the numerical simulations. This can be done by looking at the ensemble averaged gas saturation fields and see in which way they deviate from the gas saturation in a homogeneous field. It can then be considered, which flow parameters determine the corresponding features of the saturation profile. By changing these parameters a reproduction of the ensemble

averaged fields can be tried. We can then establish a qualitative understanding of how the heterogenities influence the flow behaviour.

The homogeneous case is compared to an ensemble of realizations of porous media which have a heterogeneous permeability field and a heterogeneous capillary pressure field. The fields are coupled by Leverett scaling. A capillary pressure function (3.26) was assumed with $P_{c,0} = 1000Pa$ and $\lambda_1 = 1.4$. The geometric mean of the permeability field is equal to the homogeneous value. The variance of log permeabiliy was chosen as $\sigma_f^2 = 0.67$. An ensemble of 25 realizations was generated. A plot of the radial sections of the averaged and the homogeneous gas saturation field is shown in Fig. (3.19).

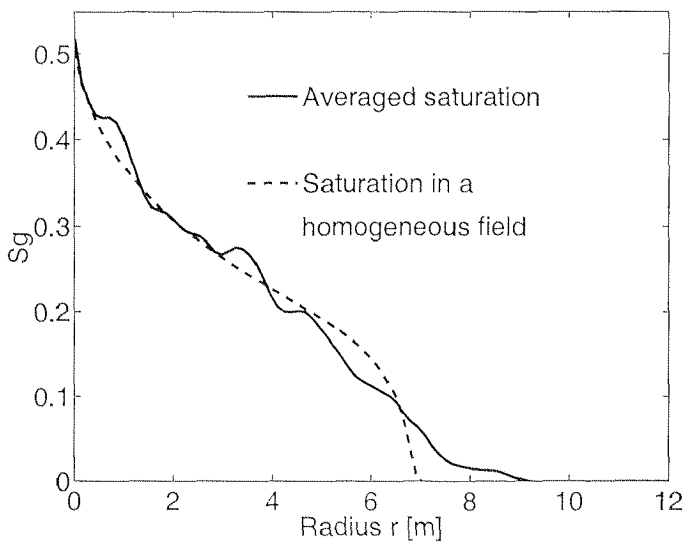

Figure 3.19: Homogeneous and averaged gas saturation profile

The averaged saturation field shows some small fluctuations. However, it is smooth enough to describe the overall influence of the heterogeneities. The saturation profile at the injection point is not different in the homogeneous and the averaged fields. However, at the front, the homogeneous profile has a steep transition zone, whereas the transition zone of the averaged field is flat and extends over a broader range of radii.

Intuitively we expect, that fluctuations in the permeability which cause fluctuations in the flow field lead to a mixing effect. This would correspond to an enhancement of the capillary pressure. It would therefore be reasonable to try whether the capillary pressure function of the homogeneous medium can be changed to obtain the flatter transition zone. At the front a higher capillary pressure would be needed to obtain smaller gas saturation. However, a higher capillary pressure affects the gas saturation also at the injection point, which is not observed in the comparison between homogeneous and averaged fields. To avoid the effect at the injection point, the parameter λ_1 in Eq. (3.26) can be changed in a way, that the capillary pressure curve gets flatter. This has been tried for the example in Fig. (3.20). However, as the effect of a change of λ_1 is limited, this could only be done up to a certain

point, where a fit shows the expected effect, but the effect is still too small. The possibilities that are provided by varying the capillary pressure are limited.

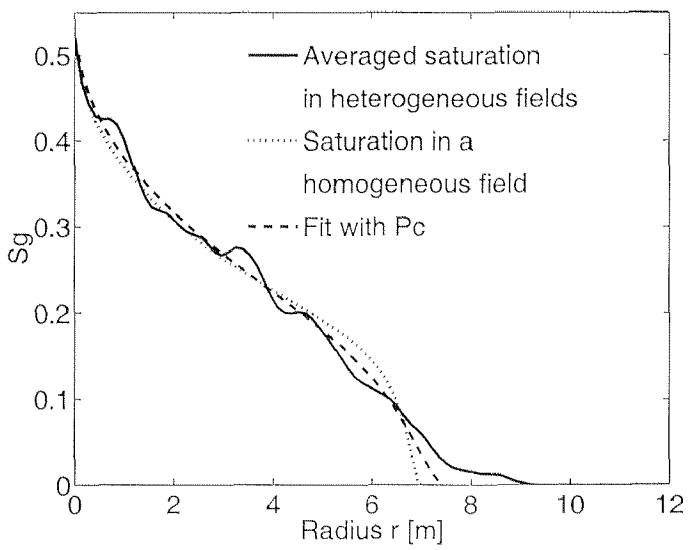

Figure 3.20: Fit of the averaged gas saturation using P_c

Another approach which would be more pragmatic is to change the behaviour of the relative permeabilities. This is something that has no intuitive motivation, as the relative permeability function is not even considered to be heterogeneously distributed. However, it has been discussed in Section 3.2.2 that the relative permeability has an impact on the selfsharpening effects of the front and therefore influences the front of the gas saturation. However, the averaged profile could not be obtained by changing the parameter λ_1 in Eq. (3.20), as the crossover from the flow behaviour of a moving front to the diffusive flow behaviour is too abrupt. By rescaling the gas saturation in the relative permeability function in a way, that the saturation cannot decrease to 0, but only to a finite value, the selfsharpening effect can be reduced. This corresponds to considering the system as a system with residual gas saturation which is smaller than the initial gas saturation. With this scaling the difference of "velocities" for different gas saturations which leads to the selfsharpening effect is reduced. The relative permeability function (3.20) then reads

$$k_{r\,\mathrm{gas}}(S_g) = \left(\frac{S_g + S_g(\mathrm{res})}{1 + S_g(\mathrm{res})}\right)^2 \cdot \left(1 - \left(1 - \left(\frac{S_g + S_g(\mathrm{res})}{1 + S_g(\mathrm{res})}\right)\right)^{(1+2/\lambda_1)}\right). \tag{3.27}$$

In this case a value of $S_g(\mathrm{res}) = 0.02$ was used to reproduce the averaged gas saturation field. The fit is shown in Fig. (3.21).

Varying the relative permeability leads to a closer reproduction of the shape of the saturation curve than the variation of the capillary pressure function. However, there is no immediate motivation why the relative permeability function should be different in an effective homogeneous medium and the possibilities to fit the averaged fields with the parameters provided in the homogeneous two-phase flow equations

(3.1) through (3.4) are limited. This issue will be considered again in the next chapter. Still, we note that the effect of heterogeneity can in principle be absorbed in a variation of the relative permeability function.

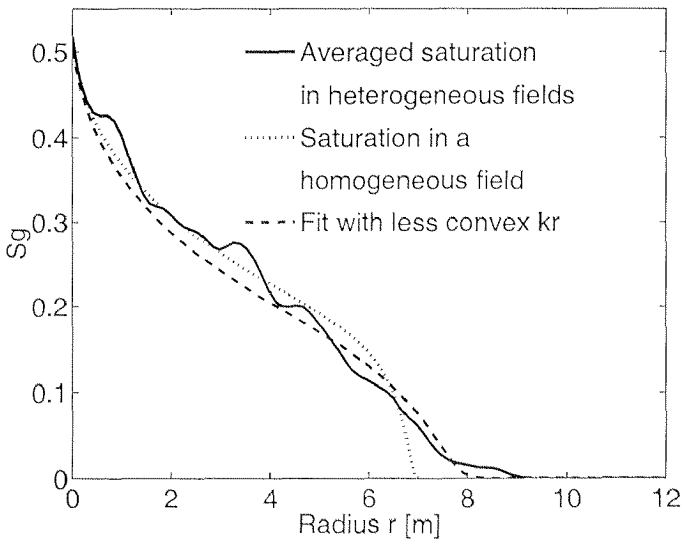

Figure 3.21: Fit of the averaged gas saturation using k_r

3.4 Comparison single realization - ensemble mean

If we want to determine effective properties from ensemble averaged quantities, an important criterion for this to succeed is the difference between single realization and ensemble mean. Even if there are no channeling effects, it is possible that the deviations between single realization and ensemble mean grow with time.

The displacement of a more viscous fluid by an immiscible viscous one is unstable. The phenomenon of viscous fingering has has been investigated extensively and is reviewed e.g. by *Homsy* [1987]. Viscous fingering can be explained easily for flow in a Hele-Shaw cell, which consists of two parallel plates with a narrow gap. If one fluid displaces the other one, the interface between them moves through the cell. If this interface is slightly disturbed, the perturbation can be enhanced and a finger can develop. Fingering surfaces develop due to two competing forces. On the one hand the surface energy is minimal if the surface is small. The surface tension is therefore stabilizing the front. On the other hand, assuming that the pressure in each phase is evenly distributed and the pressure gradient between inflow line and outflow line is constant, the conductivity at the location of the perturbation is higher due to the higher proportion of less viscous fluid. The viscosity forces enhance the finger growth. Whether or not the displacement is unstable depends on the balance of the two forces and is therefore dependent on capillary number and viscosity ratio. Criteria for the crossover between stable and unstable displacement in radial configuration have been developed e.g. by *Paterson* [1981]. In a porous medium the

mechanisms are more complicated, but it has been shown by *Yortsos* [1987] that radial displacement of a more viscous fluid by a less viscous immiscible one can lead to viscous fingering. By performing a linear stability analysis he determined a relation between the growth rate of the perturbation of the saturation and the mode of the perturbation. Both numbers scale with the capillary number, which therefore is decisive for stability. The relation also depends on the mobility ratio. Depending on the capillary number, a regime can be determined where the flow process is unconditionally stable, regardless of the porous medium characteristics. The critical capillary number below which the flow process is in the stable domain, depends on the maximal growth rate for the respective mobility ratio. An analytical expression for the maximal growth rate does not exist, however, in the numerical results of *Yortsos* [1987] the order of magnitude is 10^{-2}. The examples are for rather small mobility ratio, so we estimate that in order to be in the stable domain, the relation

$$N_{\mathrm{Ca}} < 10^{(-1)} \tag{3.28}$$

has to be fulfilled. The capillary number in the definition of *Yortsos* [1987] is based on the assumption, that the capillary pressure has the same order of magnitude as the local, pore scale capillary pressure and is therefore formulated for microscopic quantities like surface tension and wetting angle. As only an estimation of orders of magnitude is required here, it is justified to define a capillary number by

$$N_{\mathrm{Ca}} = \frac{Q_M \mu_g}{\rho_g P_c K_{\mathrm{abs}}}, \tag{3.29}$$

comparing the typical capillary pressure with an estimate for the pressure arising from the inflow of the air phase. P_c is a typical capillary pressure. It might be the entry pressure if there is one. Otherwise it might be the capillary pressure at a representative saturation value. Combining Eqns. (3.28) and (3.29) yields

$$P_c > 10 \frac{Q_M \mu_g}{\rho_g K_{\mathrm{abs}}} \simeq \frac{Q_M}{K_{\mathrm{abs}}} 10^{-4} N \ s. \tag{3.30}$$

Typical dimensions of field and laboratory experiments can take very different values, as the variability of permeability extends over some orders of magnitude. In the simulation performed in this work, care was taken that the capillary number does not exceed the critical value. Inherently unstable phenomena are very difficult to reproduce by numerical simulations, as the system is very sensitive to the form of the initial perturbation. In most cases it is only possible to reproduce generic quantities like fingering velocity. This has been investigated extensely by *Oswald* [1998], who compared numerical simulations of densitiy driven fingers with laboratory experiments. As the focus of this work is the influence of heterogeneities, it is important to compare the heterogeneous models to homogeneous ones, which behave in a stable manner. Systems which are unstable in the homogeneous state are therefore excluded from the numerical simulations.

However, it is not clear how heterogeneities will influence the stability of the growth of the air body. The dynamics of surfaces in a variety of nonlinear systems is an issue

considered extensively in the literature (e.g. *Meakin* [1993]). The two-phase flow equation does not describe the dynamics of a surface but the dynamic behaviour of the variable S. The theories of growing surfaces can therefore hardly be applied to this problem. However, if a process similar to the growth of a surface is active, it is possible that the deviations between single realization and ensemble average are growing with time. In this case it would not be reasonable to describe the heterogeneous system as an effective homogeneous one. It is therefore necessary to develop criteria to characterize the deviation between single realization and ensemble mean. Two criteria have been considered here. Firstly we consider the deviation of the saturation at a certain location from the mean saturation. Secondly the time behaviour of the mean roughness of a single realization isoline is compared to the mean radial coordinate of this isoline. The outermost isoline which circulates the injection point is chosen. This roughness of the isoline is an equivalent to the roughness of the surfaces, the dynamics of which is investigated in *Meakin* [1993] as a criterion for a growing surface. These two criteria have been considered for several test cases, where the variance of log conductivity, the capillary pressure, the correlation length and the inflow rate are varied. The parameters of the testcases are listed in Table 3.2.

No.	Variance σ_f^2 of the random field $\mathcal{Z}(\vec{x})$ $[-]$	Correlation length l_0 of $\mathcal{Z}(\vec{x})$ $[m]$	Inflow rate Q_M $[kg/s]$	Typical capillary pressure $P_c(S_g = 0.75)$ $[N/m^2]$	N_{ca} $[-]$
1	0.13	0.5	$1.23 \cdot 10^{-6}$	500	0.05
2	0.13	0.5	$1.23 \cdot 10^{-6}$	**8000**	0.003
3	**0.61**	0.5	$1.23 \cdot 10^{-6}$	500	0.05
4	**0.61**	0.5	$1.23 \cdot 10^{-6}$	**8000**	0.003
5	**2.6**	0.5	$1.23 \cdot 10^{-6}$	500	0.05
6	0.13	**0.25**	$1.23 \cdot 10^{-6}$	500	0.05
7	0.13	0.5	$\mathbf{1.23 \cdot 10^{-4}}$	500	5.0

Table 3.2: Characteristics of the different test cases

As typical capillary pressure the value at gas saturation $S_g = 0.75$ was chosen. The parameters for the parametrization (3.26) are: $P_{c\,0} = 1000Pa, \lambda = 1.42$ for $P_c(S_g = 0.75) = 500Pa$ and $P_{c\,0} = 13500Pa, \lambda = 2.0$ for $P_c(S_g = 0.75) = 8000Pa$. Gas saturation fields of a single realization and the averaged fields are shown in Appendix B. In case no 7, where the inflow rate is increased by a factor of 100, the compressibility effects become important and the relative density variations reach a value of 1.2. In this case, air was artificially set incompressible in the code in order to avoid the effects of compressibility. In this case the capillary number is higher than the critical value.

Variance of the saturation at a given location

The variance of saturation $\mathcal{D}^\star$ is defined by:

$$\mathcal{D}^\star(\vec{x},t) = \frac{\sqrt{\overline{\left(S_g(\vec{x},t) - \overline{S_g(\vec{x},t)}\right)^2}}}{\overline{S_g(\vec{x},t)}}$$

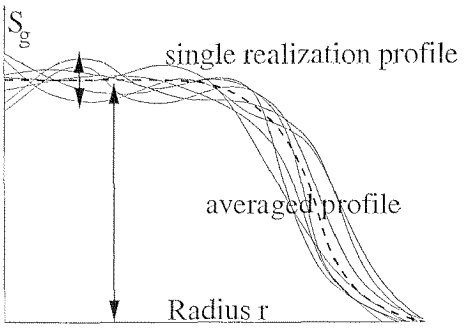

Figure 3.22: Relative variance of the gas saturation

The variance $\mathcal{D}^\star(\vec{x})$ is a measure of the fluctuations of the heterogeneous saturation field and gives an estimate for the error of a measurement of the gas saturation. For an infinitely large ensemble we would obviously assume, that the variance $\mathcal{D}^\star$ vanishes. The numbers can therefore not be interpreted as absolute values but rather in their relation to each other. They represent a sensitivity to the heterogeneities. Effective properties derived from the averaged gas saturation have been discussed in Section 3.3. $\mathcal{D}^\star$ is a measure of how reliable a parametrization with homogeneous parameters is and how good the parameters represent reality. The interpretation is qualitative. The variance $\mathcal{D}^\star$ has its highest value at the front, as can be seen in Fig. (3.23), where the variance along a radial section is plotted for two different times for the examples no 1 and no 2 from Table 3.2.

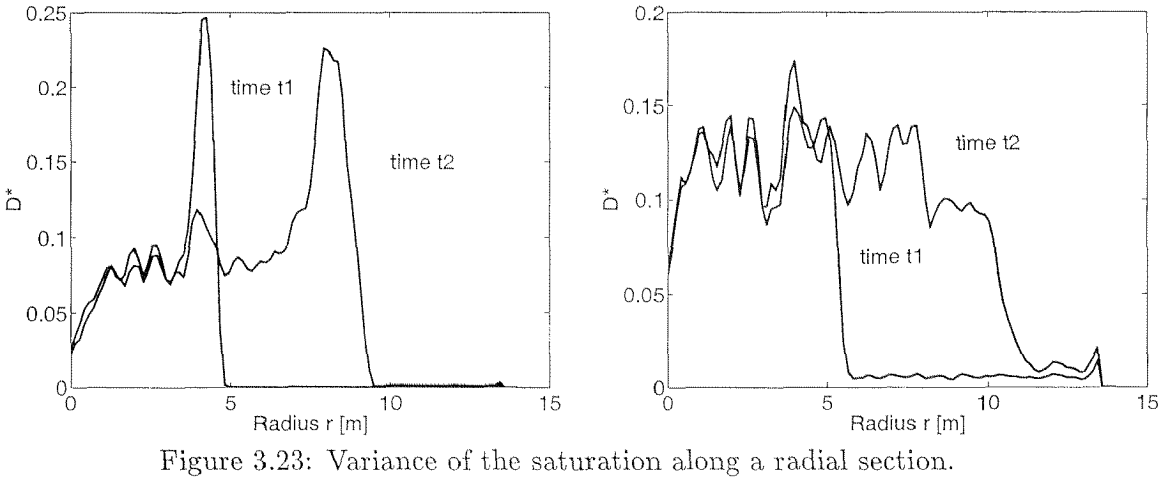

Figure 3.23: Variance of the saturation along a radial section.
Left: case no 1, right: case no 2

Behind the front it has a smaller, but nonzero value. This is intuitively reasonable, as at the front the saturation changes much over small distances. For the case no 2, where the capillary pressure is high, this is not true. The values of the deviations

at the front and behind it are almost equal. The highest value is not exactly at the front but slightly behind it. One reason for the reduction of the contrast is that the gas saturation is smaller at the injection point if the capillary pressure is large. Consequently the transition zone has a smaller saturation contrast.

The behaviour of $\mathcal{D}^\star$ with time is considered at two locations, behind the front and at the front. Both values reach a plateau. In cases no 2 and no 4 from Table 3.2, where the capillary number is small, the deviations for different locations behind the front still fluctuate considerably. However, the plateau values can be estimated by averaging over the values behind the front.

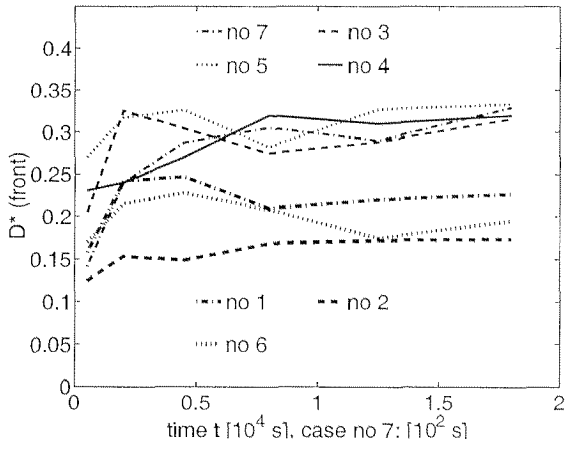

Figure 3.24: $\mathcal{D}^\star$ at the front

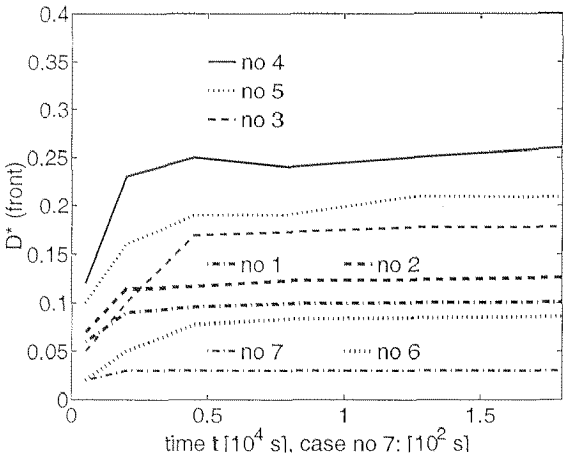

Figure 3.25: $\mathcal{D}^\star$ behind the front

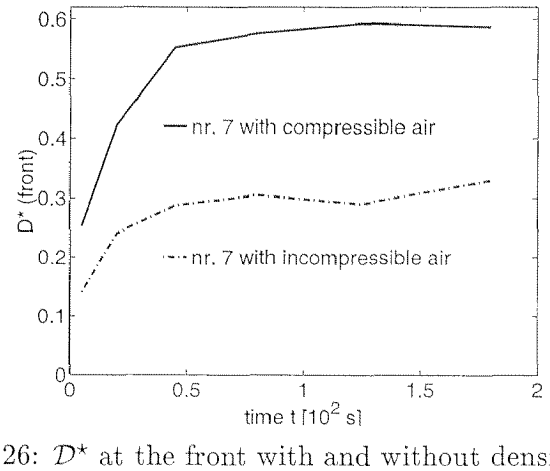

Figure 3.26: $\mathcal{D}^\star$ at the front with and without density effects

The density effects in case no 7 have an impact on the variations at the front, if air is considered as compressible. This is shown in Fig. (3.26), where the deviation at the front is plotted over time for both cases. The compressibility increases the deviations considerably.

Influence of the capillary forces

If the capillary number becomes small, the difference between the plateau values of $\mathcal{D}^\star$ at the front and behind it decreases. This can be seen in Figs. (3.24) and (3.25) by comparison of example no 7 ($N_{Ca} = 5.0$) and example no 2 ($N_{Ca} = 0.003$). In example no 7 the value behind the front is close to 0.025, whereas the value at the front is 0.3. This is an increase by a factor of about 10. In example no 2 the increase is from 0.12 to 0.15 by a factor of 1.25.

As the equilibrium of the gas saturation behind the front depends on the capillary pressure distribution, the value of $\mathcal{D}^\star$ behind the front is sensitive to the influence of the capillary pressure, which is given by the capillary number. Comparing examples no 7 ($N_{Ca} = 5.0$), no 1 ($N_{Ca} = 0.05$) and no 2 ($N_{Ca} = 0.003$), the values for $\mathcal{D}^\star$ are decreasing with increasing capillary number.

The variance $\mathcal{D}^\star$ at the front can hardly be explained by the capillary number. The flow behaviour at the front is not sensitive to the impact of the capillary forces.

Influence of the variance of log permeability and correlation length

The variance of log permeability has an impact on the behaviour behind the front. The values of $\mathcal{D}^\star$ are increasing with increasing variance (compare examples no 1, 3 and 5). However, the very high variance in example no 5 does not lead to an increase as big as the effect of the smaller capillary number from example no 4. A proportionality of $\mathcal{D}^\star$ to the capillary number or variance of the random field could not be found. As it would be expected, the correlation length does not show a big influence on the deviation behind the front.

The values for $\mathcal{D}^\star$ at the front lie in two "bands". Disregarding the case no 7, the examples with small variance of log permeability σ_f^2 lie in the lower band, whereas the examples with high σ_f^2 lie in the upper band. However, the increase of $\mathcal{D}^\star$ between cases no 3 and no 5, where the variance of the permeability field is strongly enhanced, is very small.

In the examples considered here, the plateau at and behind the front never exceeds a value of 0.35 which can be considered as a confirmation of the predictive power of the analysis of ensemble averaged saturation fields under the assumptions made here (small variance σ_f^2, no capillary entry pressure, convex relative permeability function for the gas phase). However, in case no 4 the plateau value of $\mathcal{D}^\star$ behind the front is quite large, indicating a flow behaviour, that is near the channeling domain. This can already be seen from the gas saturation field (cf. Fig. (B.7) in Appendix B).

Roughness of the surface

The roughness of the front is defined by:

$$\mathcal{R}^\star = \overline{\left(\sqrt{\langle (R(\phi) - \langle R \rangle)^2 \rangle}\right)}$$

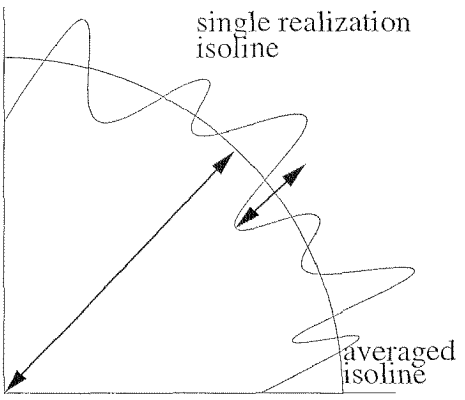

where $\langle \ \rangle \rightarrow$ sample over the angle and $\overline{\ \ } \rightarrow$ sample over an "ensemble" and $R(\phi)$ is the radial coordinate of one isoline

Figure 3.27: Roghness of an isoline

Note, that the brackets in Fig. (3.27) denote averaging not over the ensemble but over the angle. The isoline at saturation $S_g = 0.2$ was used. The roughness of the front is a space-independent property of each single realization. $\mathcal{R}^\star$ does not compare a single realization property with its ensemble mean. It gives an estimate, of how big the deviation of the radial coordinate of an isoline is in one single realization from the isoline averaged over the angle. It gives an estimate of the smoothness of the saturation at the front in a single realization.

The time behaviour of the roughness of the front $\mathcal{R}^\star$ indicates whether the flow process in the heterogeneous system is stable or whether the deviation between single realization and ensemble mean grow with time. If the roughness of the front of the air body would grow with time, a description of the single realization by a homogeneous system would not be appropriate, and measurable quantities of interest in field experiments like the point of earliest arrival or breakthrough times would be poorly estimated by homogeneous design calculations.

The quantity $\mathcal{R}^\star$ is the typical length scale for the roughness of the isoline. It has to be compared to the mean radial coordinate of the isoline, which grows with the square root of time $\sqrt{t}$ due to the constant inflow rate condition. The impact of the roughness of the front can therefore be determined by the relation of the growth rate of $\mathcal{R}^\star$ to the square root of time. If it grows with a power higher than 1/2 it will dominate the flow characteristics and a single realization cannot be represented by a homogeneous medium. If it grows slower, the fluctuations of the front become less important with time and the front essentially approaches a sharp homogeneous front.

If the growth of the roughness can be described by a power law, the power can be determined from the slope of the line in a log-log plot of roughness over time. That

this is not the case here can be seen in Fig. (3.28), where a log-log plot of the roughness for the test case no 3 is shown. As the line is not straight the dependency of $\mathcal{R}^\star$ has to be described with a more complex behaviour.

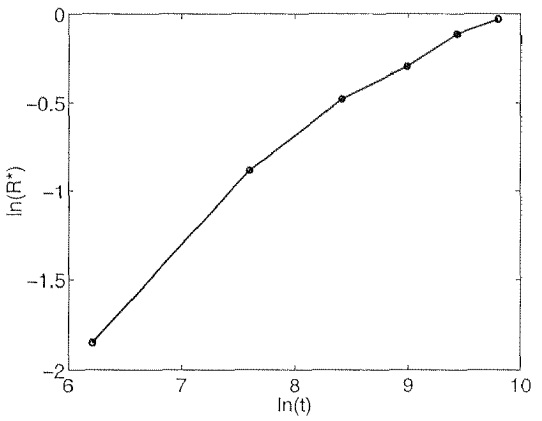

Figure 3.28: $\ln(\mathcal{R}^\star)$ over $\ln(t)$ for case no 3

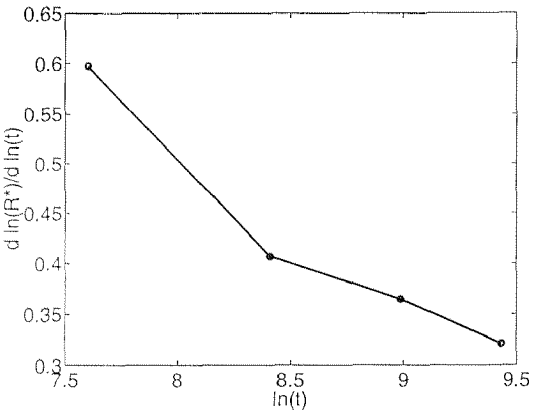

Figure 3.29: Time exponent of $\mathcal{R}^\star$ for case no 3

The slope of $\ln(\mathcal{R}^\star)$ over $\ln(t)$, which would be the time exponent of $\mathcal{R}^\star(t)$, is plotted for case no 3 in Fig. (3.29). The time exponent decreases from a value in the range of 0.5 to smaller values. In the following the time behaviour of the roughness is described phenomenologically. The initial increase is well described by a square root function. The exponent plotted in Fig. (3.29) is in the range of 0.5 at the beginning. However, after a period of time the increase gets weaker and a power law with a power smaller than 0.5 would be more appropriate. This is described here with a fit of the sum of a square root function and a linearly decreasing function,

$$\mathcal{R}^\star = a\,\sqrt{t} - b\,t. \tag{3.31}$$

Obviously, this will not describe the function up to arbitrarily large times, as at a certain point the roughness would get negative with this approach. The linear decrease rather marks the point, where the square root behaviour is no longer dominant. The larger the linear decrease compared to the increase with square root of time, the earlier is the crossover between a square root function and a function with a smaller power. The time where the crossover occurs depends on a^2/b^2. The roughness $\mathcal{R}^\star$ over time is shown for different values of σ_f^2 (case no 1, no 3 and no 5) in Fig. (3.30), for different inflow rates (cases no 1 and no 7) in Fig. (3.31), for different capillary pressure functions (cases no 1 and no 2 and cases no 3 and no 4) in Figs. (3.32) and (3.33) and for different correlation length (case no 1 and no 6) in Fig. (3.34).

During the phase where the roughness increases with the square root of time, $\mathcal{R}^\star$ is comparable to the mean radius and the fluctuations of the front have an impact on the flow behaviour. At the crossover time, the fluctuations get less important and the single realizations smooth out at the front. The increase of $\mathcal{R}^\star$ with square root of time is a measure for the early time dispersive effects, which are due to

the heterogeneous permeability field. This is the regime, where no mixing over the streamlines has occured, leading to a superdiffusive behaviour. The slower increase of the roughness of the front is due to mixing over the streamlines, leading to dispersive behaviour.

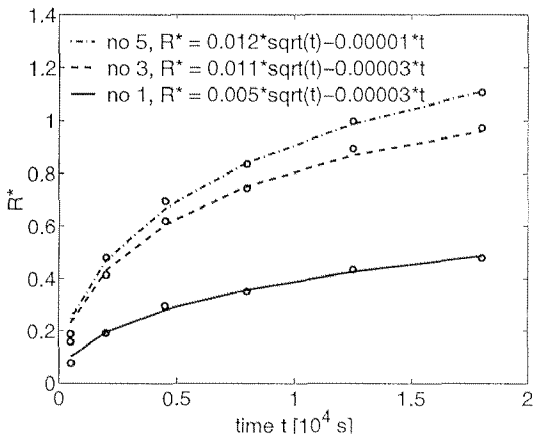

Figure 3.30: $\mathcal{R}^\star$ for different variances

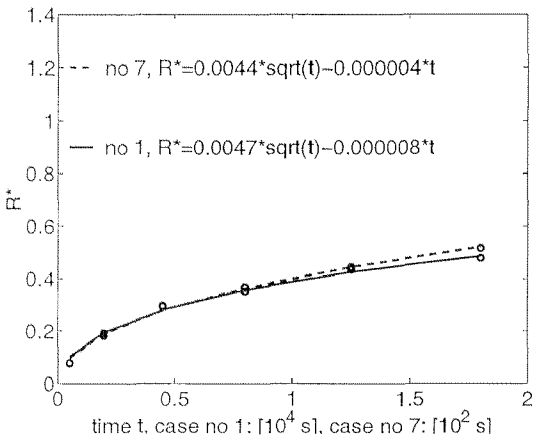

Figure 3.31: $\mathcal{R}^\star$ for different inflow rate

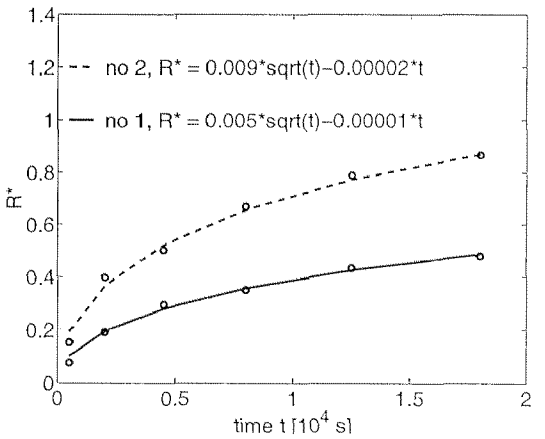

Figure 3.32: $\mathcal{R}^\star$ for different P_c (no 1 and no 2)

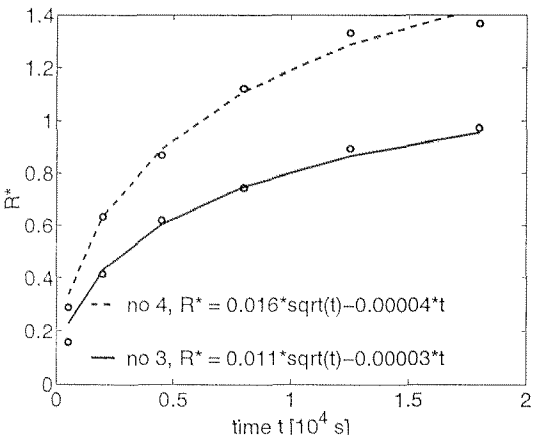

Figure 3.33: $\mathcal{R}^\star$ for different P_c (no 3 and no 4)

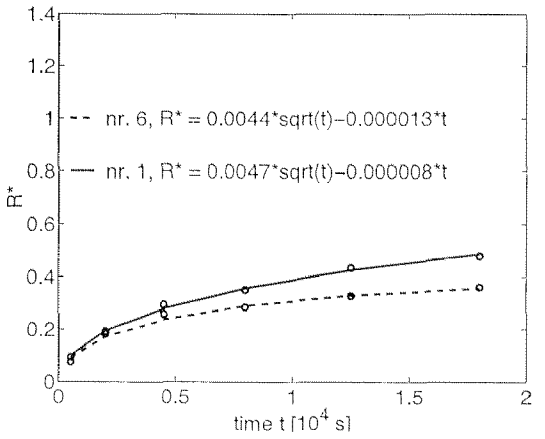

Figure 3.34: $\mathcal{R}^\star$ for different correlation length l_0

Influence of the variance of log permeability (compare Fig. 3.30)

The increase of variance of log-permeability increases the absolute growth rate in the phase of growth proportional to square root of time, as would be expected. However, a proportionality to the variance of log-permeability cannot be found. The crossover behaviour does not show a systematic trend with respect to the log-permeability variance.

Influence of the inflow rate (compare Fig. 3.31)

In contrast to that, the inflow rate increases the proportionality contrast in the initial phase, but also has an impact on the crossover time. The proportionality constant is increased by a factor of 10 if Q_M is increased by a factor of 100 (note the different scaling on the time axis). For the higher inflow rate, the crossover time is smaller as would have been expected.

Influence of the capillary pressure (compare Figs. 3.32 and 3.33)

A higher capillary pressure leads to a higher increase of the absolute growth rate in the initial phase but affects the crossover time only slightly. The capillary number seems to be not the only decisive quantity for the behaviour of the roughness of the front. It is possible that this is an effect of the coupling of the capillary pressure to the permeability field. Regarding the behaviour of the roughness of the front, the coupling leads to an effect that is similar to an increase of the depth of heterogeneity.

Influence of the correlation length (compare Fig. 3.34)

The correlation length has hardly an impact on the initial growth rate, but on the crossover time. With smaller correlation length this crossover time gets smaller. This behaviour is obviously reasonable, as the differences in the flow velocities on different streamlines are generated by the correlation structure of the medium.

None of the test cases described in Table 3.2 leads to a grow rate of the roughness $\mathcal{R}^\star$ that remains larger than 0.5. In the cases considered here, we do not have to expect roughening surfaces. However, at small times the roughness at the front has a growth rate in the same range as that of the mean radius and is therefore important. The behaviour at the front is smoothed out and the single realization is to the crossover time more similar to a homogeneous one.

3.5 Conclusions of the numerical simulations

With the help of numerical simulations the features of the parametrizations and their impact on the flow behaviour have been discussed. The flow is subject to selfsharpening effects which lead to the development of a front if the relative permeability function of gas written in terms of gas saturation is convex. This type of relative permeability function is adequate. The capillary pressure is considered to be heterogeneously distributed via a coupling with the permeability field. Entry pressure effects in the heterogeneous field can lead to channeling effects which make the ensemble averaging approach inappropriate and were therefore excluded.

An ensemble average of the gas saturation field was compared to a corresponding homogeneous field. The behaviour at the injection point in the averaged field is not changed, whereas the transition zone at the front is enhanced. This behaviour has been reproduced by an increase of the order of magnitude of the capillary pressure. The slope of the capillary pressure curve which is determined by the parameter λ has to be smaller in order to compensate for the impact at the injection point. However, the effect which can be obtained with this change of capillary pressure is limited. A larger transition zone can also be obtained by changing the relative permeability in a way that the selfsharpening effect is reduced. However, this is counterintuitive as the relative permeability is not considered to be heterogeneous.

Two characteristic quantities for the deviation of a single realization from the ensemble mean were investigated. First the variance of the gas saturation field was considered. It was observed that the variance is larger at the front zone than behind the front, if capillary effects are not important. The variance remains large behind the front if capillary effects are big. An increase of the variance of the heterogeneous field leads to an increase of the variance of the gas saturation at the front as well as behind the front. The mean roughness of an isoline at the front zone was considered, in order to quantifiy the "smoothness" of the gas saturation field at the front in the single realization. Its growth rate with time has been investigated on the one hand to estimate whether roughening surfaces have to be expected and ensemble averaging would not be justified. On the other hand the roughness is an indicator for a mixing process. Its time behaviour gives estimates of the kind of mixing induced by the heterogeneities. It therefore gives an estimate for the impact of these processes. It has been observed that the roughness grows with the square root of time at the beginning and changes to a slower growth rate after a while. The proportionality factor in the square root of time behaviour increases with the variance of the heterogeneous field, however, not linearly. It also increases with the inflow rate Q_M. An increase of the capillary pressure also leads to a larger proportionality factor, similar to the increase with the variance. The crossover time when the growth rate slows down depends on the inflow rate Q_M and on the correlation length l_0.

Chapter 4

Effective mixing effects - analytical calculations

A heterogeneous porous medium can be described as a random field making use of a stochastic approach. The method of perturbation theory has been successfully applied to determine effective large scale parameters in a number of different problems. The most important application is probably the calculation of a macrodispersion tensor in a heterogeneous flow field with uniform flow configuration. Perturbation theory can also be used to analyze the problem of radial displacement of water by air in a heterogeneous flow field. In that case however, the application is not straightforward. In this chapter we will use perturbation theory to investigate the impact of heterogeneities on the radial two-phase flow process. In Section 4.1, the flow equations described earlier are discussed in more detail. In Section 4.2 the problem of solute transport in a heterogeneous single phase flow field is considered as this problem has some analogies to the two-phase flow problem. In Section 4.3 a perturbation theory is developed for the two-phase flow problem and results which have been obtained under some restrictions and simplifications are discussed.

4.1 Formulation of the problem

The flow equations (3.1) through (3.4) can be rewritten in terms of the total flux (see e.g. *Marle* [1981])

$$\vec{q}_{\text{total}} = \vec{q}_1 + \vec{q}_2. \tag{4.1}$$

$\vec{q}_1$ denotes the volume flux of the displacing fluid, which is in this case the nonwetting fluid (air), and $\vec{q}_2$ denotes the flux of the displaced, wetting fluid (water). It is then possible to formulate the problem in terms of $\vec{q}_{\text{total}}$ instead of the pressure. Neglecting the density effects, as has been done in the last chapter, the gradient of the capillary pressure can be written as

$$\vec{\nabla} P_c = \vec{\nabla}(P_1 - P_2) = -\frac{\vec{q}_1}{K_{\text{abs}} m_1} + \frac{\vec{q}_2}{K_{\text{abs}} m_2} = -\frac{\vec{q}_1}{K_{\text{abs}} m_1} + \frac{\vec{q}_{\text{total}} - \vec{q}_1}{K_{\text{abs}} m_2}. \tag{4.2}$$

This leads to an expression for $\vec{q}_1$ depending on the capillary pressure and the total velocity

$$\vec{q}_1 = \frac{1/m_2}{1/m_1 + 1/m_2}\vec{q}_{\text{total}} - \frac{K_{\text{abs}}}{1/m_1 + 1/m_2}\frac{dP_c}{dS_1}\vec{\nabla}S_1 = \psi_1(S_1)\vec{q}_{\text{total}} - \psi_2(S_1)\vec{\nabla}S_1. \tag{4.3}$$

with

$$\begin{aligned}\psi_1(S) &= \frac{1/m_2}{1/m_1 + 1/m_2} = \frac{\mu_2/k_{r2}(S)}{\mu_1/k_{r1}(S) + \mu_2/k_{r2}(S)} \\ \psi_2(S) &= \frac{K_{\text{abs}}}{1/m_1 + 1/m_2}\frac{dP_c}{dS} = \frac{K_{\text{abs}}}{\mu_1/k_{r1}(S) + \mu_2/k_{r2}(S)}\frac{dP_c}{dS}(S).\end{aligned} \tag{4.4}$$

Inserting Eq. (4.3) into the continuity of mass equation Eq. (3.1) yields

$$\phi\partial_t S_1 + \vec{\nabla}\cdot\left[\psi_1(S_1)\vec{q}_{\text{total}} - \psi_2(S_1)\vec{\nabla}S_1\right] = s_1. \tag{4.5}$$

where the density is considered again as constant.

The heterogeneous equations will be simplified by assuming the capillary pressure to be homogeneous and therefore to be constant. We have seen in Chapter 3 that the coupling of a heterogeneously distributed permeability and a heterogeneously distributed capillary pressure has a similar effect on the flow behaviour at the front as a heterogeneous permeability field where the capillary pressure is set constant but the variance of log permeability is increased. We assume therefore, that the neglection of the heterogeneous distribution of capillary pressure is not expected to lead to a loss of important effects.

The porosity ϕ is in the following assumed to be constant and is for simplicity set to $\phi = 1$. S_1 is the saturation of the gas phase and in the following is simply denoted with S. The shapes of the functions ψ_1 and ψ_2 are dependent on the kind of parametrization chosen for the relative permeability and capillary pressure functions. Both functions are positive, as the relative permeabilities are larger than 0. The derivative of the capillary pressure with respect to the nonwetting phase saturation is also positive as is the derivative of ψ_1 with respect to S. The change of saturation with time is equal to the divergence of a flux. The flux term consists of two parts, one advective and one diffusive. Taking this into account Eq. (4.5) resembles the solute transport equation which describes transport of a miscible solute in a single phase flow field.

In the solute transport equation the advective flux is the product of an external flow field and the concentration. It describes the motion of a solute particle in the external field. In Eq. (4.5) it is the product of the total flow field and a function of the saturation. Evaluating the operators this term reads

$$\frac{d\psi_1(S)}{dS}\vec{\nabla}S\cdot\vec{q}_{\text{total}} \tag{4.6}$$

which resembles the advective part in the solute transport equation multiplied by a function of the saturation. However, the external flow field has a different interpretation in both cases. In the case of solute transport the concentration for which

the differential equation is solved is not a fluid itself, but it is dissolved in the fluid, the flux of which is described by $\vec{q}_{\text{total}}$. Darcy's equation which describes the flux $\vec{q}_{\text{total}}$ is independent of the solute concentration. In the case of two-phase flow the saturation for which the differential equation is solved is a fluid which has a flux that is one part of the total flux $\vec{q}_{\text{total}}$. The modified Darcy equation that describes the flux $\vec{q}_{\text{total}}$ is therefore dependent on the saturation, so that we obtain a system of coupled equations. In our case, however, the total flux for the homogeneous medium is given by the inflow conditions,

$$\vec{q}_{\text{total}} = \frac{Q}{2\pi r}\vec{e}_r, \tag{4.7}$$

Q being the inflow rate of gas and r being the radius $r = \sqrt{x^2 + y^2}$. The homogeneous problem with constant inflow conditions can be treated without dealing with the pressure variable. For the heterogeneous problem this is of course different. The inherent assumption in Eq. (4.7) is that the air is displacing the water completely. If this is not the case and there is a residual amount of water remaining in the medium at the inflow point the problem has to be modified. The porosity has to be recalculated in a way that the pore space per volume that is not available for the flow process due to the remaining water, is added to the porosity.

The diffusive flux looks similar for solute transport and two-phase flow, however the diffusive constant or dispersion constant in solute transport is a constant D, whereas in two-phase flow it is a function of the saturation. The mechanism is in principle the same, a mixing of the concentration or saturation. In solute transport the mixing is caused either by molecular diffusion or by dispersion, which is the mixing of the solute particles due to distribution over different flow paths on the pore scale. For two-phase flow the capillary pressure drives the water back into the air filled pores, leading to a counterflow of water opposite to the gas flow direction. These mixing mechanisms lead to a spreading of the front.

It is reasonable in a first step to look at the solute transport problem to characterize the influence of heterogeneities on the transport behaviour in a radial flow field although two-phase flow is much more complex than the solute transport due to the coupling of the equations, and due to the nonlinear behaviour caused by relative permeability and capillary pressure. Hence we can take advantage of the resemblance of the equations for these problems. This means we are looking at Eq. (4.4) for the choice

$$\psi_1(S) = \text{const.} \cdot S, \tag{4.8}$$

which would be the case for an appropriately (but not reasonably) chosen combination of lines as relative permeabilities, and

$$\psi_2(S) = \text{const.} \tag{4.9}$$

which can hardly be achieved. As an example, the funcions ψ_1 and ψ_2 are plotted for a Brook's-Corey parametrization ($P_{c0} = 1000Pa, \lambda = 2$) in Fig. (4.1). Although the

parametrizations (4.8) and (4.9) are not overly realistic, the simpler approach may be useful. The more complex phenomena can be interpreted better, if the simpler cases are well understood. Concentrating on the simplified form of the equation first, it can be investigated in a further step how to generalize the results to the two-phase flow equations.

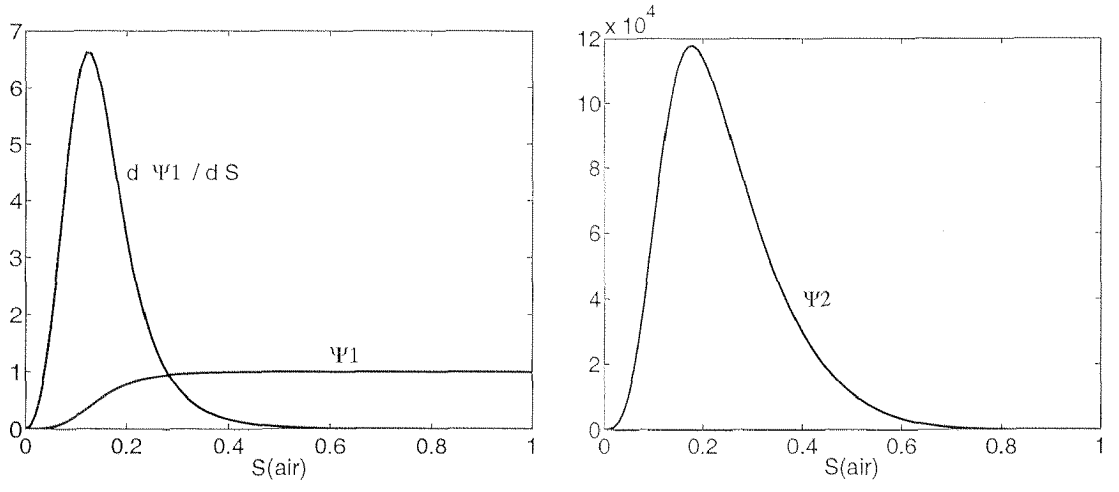

Figure 4.1: Typical functions for $\psi_1(S)$ and $\psi_2(S)$

4.2 Solute transport in a radial flow field

If we neglect the nonlinearities in the flow Eq. (4.5) and set them constant Eq. (4.5) becomes

$$\partial_t S + C_1 \vec{q}_{\text{total}} \cdot \vec{\nabla} S - C_2 \Delta S = s. \tag{4.10}$$

Setting C_1 to 1 as well as identifying C_2 with the dispersion constant D and identifying the saturation S with the solute constant c leads to the solute transport equation. However there is an important difference concerning the dispersion constant. In the two-phase flow equations it is an important characteristic that the function ψ_2 only depends on the saturation S so that C_2 is really a constant with respect to space. In solute transport it has been observed in experiments and it has also been shown analytically, that the dispersion coefficient is proportional to the flow velocity. In the radial case the velocity is not a constant, but decreases with $1/r$. Assuming that the proportionality is valid for any flow configuration, the dispersion coefficient also decreases with $1/r$. This would not be appropriate for Eq. (4.10). If there is no dispersion in the solute transport, but just molecular diffusion, the diffusion constant does not depend on time and space. The analogy between Eq. (4.5) and the solute transport equation for the radial case is therefore a transport with no dispersion, but just molecular diffusion on the small scale.

The correspondence to the heterogeneous flow field in the two-phase flow problem is a heterogeneous flow field in which the solute tracer is transported. In order to get a quantification and interpretation of the impact of the heterogeneities of the

flow field on the transport behaviour, we want to describe the transport on a scale much larger than the scale of the heterogeneities as a process in a homogeneous porous medium with effective transport parameters. There is a large body of work on the derivation of effective properties in heterogeneous porous media, which in the following we will briefly rewiew. The work presented here contributes to this field.

Many studies on effective flow and transport parameters have been performed for a uniform flow configuration in an unbounded domain, see e.g. *Gelhar* [1993] or *Dagan* [1989]. In principle heterogeneous flow fields caused by heterogeneous permeabilities lead to travel time differences of solute moving on different flow paths. Consequently, one finds strongly enhanced macro-dispersion coefficients on larger scales. Such scenarios have been investigated by *Gelhar and Axness* [1983]. With their method asymptotic (long time) macrodispersion coefficients were obtained for smoothly varying flow fields. The problem of the time behaviour of the macrodispersion was first treated by *Dagan* [1988] who used a Lagrangian approach. In later work the same problem is treated using an Eulerian approach (see e.g. the work of *Rajaram and Gelhar* [1993]).

In general the existence and the features of effective parameters will depend on boundaries and flow configurations. The studies cited above are therefore not generally applicable, but only for uniform flow conditions in unbounded domains. Some effort has been made to extend the results to more general cases. *Neuman* [1993] developed a more general formalism in order to find formulations for effective transport parameters in bounded flow fields with sinks and sources. *Indelman and Abramovich* [1994] developed a general concept for averaging nonuniform flows ending up with expressions for effective conductivities. In many cases it has been shown that the results differ considerably from the uniform flow results.

Effective flow properties for radial flow in heterogeneous porous media have been derived for several conditions. Effective conductivities were first investigated by *Shvidler* [1962]. *Indelman et al.* [1996] have calculated an equivalent transmissivity for converging flow fields with cylindrical symmetry in a three dimensional anisotropic aquifer. The head boundaries were held constant. *Sanchez-Vila* [1997] derived effective permeabilities for converging radial flow in a two-dimensional isotropic aquifer with a constant injection rate. *Neuman and Orr* [1993] numerically investigated the effective conductivity for a constant flux scenario in a two-dimensional system. Numerical results on the same subject can also be found also in the studies of *Desbarats* [1992]. In general, the effective permeability is found to be nonlocal and dependent on the chosen boundary conditions. Very close to the well the permeability is described by the harmonic or the arithmetic mean respectively. However, in the far field of the well it approaches the geometric mean value as in uniform flow configurations. *Fiori et al.* [1998] investigated three dimensional radial flow behaviour.

Solute transport in heterogeneous flow fields with radial configuration has also features differing from uniform flow. *Indelman and Dagan* [1999] used a perturbation approach in a Lagrangian formulation of the problem to calculate macrodispersion coefficients in radially divergent flow in 3d for a cylindrically symmetric and a spher-

ically symmetric flow geometry in an unbounded domain. For nonreactive tracers the mean effect is mixing due to the spatially variable velocity field, leading to macrodispersion on a larger scale. Assuming that the dispersion coefficients can be written as a product of the mean flow velocity multiplied by a factor called effective dispersivity, they derived an expression for the effective dispersivity in the limit of infinite Peclet numbers, which means vanishing small scale dispersion. The apparent dispersivities, defined via the second moments, were found to be smaller than in uniform flow situations by a factor of 3 for the cylindrical symmetry and a factor of 5 for spherical symmetry.

Neglecting the diffusion does not seem appropriate for the case considered here. On the one hand there are applications where Peclet numbers are quite small. This is especially valid for gas tracer experiments with small inflow rates. The role of diffusion in gaseous flow which has been investigated frequently (e.g. *Gimmi and Fluehler* [1996], *Popovicovca and Brusseau* [1997], *Abu-El-Sha'r and Abriola* [1997]) can have a strong influence. On the other hand we have to keep in mind that the radial tracer transport model discussed in this section stands as a simplified model for the two-phase flow process we are interested in. Typical values for the constant C_2 in Eq. (4.10) depend on the absolute permeability and can become much larger than typical diffusion constants for high permeabilities. It is therefore reasonable to include finite Peclet numbers in the analysis of solute transport.

In this section a perturbation approach for the transport equation in the Eulerian picture is used to investigate macrodispersion coefficients in a radially diverging flow field up to second order in the velocity fluctuations. The impact of finite Peclet numbers on the macrodispersion coefficients are studied. On the basis of the spatial moments of the solute concentration distribution effective transport parameters are assigned.

4.2.1 Transport model

Solute transport is described by the transport equation

$$\partial_t c(\vec{x},t) + \vec{u}(\vec{x}) \cdot \vec{\nabla} c(\vec{x},t) - \vec{\nabla} \cdot \left(D_0 \vec{\nabla} c(\vec{x},t) \right) = 0. \tag{4.11}$$

c is the solute concentration, $\vec{u}$ is the local flow velocity field and D_0 in this case is the diffusion coefficient.

Initially we write the transport equation in three dimensions with cylindrical symmetry. The mixing effects due to an extended line source in z-direction will be discussed later. It is helpful to take the z-dimension initially into account, to develop an understanding how it influences different averaging procedures. However it turns out that it has no important impact on quantitative results and will therefore be excluded later.

Injecting water into an injection well in a homogeneous saturated medium with a

constant volumetric injection rate Q yields a radially symmetric flow field

$$\vec{u}(r,\varphi,z) = \frac{Q}{2\pi r}\vec{e_r} \tag{4.12}$$

aligned in radial direction $\vec{e_r}$. Suitable to the radial symmetry, cylindrical coordinates r, φ, z are chosen for parametrization. Solute added to the groundwater flow is transported advectively in radial direction by the flow field $\vec{u}(r,\varphi,z)$ and spreads by diffusion which is assumed to be isotropic. On larger scales the permeability varies spatially due to heterogeneities of the medium which leads to a fluctuating flow field. The flow field is split into a deterministic and a random part

$$\vec{u}(r,\varphi,z) = \frac{Q}{2\pi r}\vec{e_r} + \vec{\tilde{u}}(r,\vec{\varphi},z) \tag{4.13}$$

where the random part $\vec{\tilde{u}}(r,\phi,z)$ in principle is not radially symmetric. However, due to the incompressibility of the flow field one still has $\nabla \cdot \vec{u}(r,\varphi,z) = 0$.

The initial conditions represent a pointlike instantaneous tracer injection of one unit mass at the inflow line,

$$c(\vec{x},0) = \delta(r^2)\frac{1}{L_z}\Theta(1 - z/L_z) \quad . \tag{4.14}$$

$\delta(x)$ is the Dirac delta distribution and $\Theta(x)$ is the Heavyside step function. L_z is the length of the line source in z-direction. The concentration for an injection of solute with constant mass injection rate per unit mass $\mathcal{Q}_{\text{sol}}$ can then be obtained by convolution over time

$$c(\vec{x},t)(\text{const. injection}) = \int_0^t dt' \mathcal{Q}_{\text{sol}} c(\vec{x},t')(\text{point like injection}) \tag{4.15}$$

We consider an unbounded domain and therefore have the boundary condition

$$c(\lim|\vec{x}| \to \infty, t) = 0. \tag{4.16}$$

4.2.2 General methods

In the following we make use of the stochastic approach outlined in Chapter 1. For a more detailed description of this approach see e.g. *Dagan* [1989]. We will determine effective parameters from quantities which are averaged over an ensemble of all possible realizations of the heterogeneous field.

In general the solute concentration distribution can be characterized by its spatial moments defined in an appropriately chosen coordinate system. A distribution is completely determined by its moments (see e.g. *van Kampen* [1981]). As we are interested in describing transport behaviour in a radial flow configuration it is natural to choose a radial coordinate system instead of a cartesian coordinate system as well as radial moments as characterizing transport parameters. However, the

explicit definition of appropriate transport parameters depends not only on symmetries of the system. The design of a measurement procedure decides which transport parameters are observable in a given experiment.
One possible experimental setup is to inject the solute into the well and to measure the solute concentration at different observation points distributed on circles around the well. In this case, we get information about the spatial distribution of solute particles which is characterized e.g. by the radial centre of mass and the radial width. The radial centre of mass is given by

$$\kappa_r^{(1)}(t) = \frac{m_r^{(1)}(t)}{m_r^{(0)}(t)} \tag{4.17}$$

and the squared radial width is

$$\kappa_r^{(2)}(t) = \frac{m_r^{(2)}(t)}{m_r^{(0)}(t)} - \left(\frac{m_r^{(1)}(t)}{m_r^{(0)}(t)}\right)^2. \tag{4.18}$$

Here $m^{(n)}$ denotes the n-th radial moment

$$m_r^{(n)}(t) = \int_0^\infty r dr \int_0^{2\pi} d\varphi \int_{-\infty}^{\infty} dz\, r^n c(r, \varphi, z, t), \tag{4.19}$$

with r as the distance from the injection well, φ the azimutal coordinate and z the vertical coordinate.

On the other hand, if one does not trace all particles but only particles released on one fixed radial section, we obviously obtain information about the particle distribution only on this section. This is definitely a more realistic scenario as we have mostly only a few measuring points to obtain breakthrough curves. These more local quantities

$$\kappa_r^{(1)}(t)\Big|_{\text{sect}} = \frac{m_r^{(1)}(t)\Big|_{\text{sect}}}{m_r^{(0)}(t)\Big|_{\text{sect}}} \tag{4.20}$$

and

$$\kappa_r^{(2)}(t)\Big|_{\text{sect}} = \frac{m_r^{(2)}(t)\Big|_{\text{sect}}}{m_r^{(0)}(t)\Big|_{\text{sect}}} - \left(\frac{m_r^{(1)}\Big|_{\text{sect}}}{m_r^{(0)}(t)\Big|_{\text{sect}}}\right)^2 \tag{4.21}$$

are the observable quantities. $m^{(n)}(t)\big|_{\text{sect}}$ denotes the n-th radial moment at a fixed angle

$$m_r^{(n)}\Big|_{\text{sect}} = \int_0^\infty dr \int_{-\infty}^{\infty} dz\, r^n c(r, \varphi = 0, z, t). \tag{4.22}$$

The difference between the total second cumulant and the more local one on the section is sketched in Fig. (4.2). Both types of radial cumulants, the local and the

angle-averaged one, become almost equivalent if the concentration distribution is radially symmetric and not dependent on the azimutal coordinate anymore. The transport in a homogeneous medium shows radially symmetric behaviour. However, in heterogeneous media the transport parameters depend on the spatial distribution of the heterogeneities and in general show no symmetry at all.

If there is no detailed information about the spatial distribution of the heterogeneities available it is not possible to model explicitely the transport behaviour in a given aquifer. But if one is interested in characterizing the system behaviour on larger scales only, the stochastic modeling approach offers a very useful tool: the heterogeneous model parameters are considered as one realization out of an ensemble of all possible ones. After having sampled a representative part of the heterogeneities the ensemble averaged transport parameters describe the transport behaviour in one given aquifer.

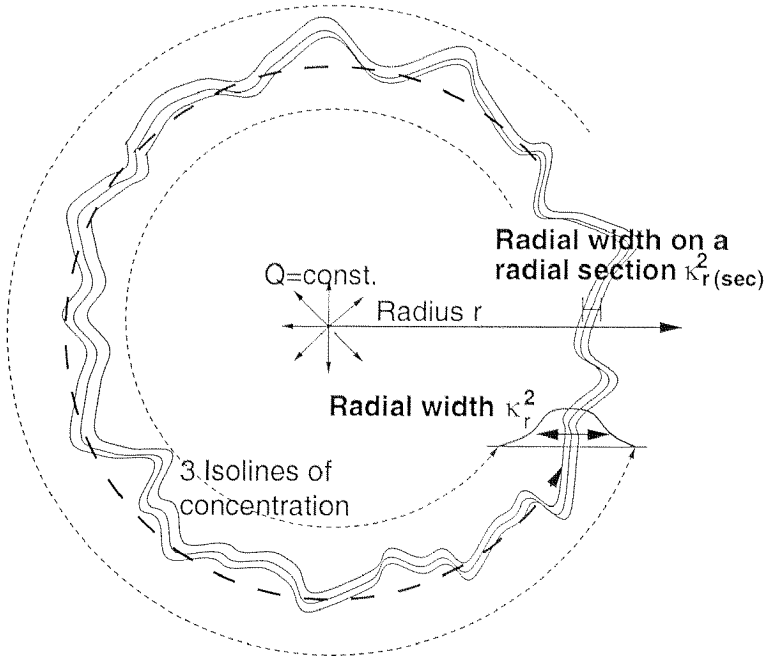

Figure 4.2: Total second radial cumulant and second radial cumulant on a radial section

Following this idea, the ensemble-averaged radial cumulants and local radial cumulants are defined by

$$\kappa_r^{(1),\mathrm{eff}}(t) = \overline{\kappa_r^{(1)}(t)}, \qquad \kappa_r^{(1),\mathrm{eff}}(t)\Big|_{\mathrm{sect}} = \overline{\kappa_r^{(1)}(t)\Big|_{\mathrm{sect}}} \tag{4.23}$$

and

$$\kappa_r^{(2),\mathrm{eff}}(t) = \overline{\kappa_r^{(2)}(t)} = \overline{\frac{m_r^{(2)}(t)}{m_r^{(0)}(t)}} - \overline{\frac{m_r^{(1)}(t)}{m_r^{(0)}(t)} \cdot \frac{m_r^{(1)}(t)}{m_r^{(0)}(t)}}, \tag{4.24}$$

$$\kappa_r^{(2),\mathrm{eff}}(t)\Big|_{\mathrm{sect}} = \overline{\kappa_r^{(2)}(t)\Big|_{\mathrm{sect}}} = \overline{\frac{m_r^{(2)}(t)\Big|_{\mathrm{sect}}}{m_r^{(0)}(t)\Big|_{\mathrm{sect}}}} - \overline{\frac{m_r^{(1)}(t)\Big|_{\mathrm{sect}}}{m_r^{(0)}(t)\Big|_{\mathrm{sect}}} \cdot \frac{m_r^{(1)}(t)\Big|_{\mathrm{sect}}}{m_r^{(0)}(t)\Big|_{\mathrm{sect}}}}.$$

In the following they are denoted as effective radial centre of mass and effective radial width, consistently with *Attinger et al.* [1999] and *Metzger et al.* [1999]. The overbar

denotes the ensemble average over all possible realizations of the heterogeneous fields.

From these quantities one has to distinguish the so called ensemble quantities characterizing the ensemble of all possible aquifer realizations. The ensemble radial centre of mass and the ensemble squared radial width are calculated from the ensemble average of the concentration distribution and are defined as

$$\kappa_r^{(1),\mathrm{ens}}(t) = \overline{\kappa_r^{(1)}(t)}, \qquad \kappa_r^{(1),\mathrm{ens}}(t)\Big|_{\mathrm{sect}} = \overline{\kappa_r^{(1)}(t)\Big|_{\mathrm{sect}}} \tag{4.25}$$

and

$$\kappa_r^{(2),\mathrm{ens}}(t) = \overline{\frac{m_r^{(2)}(t)}{m_r^{(0)}(t)}} - \overline{\frac{m_r^{(1)}(t)}{m_r^{(0)}(t)}} \cdot \overline{\frac{m_r^{(1)}(t)}{m_r^{(0)}(t)}}, \tag{4.26}$$

$$\kappa_r^{(2),\mathrm{ens}}(t)\Big|_{\mathrm{sect}} = \overline{\frac{m_r^{(2)}(t)\Big|_{\mathrm{sect}}}{m_r^{(0)}(t)\Big|_{\mathrm{sect}}}} - \overline{\frac{m_r^{(1)}(t)\Big|_{\mathrm{sect}}}{m_r^{(0)}(t)\Big|_{\mathrm{sect}}}} \cdot \overline{\frac{m_r^{(1)}(t)\Big|_{\mathrm{sect}}}{m_r^{(0)}(t)\Big|_{\mathrm{sect}}}}.$$

For the ensemble quantities, the difference between angle-averaged radial cumulants and local cumulants can be neglected as the ensemble averaged concentration distribution is radially symmetric. The difference between the two averaging methods is sketched in Fig. (4.3).

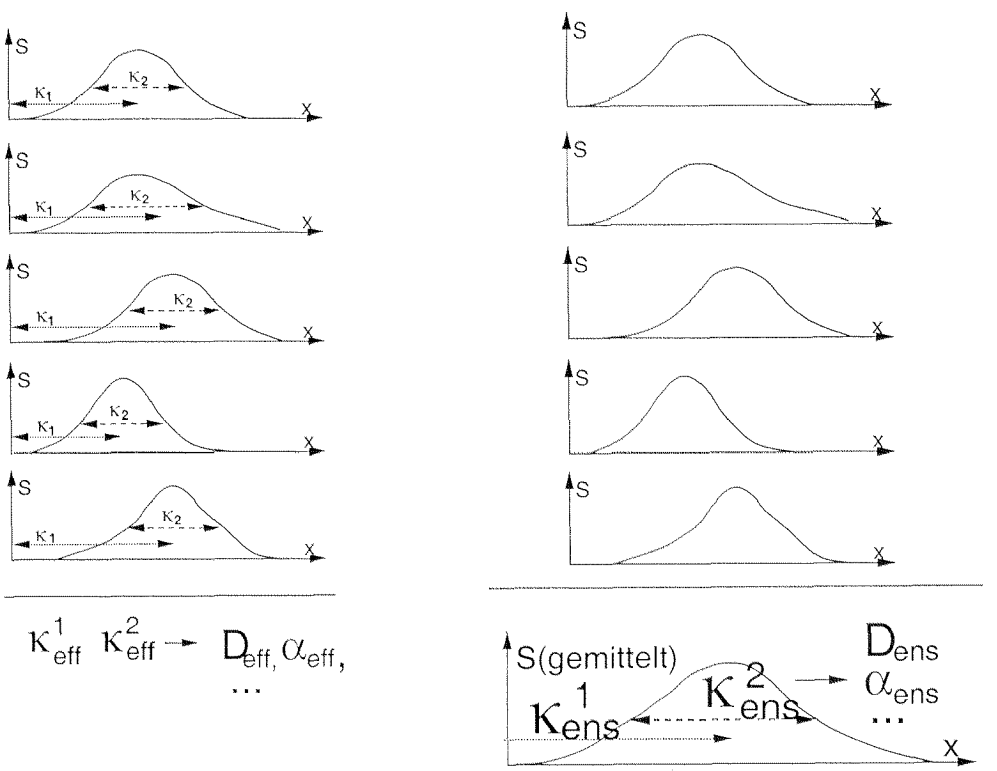

Figure 4.3: Effective and ensemble averaging

4.2.3 Transport in a homogeneous medium

To compare the ensemble averaged properties to the homogeneous ones, the homogeneous transport equation is considered at this point.

Purely advective transport behaviour

In the dispersion-free case, the transport equation reads

$$\partial_t c(\vec{x},t) + \frac{Q}{2\pi r}\,\partial_r c(\vec{x},t) = 0, \tag{4.27}$$

where ∂_r is the partial derivative with respect to the radial coordinate r. The solution for conditions described by Eq. (4.14) is simply given by a solute peak over the length L_z,

$$c(r,t) \;=\; 2\,\delta(r^2 - Q/\pi\,t)\,\frac{1}{L_z}\,\Theta(1 - z/L_z) \tag{4.28}$$

The peak is homogeneously distributed over all angles due to the radial symmetry of the problem. The radius of the solute ring grows with time according to $\kappa_r^{(1)}(t) = \sqrt{Q\,t/\pi}$. No diffusion is acting, hence the width of the ring is infinitely small, $\kappa_r^{(2)}(t) = 0$. Note that due to the decrease of the velocity field with the distance from the well, the radial centre of mass movement is much slower than the centre of mass movement for transport in a uniform flow field with the same flow rate.

Transport with diffusion

An explicit twodimensional solution for the solute distribution can be found for the case of transport in a radial velocity field and constant diffusive effects. It is given by

$$c_0(r,t) = \frac{\exp\left(-\dfrac{r^2}{4D_0t}\right)\left(\dfrac{r^2}{4D_0t}\right)^{\frac{Q}{4\pi D_0}}}{Qt\Gamma\left(\dfrac{Q}{4\pi D_0}\right)} \tag{4.29}$$

where $\Gamma(x)$ is the gamma function as defined in *Abramovitz and Stegun* [1972]. The function is plotted over radius r for different times in Fig. (4.4).

The derivation of Eq. (4.29) is discussed in Appendix C. The radial centre of mass moves according to

$$\kappa_r^{(1)}(t) \;=\; \sqrt{4D_0t}\,\frac{\Gamma\left(\frac{Q}{4\pi D_0}+\frac{3}{2}\right)}{\Gamma\left(\frac{Q}{4\pi D_0}+1\right)} \approx \sqrt{\frac{Qt}{\pi}}\left(1+\frac{3}{2}\frac{D_0\pi}{Q}+O\left(\left(\frac{D_0}{Q}\right)^2\right)\right) \tag{4.30}$$

where the result has already been expanded with respect to small inverse Peclet number $\varepsilon_1 = D_0/Q$. For small inverse Peclet numbers the centre of mass movement is dominated by advective effects reducing to the purely advective result ($\sqrt{Qt/\pi}$) in the limit of vanishing diffusion. Due to diffusion effects the squared width grows as

$$\kappa_r^{(2)}(t) = D_0 t \ (1 + O(\varepsilon_1)) \tag{4.31}$$

where O stands for the order. In the case of constant diffusion the diffusion coefficient can be identified by the operation

$$D(\varepsilon \ll 1) = \partial_t \kappa_r^{(2)}(t) \tag{4.32}$$

which except for a factor of $1/2$ is the usual difinition valid for advective-dispersive processes in uniform flow fields.

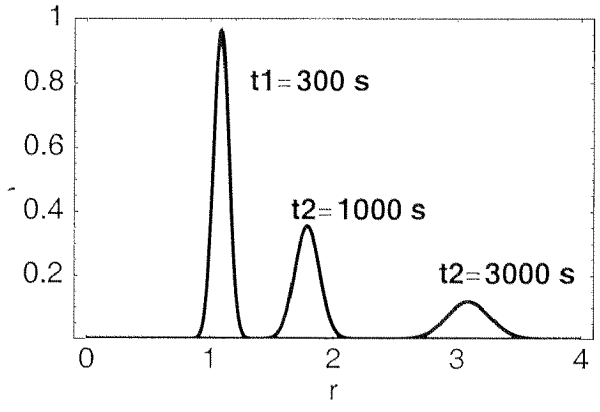

Figure 4.4: $c_0(r,t)$ at different times, for $Q = 10^{-2}m^2/s, D_0 = 10^{-5}m^2/s$

Transport with mechanical dispersion $D(r) = \alpha\frac{Q}{2\pi r}$

As will be shown later, it is also necessary to consider the case of mechanical dispersion, where the dispersion constant depends on the flow velocity. In that case the dispersion coefficient is proportional to $1/r$. To the best of our knowledge there is no closed solution for transport in a radial flow field including mechanical dispersion. *Gelhar and Collins* [1971] developed an approximate solution. *Philip* [1994] investigated solutions for the general case $D \propto r^{-n}$ with a constant solute inflow rate, but did not find an analytical solution for the case $n = 1$ either. Approximate expressions for the radial moments using a perturbation expansion in terms of the parameter $\varepsilon_2 = \alpha/\sqrt{(Qt)/\pi}$ are found (Appendix D). However, by construction the results of the perturbation theory are only true for times $t \gg \frac{\alpha^2}{Q}$ where the advective effects are dominating the dispersive effects. For the radial centre of mass and for the squared radial width of the solute distribution, we obtain

$$\kappa_r^{(1)}(t) = \sqrt{\frac{Qt}{\pi}} + \frac{2}{3}\alpha \ (1 + O(\varepsilon_2)) \tag{4.33}$$

$$\kappa_r^{(2)}(t) = \frac{2}{3}\alpha\sqrt{\frac{Q}{\pi}t} \ (1 + O(\varepsilon_2)) \tag{4.34}$$

To leading order the centre of mass movement is again given by $\sqrt{Qt/\pi}$. However, the squared radial width grows proportionally to $\sqrt{t}$ which is different from the linear growth proportional to t found in the case of transport with constant diffusion coefficient. The parameter characterizing the mechanical dispersion processes can be derived using a time dependent velocity $|\vec{u}|_t = \sqrt{Q/(\pi t)}$ instead of the local velocity $|\vec{u}| = Q/(2\pi r)$. This would be the velocity of a particle transported with the mean flow field. The dispersion length can then be defined as

$$\alpha = \frac{3\partial_t \kappa_r^{(2)}(t)}{|u|_t} = \frac{3\partial_t \kappa_r^{(2)} \sqrt{\pi t}}{\sqrt{Q}}. \tag{4.35}$$

The latter identification also works for transport in a uniform flow field, if the constant is set to 1 for the uniform case instead of 3 for the radial case. The identification of Eq. (4.32) is appropriate only for transport with constant dispersion coefficients.

4.2.4 Transport in a heterogeneous flow field - Stochastic approach

The heterogeneous transport equation can now be compared to the homogeneous one.

Statistics of the heterogeneous flow fields

In the heterogeneous system, the hydraulic conductivity fluctuates spatially. Using the stochastic approach we consider the conductivity as a stochastic field with given statistic properties. The flow velocity $\vec{u}$ is related to a heterogeneous hydraulic conductivity field by Darcy's law which allows us to derive the statistics of the flow field.

By construction the mean of the fluctuating part of the velocity field vanishes, $\overline{\tilde{u}(\vec{x})} = 0$. The autocorrelation function of the radial components of the fluctuating flow field reads

$$\overline{\tilde{u}_r(\vec{x})\tilde{u}_r(\vec{x}')} = \sigma_f^2 \frac{Q^2}{4\pi^2\, r\, r'} \exp\left(-\frac{(\vec{x}-\vec{x}')^2}{l_0^2}\right) \tag{4.36}$$

where σ_f^2 is the variance of the logarithm of the permeability field. For the autocorrelation function of the conductivity field a Gaussian function is assumed for simplicity, which leads to vanishing correlations for lengths larger than the isotropic correlation length l_0. The covariance function in this form is derived from Darcy's law (*Fiori et al.* [1998]). In its exact form it has three additional components which have their origin in the requirement of incompressibility of the flow field. However, for transport in uniform flow it has been observed that the corresponding three terms do not contribute to leading order in time to the longitudinal macrodispersion coefficients (*Dentz* [1999]). In contrast to uniform flow, these additional components

are very hard to handle in radial flow. However, by investigating the components numerically *Indelman and Dagan* [1999]) showed that their contribution is small in the purely advective transport (infinite Peclet numbers). We assume that this is also valid for finite Peclet numbers and take into account only the term (4.36) as an approximation for the two-point autocovariance.

Perturbation theory

In order to get solutions for the heterogeneous Eq. (4.11) a perturbation approach is applied. As Eq. (4.11) is linear in c the method of Green's functions can be used to transform the differential equation into an equivalent integral equation,

$$c(\vec{x},t) = c_0(\vec{x},t) + \int\int d^dx'\,dt'\,G(\vec{x},\vec{x}',t-t')\vec{\tilde{u}}(\vec{x}')\cdot\vec{\nabla}'c(\vec{x}',t'). \tag{4.37}$$

$c_0(\vec{x},t)$ is the solution of the homogeneous equation ($\vec{\tilde{u}} = \vec{0}$). $G(\vec{x},\vec{x}',t-t')$ is the Green's function which solves the homogeneous transport equation with an instantaneous solute pulse injected at $\vec{x} = \vec{x}'$ and $t = t'$

$$\partial_t G(\vec{x},\vec{x}',t-t') + \left(\frac{Q}{2\pi|\vec{x}|}\vec{e}_r\nabla - \nabla D_0(\vec{x})\nabla\right) G(\vec{x},\vec{x}',t-t') = \delta^d(\vec{x}-\vec{x}')\delta(t-t'). \tag{4.38}$$

In this form, Eq. (4.37) is not very helpul, as the solution is dependent on the solution itself. However, the right hand side of (4.37) can be inserted for $c(\vec{x}',t')$ iteratively so that it can be written as an infinite sum of integrals.

$$\begin{aligned} c(\vec{x},t) = c_0(\vec{x},t) &+ \int\int d^dx'\,dt'\,G(\vec{x},\vec{x}',t-t')\vec{\tilde{u}}(\vec{x}')\cdot\vec{\nabla}'c_0(\vec{x}',t') + \\ &\int\int d^dx'\,dt' \int\int d^dx''\,dt''\,G(\vec{x},\vec{x}',t-t')\vec{\tilde{u}}(\vec{x}')\cdot\vec{\nabla}'G(\vec{x}',\vec{x}'',t'-t'')\cdot \\ &\vec{\tilde{u}}(\vec{x}'')\cdot\vec{\nabla}''c_0(\vec{x}'',t'') + \ldots \end{aligned} \tag{4.39}$$

In this way an expression for the concentration distribution or its moments can be obtained that consists of an infinite sum of integrals. The n-th term contains the fluctuations $\tilde{u}$ n-1 times as factors. By truncating the sum after the third term the concentration distribution or its moments can be calculated to second order in the fluctuations. After ensemble averaging these expressions only depend on the mean (which vanishes by construction) and the two-point autocovariance, the radial part of which is given by (4.36).

4.2.5 Effective transport parameters for purely advective transport

In the case of purely advective transport it is possible to calculate the effective and ensemble transport parameters introduced in Section 4.2.3 explicitly.

The Green's function for the purely advective case reads

$$G_{\mathrm{ad}}(r,r',\varphi,\varphi',z,z',t,t') = 2\delta(r^2 - r'^2 - Q/\pi(t-t'))\delta(\varphi-\varphi')\delta(z-z')\Theta(t-t'). \tag{4.40}$$

Starting with a line source of length L_z in vertical direction, $s(\vec{x},t) = \delta(r^2)\,\frac{1}{L_z}\Theta(1-z/L_z)$, we find for the effective width $\kappa_r^{2,\mathrm{eff}}(t)$ and for the ensemble width $\kappa_r^{2,\mathrm{ens}}(t)$

$$\kappa_r^{2,\mathrm{ens}}(t) = \sigma_f^2\sqrt{\pi}\,\frac{1}{3}\,Qt\,\frac{l_0}{\sqrt{Qt}} \qquad \text{and} \tag{4.41}$$

$$\kappa_r^{2,\mathrm{eff}}(t) = \sigma_f^2\sqrt{\pi}\,\frac{1}{3}\,Qt\,\frac{l_0}{\sqrt{Qt}} - \sigma_f^2\,\frac{2}{9}\,\frac{l_0\sqrt{Qt}}{\pi}F\left([1/2,1,3/2],[5/4,7/4,5/2],-\frac{Qt}{\pi l_0^2}\right)\cdot$$
$$\cdot\frac{l_0^2}{L_z^2}\left(\exp(/L - z^2/l_0^2) - 1 + \sqrt{\pi}\frac{L_z}{l_0}\mathrm{erf}(L_z/l_0)\right) \tag{4.42}$$

whereas for the effective width along a radial section it yields

$$\kappa_r^{2,\mathrm{eff}}(t)\big|_{\mathrm{sect}} = \sigma_f^2\,\frac{1}{3}\,Qt\,\frac{l_0}{\sqrt{Qt}}\left(\frac{3}{2}\frac{1}{\sqrt{\pi}}\frac{\sqrt{Qt}}{sqrt\pi l_0}F\left([2,1/2],[3,3/2],-\frac{Qt}{\pi l_0^2}\right) - \right.$$
$$\left.\mathrm{erf}\left(\frac{\sqrt{Qt}}{\sqrt{\pi l_0^2}}\right)\frac{l_0^2}{L_z^2}\left(\exp(-L_z^2/l_0^2) - 1 + \sqrt{\pi}\frac{L_z}{l_0}\mathrm{erf}(L_z/l_0)\right)\right) \tag{4.43}$$

F is a hypergeometric function. $\kappa_r^{2,\mathrm{ens}}(t)$ is equal to the result obtained by *Indelman and Dagan* [1999]. For the case of vanishing initial extension of the solute plume in vertical direction, $L_z = 0$, the effective width along a radial segment reduces to zero. There are no mixing mechanisms such as dispersion processes or artificial mixing by averaging over the azimutal coordinates. Hence, the injected solute forms an infinitively thin ring with spatially varying radius. This fluctuating line stays a line characterized by a vanishing width. The situation changes completely if one describes the fluctuating solute line averaged over all angles which results in a finite radial width $\kappa_r^{2,\mathrm{eff}}(t) = \sigma_f^2\sqrt{\pi}\,\frac{1}{3}\;Qt\,l_0/\sqrt{Qt} - \sigma_f^2\frac{1}{4}l_0^2 \neq 0$. This effective width is slightly smaller than the ensemble averaged width given by $\kappa_r^{2,\mathrm{ens}}(t) = \sigma_f^2\sqrt{\pi}\,\frac{1}{3}\;Qt\,l_0/\sqrt{Qt}$. On the other hand, in the limit of an infinitively extended line source, $L_z \to \infty$, all three ensemble averaged quantities become equivalent

$$\kappa_r^{2,\mathrm{ens}}(t) = \kappa_r^{2,\mathrm{eff}}(t) = \kappa_r^{2,\mathrm{eff}}(t)\big|_{\mathrm{sect}} = \sigma_f^2\sqrt{\pi}\,\frac{1}{3}\,Qt\,\frac{l_0}{\sqrt{Qt}} \tag{4.44}$$

It is noteworthy that the ensemble width does not depend on the vertical initial extension at all. This behaviour is also found for transport in uniform flow (*Attinger et al.* [1999]).

For finite initial extension L_z one finds an intermediate behaviour. Fig. (4.5) illustrates the temporal behaviour of the width for different initial extensions.

A mixing process over the azimutal direction already gives an effective width which is only slightly smaller than the ensemble width. For initial extensions larger than

a few correlation lengths there is almost no difference. With this result in mind, the calculations are restricted to the evaluation of the ensemble width for the two-dimensional case, assuming that the dispersive mixing causes a very efficient mixing mechanism over all angles. A realistic two-dimensional application in a porous medium will generally be extended in z-direction over some correlation length. As we have seen, this causes a mixing effect which makes the ensemble averaging reasonable, but does not affect the result quantitatively. The z-dimension will be excluded in the following.

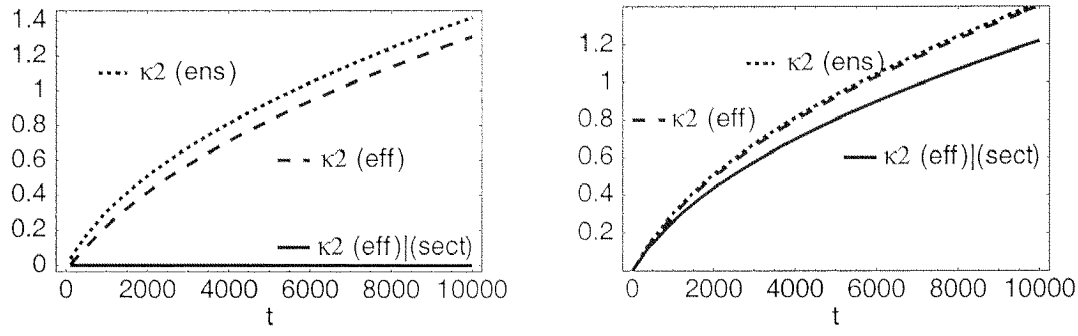

Figure 4.5: κ_2 for: $L_z/l_0 = 0.01$ $L_z/l_0 = 5$

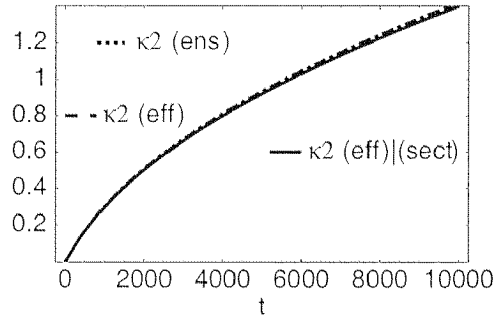

$L_z/l_0 = 50$

The cumulants κ_2 are growing with $\sqrt{t}$. Consequently, assigning an effective diffusion coefficient on the basis of Eq. (4.32) would lead to an expression that decreases with time. It is therefore more appropriate to assign to the system an effective dispersion coefficient that is proportional to the velocity field. The effective parameter would be the dispersion length α.

Following the considerations in Section 4.2.3, effective and ensemble dispersivities characterizing effective and ensemble transport behaviour can now be defined. The effective and the ensemble dispersion lengths are given by

$$\alpha^{\text{ens}} = \sigma_f^2 \frac{\sqrt{\pi}}{2} l_0 \tag{4.45}$$

$$\alpha^{\text{eff}} = \sigma_f^2 \frac{\sqrt{\pi}}{2} l_0 \left(1 - \frac{l_0^2}{L_z^2}\left(\exp(-L_z^2/l_0^2) - 1 + \sqrt{\pi}\frac{L_z}{l_0}\text{erf}(L_z/l_0)\right)\right), \tag{4.46}$$

respectively. The ensemble (4.45) and the effective dispersivity (4.46) result from travel time differences between different flow paths which are essentially determined

by the heterogeneous geometry of the medium. However, the full results for the ensemble averaged squared radial width

$$\kappa_r^{2,\mathrm{ens}} = \frac{1}{3} l_0 \sigma_f^2 \sqrt{Qt}\,\mathrm{erf}\left(\frac{\sqrt{Qt}}{\sqrt{\pi l_0^2}}\right) + l_0\sigma_f^2\left(\frac{1}{2}l_0 + \frac{1}{6}l_0^2\left(\frac{Qt}{\pi}\right)^{-1}\right)\left(1-\exp\left(-\frac{Qt}{\pi l_0^2}\right)\right) \tag{4.47}$$

show algebraic as well as exponential corrections to the asymptotic behaviour. This has also been found for transport in uniform flows (see e.g. *Dentz et al.* [1999]). In our case this behaviour at early time makes sure that the effective dispersion length is not divergent at the injection point.

$$\alpha_{\mathrm{eff}}(t\to 0) = \sigma_f^2\sqrt{\pi}/2\left[l_0\mathrm{erf}\left(\frac{\sqrt{Qt}}{\sqrt{\pi}l_0}\right) + \frac{\sqrt{Qt}}{\pi}\exp\left(-\frac{Qt}{\pi l_0^2}\right)\right], \tag{4.48}$$

4.2.6 Effective transport parameters for finite Peclet numbers

In this section the influence of local dispersion on the effective mixing process is investigated. Ensemble averaged second radial cumulants were calculated to first order in the inverse Peclet number combining Eqns. (4.50), (4.37) and (4.26). The z-dimension is not taken into account, the problem is considered as two-dimensional.

The difficulty of including dispersive effects lies in the fact that no explicit solution for the Green's function (4.38) is known. Even for transport with constant diffusion coefficients where the concentration distribution starting with a pulse-like solute injection at the injection well is known the different initial condition of injecting at an arbitrary point in space makes it inpossible to solve Eq. (4.38). Therefore, analogously to Section 4.2.3 a perturbation theory with respect to small inverse Peclet numbers is constructed. The derivatives with respect to the angle are neglected in the operator Δ. Using the purely advective part of the Green's function

$$G_{\mathrm{ad}}(r,r',\varphi,\varphi',t,t') = 2\delta(r^2 - r'^2 - \frac{Q}{\pi}(t-t'))\Theta(t-t')\delta(\varphi-\varphi') \tag{4.49}$$

the solution for the Green's function up to first order in the inverse Peclet number can be written as

$$G(r,r',\varphi,\varphi',t,t') = G_{\mathrm{ad}}(r,r',\varphi,\varphi',t,t') + \int r''dr'' \int d\varphi'' \int dt'' G_{\mathrm{ad}}(r,r'',\varphi,\varphi'',t,t'')\cdot \left(\frac{D_0}{r''}\partial_{r''}\left(r''\partial_{r''}\right)\right)\cdot G_{\mathrm{ad}}(r'',r',\varphi'',\varphi',t'',t') + \dots . \tag{4.50}$$

The approach (4.50) was tested by applying it to the homogeneous Eq. (4.11) where an exact homogeneous solution can be found. The moments were calculated

up to first order in the Peclet number. They reproduced exactly the cumulants (4.31) and (4.34) which was considered a confirmation of the approximation for the Green's function. Nevertheless, the validity of this approximation is limited. The expansion in D_0/Q to first order is only reasonable if diffusive effects do not dominate the transport behaviour on the scale of the heterogeneities. The Peclet number defined on this scale, $\sqrt{Q/\pi t}l_0/D_0$ has therefore to be larger than 1. This requirement leads to a restriction of the time domain and the results are only valid for times $t < (l_0^2 Q)/D_0^2$. However, for many realistic experimental setups, these are the times one is mainly interested in. Even for relatively high diffusion coefficients (e .g $D_0 = 10^{-5} m^2/s$) the time scale $(l_0^2 Q)/D_0^2$ is in the range of 100 days assuming a typical correlation length of about 1 meter.

Using Eq. (4.37) as concentration, the approximation (4.50) as Green's function, and (4.36) as autocovariance function the ensemble radial width in lowest order of small inverse Peclet numbers is obtained. The full expression is given in Appendix E.

In general, different time scales can be identified to characterize different time behaviour of the transport parameters. There are the advective time scale $\tau_{\text{adv}} = l_0^2/Q$ and, taking the diffusive effect into account, a further time scale: $\tau_{\text{disp}} = (l_0^2 Q)/D_0^2$. The advective time scale is usually much smaller than the diffusive one.

$$\tau_{\text{adv}} \ll \tau_{\text{disp}} \tag{4.51}$$

For times $t > \tau_{\text{adv}}$ we again find an enhanced spreading of the solute plume. The heterogeneous flow fields first of all cause the same advectively dominated mixing process as was found already in the purely advective transport. However, taking into account diffusion effects additional contributions to the enhanced ensemble width become prevalent. While the asymptotic value for the ensemble width of the solute distribution is reached very fast, namely already for times $t > \tau_{\text{adv}}$, the time to reach the asymptotic behaviour for transport including diffusive effects is in general much larger and given by $t \gg \tau_{\text{disp}}$.
For intermediate times, $\tau_{\text{adv}} < t < \tau_{\text{disp}}$, which are realistic times for measurment to be taken, one sees still a linear increase of the ensemble width with time which is caused by the diffusive processes which is enhanced due to the heterogeneities.

Explicitly, for times $(l_0^2)/Q < t < (l_0^2 Q)/D_0^2$, the second radial cumulant writes

$$\kappa_r^{2,\text{ens}} = D_0\, t + \sigma_f^2 \left(\frac{1}{3} l_0 \sqrt{Qt} + D_0\, t\right) \tag{4.52}$$

Using the analogy to mechanical dispersion, where the dispersion coefficient is proportional to the velocity field, an effective diffusion coefficient D^{eff} and an effective dispersivity α^{eff} can be defined as

$$\begin{aligned} D^{\text{eff}} &= (1 + \sigma_f^2)\, D_0 \\ \alpha^{\text{eff}} &= \sigma_f^2 \frac{\sqrt{\pi}}{2} l_0. \end{aligned} \tag{4.53}$$

Figs. (4.6) through (4.8) illustrate the role of the Peclet number for intermediate times. The second radial cumulant, representing the quantity that would be measured in an experiment, is plotted over time. Two parts of Eq. (4.52) are considered, the first part of which includes only purely advective macrodispersion

$$(\kappa_r^{2,\mathrm{ens}})(\mathrm{adv}) = \sigma_f^2 \, (\frac{1}{3} l_0 \sqrt{Qt}) \tag{4.54}$$

This would correspond to the result obtained for infinite Peclet number. Second, the whole expression for the cumulant Eq. $(\kappa_r^{2,\mathrm{ens}})$ in (4.52) is considered. The parameters are chosen as: $Q = 10^{-2} m^2/s$, $D_0 = 10^{-5} m^2/s$, $l_0 = 1m$ and $\sigma_f^2 = 0.5$. This choice of numbers leads to small Peclet numbers, $Q/D = 10^{-3}$, which can be found in gas flow experiments (compare *Ng and Mei* [1996]). In Fig. (4.7) the dispersion length calculated from the two parts of $\kappa_r^{2,\mathrm{ens}}$ using (4.35) is plotted. The advective part is denoted by $\alpha^{\mathrm{ens}}(\mathrm{adv})$. In Fig. (4.8) the effective diffusion, which is the more relevant quantity for the comparison to the two-phase flow process is calculated from the two parts of $\kappa_r^{2,\mathrm{ens}}$ using Eq. (4.32) is plotted. The advective part is denoted by $D(\mathrm{adv})$.

On larger time-scales the impact of the linear increase of $\kappa_r^{2,\mathrm{ens}}$ with time due to the diffusive effects is already visible. On a time scale of 10^4 seconds 10 per cent of the whole dispersivity is already diffusive. This is the time needed to transport the solute over the radial length of some meters. In experiments with small Peclet numbers neglecting of these effects can lead to an overestimation of the mechanical dispersion effects.

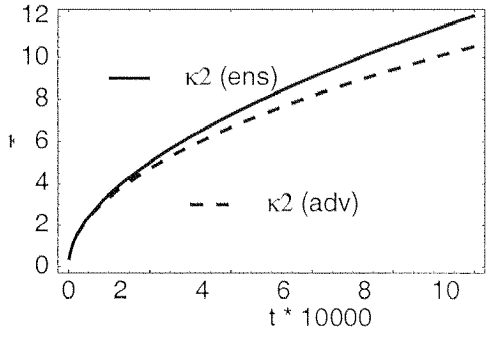

Figure 4.6: $(\kappa_r^{2,\mathrm{ens}})$ and $(\kappa_r^{2,\mathrm{ens}})(\mathrm{adv})$

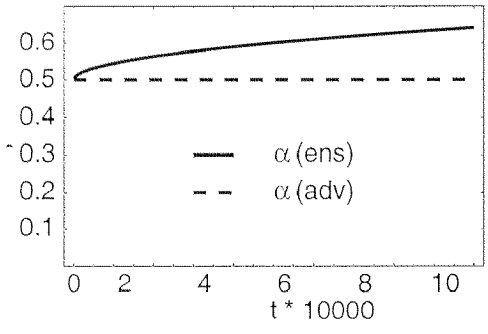

Figure 4.7: α^{ens} and $\alpha^{\mathrm{ens}}(\mathrm{adv})$

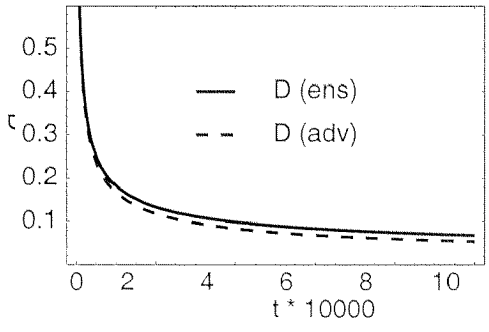

Figure 4.8: D and $D(\mathrm{adv})$

If parameters are chosen which are realistic for solute transport in the water phase, such as $Q = 10^{-3}m^2/s$, $D_0 = 10^{-8}m^2/s$, $\alpha = 0.01m$, $l_0 = 1m$ and $\sigma_f^2 = 0.5$, leading to $Q/D = 10^{-5}$, the diffusive effects are hardly visible and can be neglected.

To summarize, we have discussed the effective parameters for tracer transport in a radially diverging flow field considering diffusion only. It has been observed, that at intermediate times the diffusion is enhanced due to the heterogeneous flow field. However, the increase measured in units of the homogeneous dispersion coefficient is just the variance of the permeability field and is therefore small. Another effect that is dominant at small times is a dispersion effect due to the fluctuations of the solute center of mass in the heterogeneous flow field, where the dispersion constant can be written as a product of the dispersion length and the velocity field. The effective dispersion length is proportional to the variance of the permeability field and its correlation length. This result is valid for finite but small Peclet numbers and for intermediate times.

4.3 Radial two-phase flow

As the effective mixing processes for solute transport are known similar approaches will in the following be compared to the two-phase flow problem, which will also be treated in the framework of a perturbation theory.

Some progress in the determination of effective properties has also been made in two-phase flow with the methods based on the stochastic approach. Numerical investigations such Monte Carlo simulations can be performed in a straightforward manner (e.g. *Abdin et al.*, [1995]). Also grid oriented upscaling with renormalization techniques, well established for single phase flow, have been extended to two-phase flow in order to determine effective permeability (*King et al.*, [1993] or *Hansen et al.*, [1997]). However, analytical methods based on a continuum approach are difficult to apply. Effective properties calculated analytically were obtained with methods such as volume averaging (see e.g. *Dale et al.* [1997], or *Quintard and Whittaker*, [1988]) or homogenization theory (e.g. *Bourgeat*, [1997] or *Amaziane et al.*, [1991]). However, these results are usually for boundary conditions different from the ones used here and it is hard to obtain explicit results.

Also, perturbation theory was used to investigate the influence of small scale heterogeneities on the large scale flow behaviour in two-phase flow. In most cases this has been done for water flow through the unsaturated zone, a two-phase flow system of air and water, where the pressure in the gas phase is assumed to be in equilibrium instantaneously and therefore to have no gradients. *Mantoglou and Gelhar* [1987], *Yeh et al.* [1985] or *Zhang* [1999] investigated systems like these using a perturbation theory to second order in the variability of log conductivity and capillary pressure. Their theory has been extended to the general two-phase flow with pressure gradients in both phases by *Chang et al.* [1995] and for three-phase flow by *Abdin and Kaluarachchi* [1997]. They investigated the impact of the variability of absolute permeability and capillary pressure on the pressure and flow variances and

on effective permeability. The results were confirmed by additional Monte Carlo calculations (*Abdin et al.*, [1995]). These studies are performed for steady state conditions. However, steady state conditions are not given in the problem we are considering here and the dynamics have to be included.

The nonlinearities of the flow equations make it difficult to use perturbation theory methods. For example by linearizing the equations essential features of the nonlinear behaviour cannot be captured. It is therefore an important task to take into account the nonlinearities as thoroughly as possible. Therefore, a functional perturbation expansion for the two-phase flow equation around the homogeneous fully nonlinear solution for the saturation distribution is applied in this section. A similar approach has been used by *Foussereau et al.* [1999] for the analysis of solute transport through the unsaturated zone. In their analysis the pressure gradient in the water phase is equal to the gradient of capillary pressure. It is therefore possible to establish a system of equations that depends on a single variable only which is the water saturation. For the general two-phase flow equations used here, this is not possible due to the coupling of the continuity equation and Darcy's law via the saturations. It is however reasonable to take the fluctuations of the flow field itself as a functional expansion parameter.

The perturbation approach used here was also applied to the problem of solute transport with a nonlinear isotherm by *Attinger and Kinzelbach* [1999] who derived an effective dispersion coefficient.

In the following the perturbation approach is explained and we describe the features of the important quantities in more detail. Then the approach is applied to the Buckley Leverett problem where the capillary pressure is neglected. The result is compared and improved with the methods of homogenization theory. Finally, the result is compared to numerical simulations.

4.3.1 Effective mixing parameters: Perturbation theory

In order to develop an expression for the gas saturation in the heterogeneous flow field, a more general perturbation formulation than the one in Section 4.2 has to be established. The flow field varies in space and is, in analogy to Section 4.2, divided into its average part and the fluctuations.

$$\vec{q}_{\text{total}} = \overline{\vec{q}_{\text{total}}} + \tilde{q}_{\text{total}}(\vec{x}) = \frac{Q}{2\pi r}\vec{e}_r + \tilde{q}_{\text{total}}(\vec{x}), \qquad \overline{\tilde{q}_{\text{total}}(\vec{x})} = 0. \tag{4.55}$$

Here, $\vec{q}_{\text{total}}$ denotes the total flux and in the following is simply written as $\vec{q}$. It has to be emphasized, that the capillary pressure is assumed to be constant and homogeneous. Of course this is an approximation, as in general the properties of the capillary pressure are coupled to the permeability over a Leverett scaling as explained in Chapter 3. The formulation (4.55) is therefore only valid if capillary effects are very small. In this work they will be excluded later, and we only consider the Buckley Leverett case.

The gas saturation can be expanded into a functional expansion with respect to the fluctuations of the flow field $\tilde{q}$. This functional expansion can be considered as an infinitely dimensional Taylor expansion, where each location $\vec{x}'$ represents one dimension. Considering the space not as a continuum but as a grid with gridpoints at x_{ij}, the saturation would be expanded with respect to the fluctuations at each grid point x_{ij}.

$$S = S_0 + \sum_k \sum_{i,j} \frac{\delta S}{\delta \tilde{q}_k(x_{ij})} \tilde{q}_k(x_{ij}) + \sum_{k,k'} \sum_{i,j,i',j'} \frac{1}{2} \frac{\delta^2 S}{\delta \tilde{q}_k(x_{ij}) \delta \tilde{q}_{k'}(x_{i'j'})} \tilde{q}_k(x_{ij}) \tilde{q}_{k'}(x_{i'j'}) + \dots \tag{4.56}$$

In the transition from grid to continuum, the sum over the dimensions (i, j) becomes an integral over space. S_n contains the part of the total saturation, that is influenced by the n-fold product by the fluctuations $\tilde{q}$.

$$\begin{aligned} S(\vec{x}, t) = S_0(\vec{x}, t) + \int d^d x' \, \frac{\delta S}{\delta \{\tilde{q}_{\text{total}}(\vec{x'})\}} \tilde{q}_{\text{total}}(\vec{x'}) + \\ \frac{1}{2} \int d^d x' \int d^d x'' \, \frac{\delta^2 S}{\delta \{\tilde{q}_{\text{total}}(\vec{x'})\} \delta \{\tilde{q}_{\text{total}}(\vec{x''})\}} \tilde{q}_{\text{total}}(\vec{x'}) \tilde{q}_{\text{total}}(\vec{x''}) + \dots \equiv \\ \equiv S_0(\vec{x}, t) + S_1(\vec{x}, t, \{\tilde{q}\}) + S_2(\vec{x}, t, \{\tilde{q}\tilde{q}\}) + \dots \end{aligned} \tag{4.57}$$

The functions ψ_1 and ψ_2 can be expanded around the homogeneous solution S_0,

$$\psi_i(S) = \psi_i|_{S_0} + \left.\frac{\partial \psi_i}{\partial S}\right|_{S_0} (S_1 + S_2 + \dots) + \frac{1}{2} \left.\frac{\partial^2 \psi_i}{\partial S^2}\right|_{S_0} (S_1 + S_2 + \dots)^2 + \dots . \tag{4.58}$$

Inserting Eqns. (4.57) and (4.58) into the flow equations (4.5) yields

$$\begin{aligned} &\partial_t (S_0 + S_1 + S_2 + \dots) + \\ &\vec{\nabla} \cdot \left\{ \left[\psi_1|_{S_0} + \tfrac{\partial \psi_1}{\partial S}|_{S_0} (S_1 + S_2 + \dots) + \tfrac{1}{2} \left.\tfrac{\partial^2 \psi_1}{\partial S^2}\right|_{S_0} (S_1 + S_2 + \dots)^2 + \dots \right] \cdot \right. \\ &\cdot (\overline{q} + \tilde{q}) - \left[\psi_2|_{S_0} + \tfrac{\partial \psi_2}{\partial S}|_{S_0} (S_1 + S_2 + \dots) + \tfrac{1}{2} \left.\tfrac{\partial^2 \psi_2}{\partial S^2}\right|_{S_0} (S_1 + S_2 + \dots)^2 + \dots \right] \\ &\left. \cdot \vec{\nabla} (S_0 + S_1 + S_2 + \dots) \right\} = 0 \end{aligned} \tag{4.59}$$

This equation can be arranged in orders of the fluctuation $\tilde{q}$, leading to an infinite set of coupled differential equations for the single orders of the contributions of the fluctuation to the gas saturation. This makes it possible to investigate explicitly a

certain order of the fluctuations in the gas saturation.

$$
\begin{aligned}
&\rightarrow \text{ 0-th order:} \\
&\partial_t S_0 + \vec{\nabla} \cdot \left[\psi_1|_{S_0} \, \bar{\vec{q}} - \psi_2|_{S_0} \, \vec{\nabla} S_0 \right] = 0 \\
&\rightarrow \text{ 1-th order:} \\
&\partial_t S_1 + \vec{\nabla} \cdot \left[\psi_1|_{S_0} \, \tilde{q} + \left. \frac{\partial \psi_1}{\partial S} \right|_{S_0} S_1 \bar{\vec{q}} - \vec{\nabla} (\psi_2|_{S_0} \, S_1) \right] = 0 \\
&\rightarrow \text{ 2-nd order:} \\
&\partial_t S_2 + \vec{\nabla} \cdot \left[\left. \frac{\partial \psi_1}{\partial S} \right|_{S_0} S_1 \tilde{q} + \left. \frac{\partial \psi_1}{\partial S} \right|_{S_0} S_2 \bar{\vec{q}} + \frac{1}{2} \left. \frac{\partial^2 \psi_1}{\partial S^2} \right|_{S_0} S_1^2 \bar{\vec{q}} \right. \\
&\left. - \vec{\nabla} (\psi_2|_{S_0} \, S_2) - \frac{1}{2} \vec{\nabla} \left(\left. \frac{\partial \psi_2}{\partial S} \right|_{S_0} S_1^2 \right) \right] = 0 \\
&\quad \vdots
\end{aligned}
\tag{4.60}
$$

The equation for the 0-th order is the homogeneous flow equation. It includes all nonlinearities. The equations for the higher orders are nonlinear in time and space, but by construction they are all linear in S_n. Therefore we can transform the differential equation for S_n into an integral equation with the help of Green's functions. The solution for S_n depends on the lower orders $S_{n-1}, S_{n-2}, \ldots, S_0$ and as there is no known solution for S_0 the equations cannot be solved explicitly. The integral equation for S_n reads

$$
S_n = \int d^d x' \, dt' \; G_n(\vec{x}, \vec{x}', t, t') \mathcal{O}_n(\vec{x}', t'). \tag{4.61}
$$

where G is the Green's function solving

$$
\partial_t G + \vec{\nabla} \cdot \left[\left. \frac{\partial \psi_1}{\partial S} \right|_{S_0} \bar{\vec{q}} G - \vec{\nabla} (\psi_2|_{S_0} \, G) \right] = \delta^d(\vec{x} - \vec{x}') \delta(t - t'). \tag{4.62}
$$

G is the same function for all orders n. On the other hand The right hand side of the differential equation, $\mathcal{O}_n(\vec{x}', t')$, is dependent on the order n. The lower orders $n-1, n-2, \ldots$ of S enter the equations via $\mathcal{O}_n$.

The first and second order of $\mathcal{O}$ read

$$
\begin{aligned}
\mathcal{O}_1(\vec{x}, t) &= \vec{\nabla} \left[\psi_1|_{S_0(x,t)} \, \tilde{q}(\vec{x}) \right] \\
\mathcal{O}_2(\vec{x}, t) &= \vec{\nabla} \left[\left. \frac{\partial \psi_1}{\partial S} \right|_{S_0(x,t)} S_1(\vec{x}, t) \tilde{q} + \frac{1}{2} \left. \frac{\partial^2 \psi_1}{\partial S^2} \right|_{S_0(x,t)} (S_1(\vec{x}, t))^2 \, \bar{\vec{q}} - \right. \\
&\quad \left. - \frac{1}{2} \vec{\nabla} \left(\left. \frac{\partial \psi_2}{\partial S} \right|_{S_0(x,t)} (S_1(\vec{x}, t))^2 \right) \right].
\end{aligned}
\tag{4.63}
$$

Inserting Eq. (4.63) in (4.61) leads to an integral equation for the contributions of the first and second order of the fluctuations to the saturation,

$$S_1(\vec{x},t) = \int d^dx' \int dt'\, G(\vec{x},\vec{x}',t,t') \left.\frac{\partial\psi_1}{\partial S}\right|_{S_0(x',t')} \tilde{q}(\vec{x}')\vec{\nabla}' S_0(\vec{x}',t'). \tag{4.64}$$

$$\begin{aligned} S_2(\vec{x},t) = & \int d^dx' \int d^dx'' \int dt' \int dt''\, G(\vec{x},\vec{x}',t,t')\vec{\nabla}' \cdot \\ & \left[\left.\frac{\partial\psi_1}{\partial S}\right|_{S_0(x',t')} \tilde{q}(\vec{x}') G(\vec{x}',\vec{x}'',t',t'') \left.\frac{\partial\psi_1}{\partial S}\right|_{S_0(x'',t'')} \tilde{q}(\vec{x}'')\vec{\nabla}'' S_0(\vec{x}'',t'') \right] + \\ & + \frac{1}{2} \int d^dx' \int d^dx'' \int d^dx''' \int dt' \int dt'' \int dt'''\, G(\vec{x},\vec{x}',t,t')\vec{\nabla}' \cdot \\ & \left[\left(\left.\frac{\partial^2\psi_1}{\partial S^2}\right|_{S_0(x',t')} \vec{q} - \vec{\nabla}' \left.\frac{\partial\psi_2}{\partial S}\right|_{S_0(x',t')} \right) G(\vec{x}',\vec{x}'',t',t'') \left.\frac{\partial\psi_1}{\partial S}\right|_{S_0(x'',t'')} \tilde{q}(\vec{x}'') \right. \\ & \left. \vec{\nabla}'' S_0(\vec{x}'',t'') G(\vec{x}',\vec{x}''',t',t''') \left.\frac{\partial\psi_1}{\partial S}\right|_{S_0(x''',t''')} \tilde{q}(\vec{x}''')\vec{\nabla}''' S_0(\vec{x}''',t''') \right]. \end{aligned} \tag{4.65}$$

If the functions ψ_1 and ψ_2 are chosen as $\psi_1 = C_1 \cdot S$ and $\psi_2 = C_2$ (which leads to the solute transport problem as described in Section 4.2), the perturbation expansion reduces to the linear perturbation expansion (4.39). In order to analyze the effective parameters, three issues have to be discussed in more detail. First, the homogeneous solution has to be known. Moreover, the Green's function of the system, $G(x,x',t,t')$, has to be known and finally, the stochastic properties of the fluctuations of the flow field have to be given. Since none of these quantities can be derived exactly, approximations have to be used.

Homogeneous solution - scaling functions

The homogeneous flow equation in cylindrical coordinates and with a constant volumetric fluid injection rate is given by

$$\partial_t S_0 + \frac{d\psi_1(S_0)}{dS_0}\partial_r S_0 \frac{Q}{2\pi r} - \frac{d\psi_2(S_0)}{dS_0}(\partial_r S_0)^2 - \psi_2(S_0)\frac{1}{r}\partial_r S_0 - \psi_2(S_0)\partial_r^2 S_0 = 0. \tag{4.66}$$

Here it is assumed that in the homogeneous case the solution has no dependence on the angle which is a reasonable assumption as the inflow condition is also cylindrically symmetric. The initial- and the boundary conditions read

$$\begin{aligned} & S_0(r,0) = 0 \quad \text{for} \quad r \neq 0, \qquad S_0(0,t) = 1 \quad \text{for} \quad t \neq 0, \\ & S_0(r \to \infty, t) = 0 \quad \text{for finite time } t. \end{aligned} \tag{4.67}$$

The more realistic condition $S_0(0,t) = \text{const.}$ corresponds to the condition $S_0(0,t) = 1$ for a porous medium with normalized porosity. Considering an ensemble of porous

media, this condition is only reasonable if the capillary pressure is assumed to be constant. Otherwise the constant initial saturation would change from realization to realization and the corresponding media with initial saturation $S_0(0,t) = 1$ would have different mean flow velocities due to the different porosities.

To the best of our knowledge, there is no solution for this system of equations for any nontrivial choice of ψ_1 or ψ_2. However, a similarity solution can be found for this problem. For this purpose we write a polynomial expansion of ψ_1 and ψ_2.

$$\psi_1(S_0) = \sum_i c_i S_0^{\gamma_i}, \qquad \psi_2(S_0) = \sum_i d_i S_0^{\delta_i}. \tag{4.68}$$

A similarity variable is defined as

$$\eta = \frac{r}{t^a} \tag{4.69}$$

and the saturation is assumed to have the behaviour

$$S_0 = t^b S^\star(\eta) \quad \text{for} \quad t \to \infty. \tag{4.70}$$

With this, Eq. (4.66) becomes

$$\begin{aligned} &bS^\star - \eta\partial_\eta S^\star + \frac{Q}{2\pi\eta}\partial_\eta S^\star \sum_i c_i\gamma_i t^{(1+(\gamma_i-1)b-2a)}(S^\star)^{\gamma_i-1} - \\ &(\partial_\eta S^\star)^2 \sum_i d_i\delta_i t^{(1+\delta_i b-2a)}(S^\star)^{\delta_i-1} - \frac{1}{\eta}\partial_\eta S^\star \sum_i d_i t^{(1+\delta_i b-2a)}(S^\star)^{\delta_i} - \\ &\partial_\eta^2 S^\star \sum_i d_i t^{(1+\delta_i b-2a)}(S^\star)^{\delta_i} = 0 \end{aligned} \tag{4.71}$$

The choice of a and b is determined by the boundary conditions and by the polynomial orders γ_i and δ_i. First of all, since S_0 has a constant value at $r = 0$ and $t = 0$ and cannot exceed the value 1, positive values for b would be unphysical. Taking this into account the requirement that $S^\star$ does not depend on the time t explicitly in the limit of long times leads to the relation

$$\begin{aligned} 1 + (\min(\gamma_i) - 1)b - 2a = 0 \qquad &\text{for} \quad \min(\gamma_i) < \min(\delta_i) + 1 \\ 1 + (\min(\delta_i))b - 2a = 0 \qquad &\text{for} \quad \min(\gamma_i) > \min(\delta_i) + 1, \end{aligned} \tag{4.72}$$

as $S^\star$ is supposed to become independent of time t. In general it would be sufficient to restrict the left hand side of (4.72) to values which are smaller than the right hand side, but the inequality would lead to an unphysical solution of the gas saturation in the long time limit. The case distinction (4.72) also decides, which process dominates the shape of the gas saturation for long times. In the first case where $(\min(\gamma_i) < \min(\delta_i)+1)$ the "advective" part is prevalant, whereas in the second case $(\min(\gamma_i) > \min(\delta_i) + 1)$ the "diffusive" part is dominant.

The conservation of mass gives another constraint for the parameters a and b. Under the assumption of incompressibility we have

$$\int_0^{2\pi} d\varphi \int_0^\infty r\, dr S(r,t) = 2\pi t^{(2a+b)} \int_0^\infty d\eta\eta S^\star(\eta) = V(S_0)(t). \tag{4.73}$$

V is the volume of gas at time t. We are considering two cases, on the one hand the constant injection of air and on the other hand the flow of one unit volume of air in a radial flow of water. The second case is chosen to have a comparison to the transport of one unit mass of solute in the solute transport case. The second case leads to

$$V(S_0)(t) = 1 \rightarrow 2a + b = 0 \tag{4.74}$$

which combines with (4.72) to

$$\min(\gamma_i)b = -1 \rightarrow b = -\frac{1}{\min(\gamma_i)} \rightarrow a = \frac{1}{2\min(\gamma_i)} \tag{4.75}$$

or

$$b = -\frac{1}{\min(\delta_i) + 1} \rightarrow a = \frac{1}{2(\min(\delta_i) + 1)} \tag{4.76}$$

respectively.

For the parametrizations chosen in Fig. (4.1), we would have the case $\min(\gamma_i) = 3$ and $\min(\delta_i) = 3$, which means the gas saturation has a similarity solution

$$\lim_{t\rightarrow\infty} S(r,t) = t^{-1/3} S^\star\left(\frac{r}{t^{1/6}}\right). \tag{4.77}$$

For the constant inflow rate we get

$$V(S_0)(t) = Qt \rightarrow 2a + b = 1 \tag{4.78}$$

which leads to the condition

$$b = 0 \rightarrow a = \frac{1}{2}. \tag{4.79}$$

This is valid, independently of the choice of the functions ψ_1 and ψ_2. The similarity solution has the form

$$\lim_{t\rightarrow\infty} S(r,t) = S^\star\left(\frac{r}{t^{1/2}}\right). \tag{4.80}$$

In this special case the nonlinearities have no influence on the longtime behaviour of the solution and the scaling behaviour is the same for the linear or the nonlinear case. The boundary conditions can be transformed into

$$S^\star(0) = 1, \qquad S^\star(\lim \eta \rightarrow \infty) \rightarrow 0 \tag{4.81}$$

With the scaling function, the leading time behaviour of the radial moments of the gas saturation can be estimated. For the general case we get

$$m_r^{(n)}(t) = \int_0^{2\pi} d\varphi \int_0^\infty r\, dr r^n t^b S^\star(\eta) = 2\pi t^{((n+2)a+b)} \int_0^\infty d\eta \eta^{n+1} S^\star(\eta) \tag{4.82}$$

A necessary condition for the existence of the solution is the existence of all moments of the saturation. Therefore, the rescaled solution $S^\star$ has to decrease to 0 faster than all algebraic orders for $\eta \to \infty$ if the moments do not vanish due to symmetry reasons. The zeroth, first and second moment of the saturation for the case of flow of one mass unit of gas and for $\min(\gamma_i) = 3$ read

$$m_r^{(n)}(t) \propto t^{n/(2\min(\gamma_i))} \quad \to \quad m_r^{(0)}(t) \propto \text{const.}, \quad m_r^{(1)}(t) \propto t^{1/6}, \quad m_r^{(2)}(t) \propto t^{1/3}. \tag{4.83}$$

For the case of constant inflow rate the moments we get are

$$m_r^{(0)}(t) \propto t, \quad m_r^{(1)}(t) \propto t^{3/2}, \quad m_r^{(2)}(t) \propto t^2 \quad \to \quad \frac{m_r^{(1)}}{m_r^{(0)}} \propto \sqrt{t}, \quad \frac{m_r^{(2)}}{m_r^{(0)}} \propto t. \tag{4.84}$$

If we compare the leading time behaviour of the moments with the leading time behaviour of solute transport Eqns. (4.30) and (4.31), we note, that the time behaviour is the same for the case of constant inflow. It differs for the flow of one mass unit of gas and the transport of one mass unit of tracer. In this case, depending on the form of the nonlinearities, the moments of the gas saturation grow slower than in the moments of solute concentration. It is only in the special case of constant inflow rate, that the equivalence of linear and nonlinear case in the leading time behaviour of the moments is independent of the choice of ψ_1 and ψ_2.

Green's functions

The differential equation for the Green's function in cylindrical coordinates reads

$$\begin{aligned} &\partial_t G + \partial_r \left(\frac{d\psi_1(S_0)}{dS_0} \frac{Q}{2\pi r} G \right) - \frac{1}{r} \partial_r \left(\psi_2(S_0) G \right) - \\ &\partial_r^2 \left(\psi_2(S_0) G \right) - \psi_2(S_0) \frac{1}{r^2} \partial_\varphi^2 G = \frac{1}{r} \delta(r - r') \delta(\varphi - \varphi') \delta(t - t'). \end{aligned} \tag{4.85}$$

The equation has a translation symmetry in the angle φ, which can be transferred to $\varphi^\star = \varphi - \varphi'$. Due to the nonlinear behaviour in time and space this equation cannot be simplified further. However, for the point $\vec{x}' = 0, t' = 0$ a similarity solution can be found for G. Under these conditions G does not depend on the angle φ. For S_0 we assume the similarity solution for constant inflow $S_0(r,t) = S_0(\eta) = S_0(r/t^{1/2})$. Introducing again

$$\zeta = \frac{r}{t^a} \quad \text{and} \quad \lim_{t \to \infty} \quad G(r,0,t,0) = t^b G^\star(\zeta) \tag{4.86}$$

leads to

$$\begin{aligned} &bG^\star - \zeta\partial_\zeta G^\star + t^{1-2a}\frac{d^2\psi_1(S_0)}{dS_0^2}\frac{Q}{2\pi\zeta}\partial_\eta S_0 G^\star + t^{1-2a}\frac{d\psi_1(S_0)}{dS_0}\frac{Q}{2\pi\zeta}\partial_\zeta G^\star - \\ &t^{1-2a}\psi_2(S_0)\frac{1}{\zeta}\partial_\zeta G^\star - t^{1-2a}\psi_2(S_0)\partial_\zeta^2 G^\star - \\ &t^{1/2-a}2\frac{d\psi_2(S_0)}{dS_0}\partial_\eta S_0\partial_\zeta G^\star - t^{1/2-a}\frac{d\psi_2(S_0)}{dS_0}\frac{1}{\zeta}\partial_\eta S_0 G^\star - \\ &\frac{d\psi_2(S_0)}{dS_0}\partial_\eta^2 S_0 G^\star - \frac{d^2\psi_2(S_0)}{dS_0^2}(\partial_\eta S_0)^2 G^\star = t^{1-b-2a}\frac{1}{\zeta}\delta(\zeta)\delta(\varphi)\delta(t). \end{aligned} \tag{4.87}$$

Combined with the normalization condition, that the integral of the Green's function over space has to be equal to 1, we get

$$b=-1, a=1/2 \quad \rightarrow \quad \zeta=\eta \quad \rightarrow \quad G(r,0,t,0)=\frac{1}{t}G^\star\left(\frac{r}{t^{1/2}}\right)=\frac{1}{t}G^\star(\eta). \tag{4.88}$$

The time behaviour of the Green's function for $r'=0$ and $t'=0$ does not depend on the functions ψ_1 and ψ_2 if the inflow rate is constant over time. However, more information about the Green's function is not available and in the general case we have

$$G = G(r, r', \varphi-\varphi', t, t') \tag{4.89}$$

Covariance of the flow field

The fluctuations of the flow field are derived from Darcy's law. For the two-phase flow, the Darcy equation depends on the saturation via the relative permeability. The covariance of the fluctuations of the velocity field depends on the saturation S_0 as well and its derivation is rather complicated. As a simplification we therefore assume that the main influence on the radial moments is caused by the fluctuations of the radial part of the flow field, as in the case of solute transport. Furthermore we assume a simple Gaussian covariance, as in the solute transport case, and neglect all dependencies on the saturation.

$$\overline{\tilde{q}(\vec{x})\tilde{q}(\vec{x}')} = \sigma_f^2\frac{Q^2}{4\pi^2 rr'}\exp\left(-\frac{(r-r')^2}{l_0^2}\right), \tag{4.90}$$

where σ_f^2 is the variance of the log permeability field and l_0 the correlation length. This approximation is reasonable if the main influence of the fluctuations is given by the permeabilities and the differences in the relative permeabilities are not too high. Therefore on the one hand we need to restrict the variance of log permeability to not too high values, as we truncate the perturbation expansion after the second order, but on the other hand it should not be too small, as in this case the approximation of the covariance is not reasonable. The region where this approach is most questionable is at the front of the gas saturation, as in this region big changes of saturation occur over small distances.

It is also assumed that the reaction of the gas to the permeabilities is similar to the one of water.

In the limit of small correlation length $l_0 \to 0$ the covariance (4.90) reads

$$\lim_{l_0 \to 0} \overline{\tilde{q}(\vec{x})\tilde{q}(\vec{x}')} = \sigma_f^2 \frac{Q^2}{4\pi^2 r r'} l_0 \sqrt{\pi} \delta(r - r') \tag{4.91}$$

Buckley-Leverett flow: Results

As the possibilities of applying perturbation theory to nonlinear systems are limited the following considerations are restricted to the problem of Buckley-Leverett flow. In Buckley-Leverett flow the assumption is made that the influence of capillary forces can be neglected compared to the pressure gradients. The flow is purely "advective", but still nonlinear due to the relative permeabilities. For Eq. (4.5) this means that the function ψ_2 vanishes. We have seen in the problem of radial solute transport that the main effect of the fluctuating velocity field is due to the purely advective part, which leads to a macrodispersion term. The influence of finite Peclet number is not negligible for all cases. However, if the Peclet numbers are small the main effect is still the caused by the advective part. With this result in mind and knowing that the analysis for the nonlinear problem is based on strong assumptions and can only lead to qualitative results, it seems reasonable to concentrate on the part of the whole problem from which the most important effect is expected. Typical behaviour for Buckley-Leverett solutions is a sharp front of the gas saturation (see e.g. *Marle* [1981]). An example of the outcome of a numerical simulation for the radial Buckley Leverett problem in a homogeneous medium is shown in Fig. (4.9).

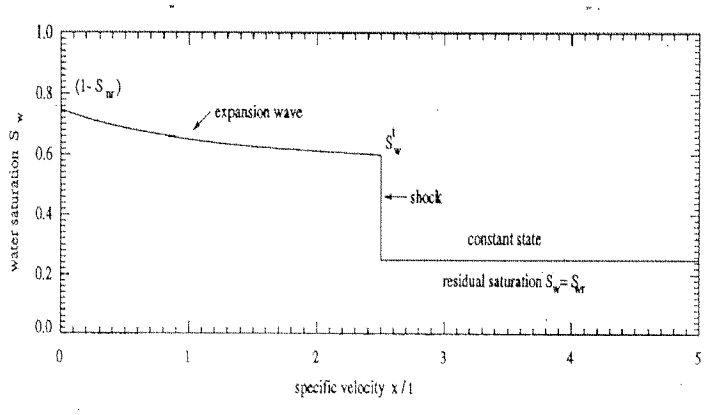

Figure 4.9: Buckley Leverett profile, taken from *Helmig* [1997]

We expect an effective mixing process for the Buckley Leverett case, similar to the purely advective solute transport problem. However, here the effective mixing parameter cannot be obtained from the radial moments, but has to be derived appropriately from the homogeneous problem. We consider two different types of mixing process. First we assume that the mixing is purely diffusive, leading to the

flow equation:

$$\partial_t S + \partial_r \psi_1(S) \frac{Q}{2\pi r} - \frac{D_0}{r} \partial_r \psi_3(S) - D_0 \partial_r^2 \psi_3(S) = 0. \tag{4.92}$$

ψ_3 is an unknown function of S and D_0 is the diffusion coefficient. We assume that the solution S is cylindrically symmetric. The diffusion coefficient D_0 can then be obtained by the definition

$$D_0 = \frac{1}{4} \frac{\int_0^\infty r\, dr\, r^2 \partial_t S - \frac{Q}{\pi} \int_0^\infty r\, dr\, \psi_1(S)}{\int_0^\infty r\, dr\, \psi_3(S)}. \tag{4.93}$$

Alternatively we assume a dispersive mixing process, where the dispersion coefficient is proportional to the flow velocity field, leading to the flow equation

$$\partial_t S + \partial_r \psi_1(S) \frac{Q}{2\pi r} - \frac{\alpha Q}{2\pi r} \partial_r^2 \psi_3(S) = 0. \tag{4.94}$$

α is the dispersivity. We can then obtain the dispersivity via the definition

$$\alpha = \frac{1}{6Q} \frac{\int_0^\infty r\, dr\, r^3 \partial_t S - \frac{3}{2} \frac{Q}{\pi} \int_0^\infty r\, dr\, r \psi_1(S)}{\int_0^\infty r\, dr\, \psi_3(S)}. \tag{4.95}$$

To derive effective properties for the heterogeneous problem we have to perform the ensemble average of (4.93) or (4.95) in a perturbation theory approach. If the effective parameters are not constant in time in the long time limit, the approach for the large scale mixing process is not appropriate.

If we insert(4.57) for the saturation S, use the flow equation (4.60) for each part and take into account that the homogeneous problem is purely advective and has no mixing process, we obtain for D_{eff} and α_{eff} to the second order of perturbation

$$D_{\text{eff}} = \frac{\overline{\int_0^\infty r\, dr\, r \left. \frac{d\psi_1}{dS} \right|_{S_0} S_1 \tilde{q}}}{2 \int_0^\infty r\, dr\ \psi_3|_{S_0}} - \frac{\overline{\int_0^\infty r\, dr\, r\, \psi_1|_{S_0}\, \tilde{q} \int_0^\infty r'\, dr' \left. \frac{d\psi_3}{dS} \right|_{S_0} S_1}}{2 \left(\int_0^\infty r\, dr\ \psi_3|_{S_0} \right)^2} \tag{4.96}$$

and

$$\alpha_{\text{eff}} = \frac{\overline{\int_0^\infty r\, dr\, r^2 \left. \frac{d\psi_1}{dS} \right|_{S_0} S_1 \tilde{q}}}{2Q \int_0^\infty r\, dr\ \psi_3|_{S_0}} - \frac{\overline{\int_0^\infty r\, dr\, r^2\, \psi_1|_{S_0}\, \tilde{q} \int_0^\infty r'\, dr' \left. \frac{d\psi_3}{dS} \right|_{S_0} S_1}}{2Q \left(\int_0^\infty r\, dr\ \psi_3|_{S_0} \right)^2}. \tag{4.97}$$

To determine the leading time behaviour of D_{eff} and α_{eff}, some assumptions have to be made. First, we assume that the homogeneous solution can be approximated by a

Heaviside step function. The underlying assumption is that the mean effect is due to the sharp front of the solution. The considerations outlined in this section regarding the scaling behaviour of the homogeneous solution and the Green's function are also valid for the purely advective case. We assume for the saturation the following approximation.

$$S_0(r/t^{1/2}) = \Theta\left(\frac{r^2\pi}{Qt} - 1\right) \rightarrow \partial_{r^2} S_0 = \delta\left(r^2 - \frac{Qt}{\pi}\right). \tag{4.98}$$

Furthermore we restrict the covariance function to the limit of small correlation length (4.91) in order to get the leading time order. It has been checked by numerical integrations that this limit yields the main contribution for times $t > l_0^2/Q$. Explicit results cannot be obtained as the Green's functions are still unknown and the function ψ_3 is not further specified. However, due to our knowledge about the scaling behaviour of the functions, the leading time behaviour can be determined as

$$\begin{aligned} D_{\text{eff}} &\propto \sigma_f^2 \frac{l_0\sqrt{Q}}{\sqrt{t}} \\ \alpha_{\text{eff}} &\propto \sigma_f^2\, l_0 \end{aligned} \tag{4.99}$$

The explicit derivation of the result is shown in Appendix F.

The approach of a diffusive mixing process leads to an effective diffusion coefficient which is decreasing with $1/\sqrt{t}$, whereas the approach of a dispersive mixing process leads to a dispersivity which is constant with time. It can therefore be assumed that the heterogeneities of the flow field lead to a similar effect as in the solute transport case, a mixing that is proportional to the mean velocity field and therefore decreasing with $1/r$. The effective dispersion length cannot be determined explicitly as it depends on the function ψ_1 at $S_0(1)$ and on ψ_3, which are not known, and also on integrals over the scaling functions which cannot be performed.

However, the interpretation of the effective mixing effect as an effect similar to the one seen in the solute transport problem leads to a qualitative difference from the solute transport problem. As opposed to solute transport the small scale system has no diffusion or dispersion included. The capillary forces lead to an effect similar to diffusion, but in a homogeneous medium it is assumed to depend on saturation only and not on time or space explicitely. The heterogeneous medium can therefore not be described as an effectively homogeneous one without including an additional effect, a dispersive process which is proportional to the velocity. The small scale homogeneous system and the effective large scale system are not equivalent under the assumptions made in this analysis.

4.3.2 Averaged flow equations for the Buckley Leverett problem: Homogenization theory

The explicit dependency of the effective mixing effect on the system parameters and on the saturation can be determined by means of homogenization theory. In homogenization theory the long time behaviour of the effective differential equation for the

investigated problem can be determined. The method will be explained briefly in the next section. A more detailed discussion of the methods of homogenization theory can be found e.g. in *Hornung* [1997]. Its application to the Buckley Leverett problem and the results will be discussed afterwards.

Method of homogenization theory

The basic idea of homogenization is the separation of the problem into two explicitely different spatial scales, a large and a small one. The fluctuations act on a small scale, whereas we are interested in the flow behaviour on a large scale, where the detailed description of the fluctuations is no longer necessary.

There are different methods to extrapolate the system behaviour from smaller to larger scales. One way is to hold the micro length scale fixed, but increase the size of the domain continuously. The large scale is reached asymptotically in the limit of an infinite domain size. It describes the usual upscaling approach in a way all methods using REVs do (e.g. the perturbation theory method used before). On the other hand, one can also consider the large length scale as the fixed length scale diminishing the small length scale step by step. Now, the asymptotic limit is reached with vanishing small length scale. This is the approach of homogenization theory. Both approaches are fully equivalent. The important parameter indicating the transition from the small- to the large scale system is the ratio of a typical length on the micro- scale y, which would be given by the correlation length of the medium, to a typical length on the macro-scale x, a length scale in the order of the medium size. The ratio of these scales is defined in the following as $\varepsilon \equiv y/x$. The asymptotic large scale behaviour is found in the limit $\varepsilon \to 0$. Note that the whole idea only works if the two scales are clearly separated from each other: the large length scale x and the much smaller length scale, $y \equiv x/\varepsilon$.

The method has been applied to investigate macrodispersion effects in linear advective flow processes e.g. by *Avellaned and Majda* [1991], *Bensoussau et al.* [1978] or *Attinger at al.* [1999]. It has also been applied to two-phase flow e.g. by *Amaziane et al.* [1991], however for different flow conditions.

Application to the radial Buckley Leverett problem

The method of homogenization theory is applied to the Buckley Leverett problem:

$$\partial_t S + \frac{Q}{2\pi r}\vec{e}_r\vec{\nabla}\psi_1(S) + \vec{\tilde{q}}\vec{\nabla}\psi_1(S) = 0 \tag{4.100}$$

The space coordinates and the derivatives with respect to space coordinates are split into the small scale y and the large scale x

$$\vec{x} \to \vec{x}, \vec{y} = \frac{\vec{x}}{\varepsilon}, \qquad \vec{\nabla} \to \vec{\nabla}_x + \frac{1}{\varepsilon}\vec{\nabla}_y \tag{4.101}$$

The fluctuations $\tilde{q}$ are supposed to occur on the small scale only. The total flow field has a large scale part $\vec{q}(\vec{x})$ and a small scale part $\vec{q}(\vec{y})$ which scale as

$$\vec{q}(\vec{x}) = \frac{Q}{2\pi|\vec{x}|}\vec{e}_r \qquad \vec{q}(\vec{y}) = \frac{Q}{\varepsilon 2\pi|\vec{y}|}\vec{e}_r + \frac{1}{\varepsilon}\tilde{q}(\vec{y}). \tag{4.102}$$

The saturation is split into a part independent of the fluctuations and which therefore is dependent on the large scale only, and into the expansions around it, which depend on both scales. The expansion terms are supposed to be small compared to the large scale part, so that we can write the function ψ_1 in a Taylor series,

$$\begin{aligned} S &= S_0(\vec{x}) + \varepsilon S_1(\vec{x},\vec{y}) + \varepsilon^2 S_2(\vec{x},\vec{y}) + \dots \\ \psi_1(S) &= \psi_1(S_0) + \varepsilon \left.\frac{d\psi_1(S)}{dS}\right|_{S=S_0} S_1 + \\ &\quad \varepsilon^2 \left(\left.\frac{d\psi_1(S)}{dS}\right|_{S=S_0} S_2 + \frac{1}{2}\left.\frac{d^2\psi_1(S)}{dS^2}\right|_{S=S_0} S_1^2 \right) + \dots . \end{aligned} \tag{4.103}$$

Inserting these expressions into Eq. (4.100) leads to a differential equation with terms in different orders in ε. In order to fulfil Eq. (4.100) all the orders of ε have to vanish seperately. As finally we only consider the limit $\varepsilon \to 0$ only the orders smaller or equal to 0 have to be taken into account. For these orders we get

$$\begin{aligned} O(\varepsilon^0): \;& \partial_t S_0 + \frac{Q}{2\pi|\vec{x}|}\vec{e}_r\vec{\nabla}_x\psi_1(S_0) + \frac{Q}{2\pi|\vec{y}|}\vec{e}_r\vec{\nabla}_y\Big(\left.\frac{d\psi_1(S)}{dS}\right|_{S=S_0} S_2\Big) + \\ & \frac{1}{2}\frac{Q}{2\pi|\vec{y}|}\vec{e}_r\vec{\nabla}_y\Big(\left.\frac{d^2\psi_1(S)}{dS^2}\right|_{S=S_0} S_1^2\Big) + \tilde{q}(\vec{y})\vec{\nabla}_x\Big(\left.\frac{d\psi_1(S)}{dS}\right|_{S=S_0} S_1\Big) + \\ & \tilde{q}(\vec{y})\vec{\nabla}_y\Big(\left.\frac{d\psi_1(S)}{dS}\right|_{S=S_0} S_2\Big) + \frac{1}{2}\tilde{q}(\vec{y})\vec{\nabla}_y\Big(\left.\frac{d^2\psi_1(S)}{dS^2}\right|_{S=S_0} S_1^2\Big) = 0 \\ O(\varepsilon^{-1}): \;& \frac{Q}{2\pi|\vec{y}|}\vec{e}_r\vec{\nabla}_y\Big(\left.\frac{d\psi_1(S)}{dS}\right|_{S=S_0} S_1\Big) + \tilde{q}(\vec{y})\vec{\nabla}_x\psi_1(S_0) + \\ & \tilde{q}(\vec{y})\vec{\nabla}_y\Big(\left.\frac{d\psi_1(S)}{dS}\right|_{S=S_0} S_1\Big) = 0 \\ O(\varepsilon^{-2}): \;& \frac{Q}{2\pi|\vec{y}|}\vec{e}_r\vec{\nabla}_y\psi_1(S_0) + \tilde{q}(\vec{y})\vec{\nabla}_y\psi_1(S_0) = 0. \end{aligned} \tag{4.104}$$

The equation for order ε^{-2} is always fulfilled as the gradient on the small scale y does not act on the part of the saturation that is only dependent on the large scale x.

The order ε^0 is assumed to be fulfilled on the large scale, where the small scale fluctuations are no longer resolved. For this reason the integral of the equation over the small scale is required to vanish.

$$\int d^d y f(\vec{y}) O(\varepsilon^0) = 0, \qquad \text{where} \qquad \int d^d y f(\vec{y}) = 1. \tag{4.105}$$

We now make the assumption that the dependence of the higher orders $S_n(\vec{x},\vec{y})$ for $n>0$ on the small and the large scale can be separated into two factors so that we can write $S_n(\vec{x},\vec{y}) = f_{1,n}(\vec{x})f_{2,n}(\vec{y})$. As the part $f_{2,n}(y)$ has to vanish at infinity, all terms that can be written as divergence on y-scale vanish in the integration over the small scale. For the other terms we make the assumption of the stochastic approach, which stats that under appropriate conditions the spatial average can be interchanged with an ensemble mean. If we consider in this sense only terms up to second order in the fluctuations, the averaged equation for the 0-th order is reduced to

$$\partial_t S_0 + \frac{Q}{2\pi|\vec{x}|}\vec{e}_r\vec{\nabla}_x\psi_1(S_0) + \overline{\vec{\tilde{q}}(\vec{y})\vec{\nabla}_x \left.\frac{d\psi_1(S)}{dS}\right|_{S=S_0} S_1} = 0. \tag{4.106}$$

Note that S_0 does not correspond to the S_0 from the perturbation theory in the last section since it does not have the same scaling solution $S_0 = S_0(r/\sqrt{t})$. The first correction to the saturation S_1 is determined from the order ε^{-1}. For S_1 the following ansatz is made.

$$S_1 = \vec{\chi}(\vec{y})\vec{\nabla}_x S_0 \tag{4.107}$$

Inserting Eq. (4.107) into the equation for order ε^{-1} yields

$$\frac{Q}{2\pi|\vec{y}|}\vec{e}_r\vec{\nabla}_y\chi_i(\vec{y}) = -\vec{\tilde{q}}(\vec{y})\vec{\nabla}_y\chi_i(\vec{y}) - \vec{\tilde{q}}_i(\vec{y}) \tag{4.108}$$

Expanding into a perturbation series to second order we get the covariance $\tilde{q}\chi$ needed for the 0-th order equation

$$\overline{\tilde{q}_i(\vec{y})\chi_j(\vec{y})} = -\int d^d y' G(\vec{y},\vec{y}')\overline{\tilde{q}_i(\vec{y})\tilde{q}_j(\vec{y}')}. \tag{4.109}$$

where $G(\vec{y},\vec{y}')$ is the Green's function of the system

$$\frac{Q}{2\pi|\vec{y}|}\vec{e}_r\vec{\nabla}_y G(\vec{y},\vec{y}')) = \delta(\vec{y}-\vec{y}') \quad \rightarrow \quad G(\vec{y},\vec{y}') = \frac{2\pi}{Q}\Theta\left(\frac{r^2}{r'^2}-1\right)\delta(\varphi-\varphi'). \tag{4.110}$$

If for the fluctuations of the velocity field the same covariance function is applied as used in the perturbation theory approach, the final result for the averaged homogenized equation reads

$$\partial_t S_0 + \frac{Q}{2\pi|\vec{x}|}\vec{e}_r\vec{\nabla}_x(\psi_1(S_0)) + \vec{\nabla}_x\left(\frac{Q}{2\pi|\vec{x}|}\sigma_f^2 l_0\frac{\sqrt{\pi}}{2}\vec{\nabla}_x\psi_1(S_0)\right) = 0. \tag{4.111}$$

This result shows the effective mixing term to be dependent on $1/r$, which has been seen already in the discussion of the time behaviour of the moments. This result is valid for large times only. For early times, there will be corrections to the dispersion, analogous to the solute transport case, that make sure, that the "macrodispersion"

effect will vanish at the injection point. In the form (4.111), the macrodispersion coefficient would diverge at the injection point.

The result also shows that this mixing term depends in a nonlinear way on the saturation. To interpret the effective mixing term as an effective capillary pressure does not seem reasonable. Rather it has to be seen as an additional large scale effect that does not have an equivalent in the small scale equations.

4.3.3 Comparison with numerical simulations

In order to validate the results of Section 4.3.1 and 4.3.2 they have to be compared with numerical simulations. The comparable quantity is the effective flow parameter (4.95), calculated from the ensemble averaged gas saturation field or its time behaviour, respectively. As we have restricted the problem to the Buckley-Leverett case, a code was used that was constructed for problems without capillary problems. The streamline code written by *Batycky* [1997] (see also *Batycky et al.* [1997]) was applied, as the method of streamlines minimizes the effect of numerical dispersion. The effects we want to see are small and for this reason it is important to keep numerical effects as small as possible. The streamline method used by *Batycky* [1997] is briefly described in the following. A detailed description of the code and the underlying principles are thoroughly discussed in his work.

Streamline code

The streamline code has been developed for the Buckley Leverett flow equations including gravity, which is not taken into account here. The basic concept is to calculate streamlines from the solution of the pressure field and to calculate the saturation on each streamline for the time $t + \Delta t$. With this procedure the problem is reduced to a quasi one-dimensional problem, which is advantageous with respect to CPU time and also reduces the numerical dispersion. The equation we start off with is Eq. (3.2). As capillary pressure is assumed to vanish, there is only one pressure variable.

- The flux of fluid i $\vec{q}_i$ is given by Darcy's law and is assumed to be free of divergence,

$$\vec{\nabla} \cdot \vec{q}_{\text{total}} = \vec{\nabla} \left(\frac{K_{\text{abs}} k_{r,1}(S(\vec{x},t))}{\mu_1} + \frac{K_{\text{abs}} k_{r,2}(S(\vec{x},t))}{\mu_2} \right) \vec{\nabla} P = 0. \tag{4.112}$$

  For the parameters at initial time t Eq. (4.112) is solved numerically for the pressure field at time $t + \Delta t$ with a finite difference method on a Cartesian grid. The velocity components on the interfaces between the cells around the grid nodes are calculated from Darcy's law.

- The streamlines for which the starting points are given, are traced in the following way: The particle travel time from the inlet point to each possible

outlet point of the line at the cell boundaries can be determined on the basis of a linear interpolation of the velocity components at the cell boundaries (see Fig. 4.10). The outlet point is determined by minimizing the particle travel time. Streamlines are traced from an injection well until they reach an extraction well. The inlet- and outlet points and the velocities at these points determine the streamline.

- Each point on a streamline can be assigned to the "time of flight" τ at this point, the particle travel time to that point, given by our knowledge of the velocity field. Thus the space dimension can be transformed to an equivalent time dimension. The flow equation along the streamline can be written in terms of time t and time of flight τ.

- The saturation on each streamline is calculated for the time $t + \Delta t$. This can be done with analytical or numerical methods. In this work the numerical methods were used. The information about saturation on the inlet- and outlet points of the streamline is picked, as well as the time of flight τ. The initial saturation is then given on an irregular τ grid, which has to be transformed to a regular τ grid. On the regular grid, the saturation at time $t+\Delta t$ is calculated numerically using an upstream weighting scheme that is explicit in time. The saturation has then to be mapped back onto the irregular τ grid.

- With the saturation field at $t + \Delta t$ the permeabilities can be calculated for this time and the steps described above are repeated.

- There are two main sources of error. On the one hand there is numerical dispersion in the calculation of the one-dimensional solution of the saturation on a streamline. A second point is, that often more than one streamline is passing through a cell. After the calculation of the saturation on the streamlines at the new time step, the properties that are assigned to the cell have to be averaged over all streamlines passing the cell. *Batycky* [1997] considered the second source of error to be more important for the flow problem which corresponds to the problem considered here, as the flow is selfsharpening and the one-dimensional numerical dispersion is reduced by this process.

In the simulation performed here, the full radial problem was modelled, as the boundary effects in the quarter model described in Chapter 3 are already large enough to spoil the result. Boundary conditions of constant pressure can be incorporated into the code of *Bartycky* [1997] by wells with constant pressure only, a Dirichlet condition for the saturation is not reasonable. In the simulations performed here, the boundary was modeled as a ring of wells with constant pressure, arranged in a circle around an injection well in the center, where air is injected with a constant rate of $10^{-6} m^3/s$.

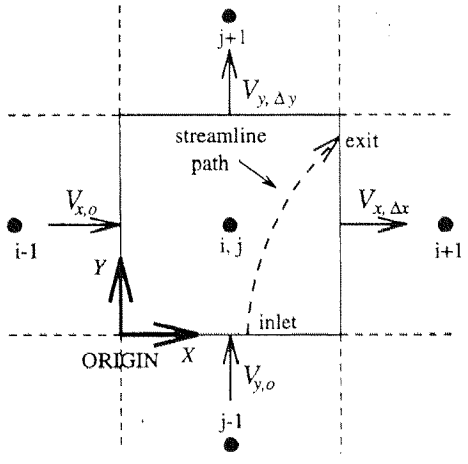

Figure 4.10: Schematic of a streamline path through a 2D gridblock, taken from *Batycky* [1997]

However, as the boundary realized in this way does not lead to vanishing gas saturation, the results can only be analyzed if the gas front is still far away from the boundary. Simulations for one ensemble of 50 realizations were performed on a 451x451x1 grid with a cell size of 0.1 meter in x- y-direction and of 0.01 meter in z-direction. The porosity was set to $\phi = 0.2$ and the geometric mean of the absolut permeability is $\overline{K_{\text{absgeom}}} = 3.53 \cdot 10^{-11} m^2$. The relative permeabilities were modelled as Brook's-Corey functions with $\lambda = 2$. About 3000 streamlines were calculated for 384 time steps with a duration of $1350s$ each. This large field was chosen to obtain a result in the asymptotic time regime. For the same reason the correlation length of the fields was set to a small value of $0.3m$. The variance was chosen as $\sigma_f^2 = 0.5$. Further simulations for three ensembles of 65 realizations each were performed on a 300x300x1 grid with the same parameters as the large field. In this case 192 time steps with duration of $1350s$ were calculated. The properties of the stochastic permeability fields for the three cases are given in Table 4.1. The large field was chosen to confirm the kind of mixing mechanism obtained in (4.94). The smaller fields were chosen to test the dependency of the effective parameter on the stochastic properties of the field.

No ensemble	Variance $\sigma_f^2[m^4]$	Correlation length $l_0[m]$
1	$0.67 \cdot 16 \cdot 10^{-22}$	0.5
2	$0.35 \cdot 16 \cdot 10^{-22}$	0.5
3	$0.67 \cdot 16 \cdot 10^{-22}$	0.8

Table 4.1: Stochastic properties of the random permeability fields

In order to get an estimate for the numerical artefacts, a simulation of the large field was also performed for a homogeneous field. The effective dispersivity α_{eff}

is obtained from the ensemble averaged definition (4.95) using numerical spatial integrations and numerical time derivatives. As theoretical results we would expect $\alpha_{\text{eff}} = \sigma_f^2 \, l_0 \, \sqrt{\pi}/2 = 0.13m$ for the ensemble of the large fields and $\alpha_{\text{eff}} = 0m$ for the homogeneous large field. The numerically obtained results are compared to the analytical ones in Fig. 4.11.

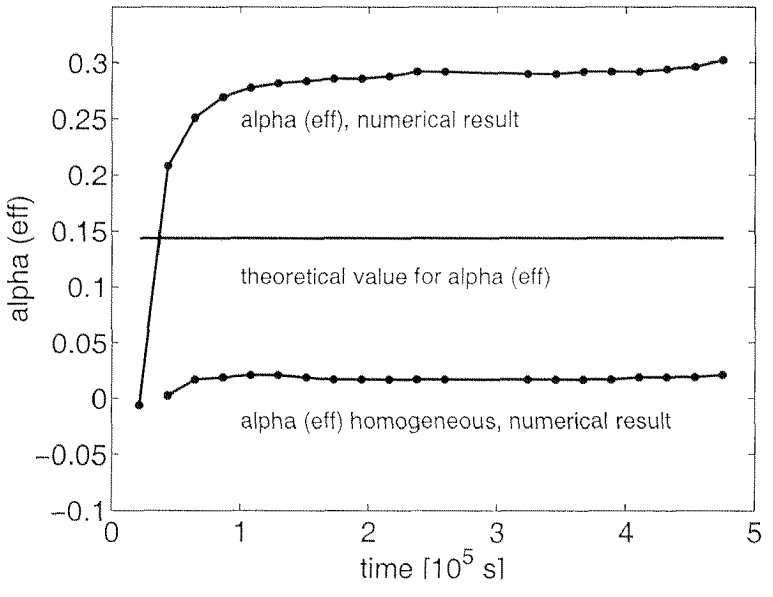

Figure 4.11: α_{eff} calculated from the large field

From these simulations we can conclude, that the approach of an effective dispersion mechanism described by (4.94) is confirmed very well with the numerical calculations. The effective dispersivity is growing at early times until it reaches a value which remains constant with time. The quantitative value of α_{eff} obtained from the numerical calulations is in the same order of magnitude as the analytically obtained one, however it is larger by a factor of 2. From the results of the numerically obtained value of α_{eff} in the homogeneous field we can see that there is an effect which is caused by numerical artifacts. However, this effect is rather small, which makes the interpretation of the factor 2 as a numerical artefact unlikely. On the other hand it is very well possible that the enhancement of α_{eff} is caused by effects that are not captured in the analytical calculations due to the approximations made. For example it is possible, that the dependency of the fluctuating velocity field on the saturation, which has been neglected in the analytical calculations, leads to corrections of the results. In general the relative permeabilities lead to an enhancement of the heterogeneities of the absolute permeability which would lead to a higher variance of the total velocity field. It is also possible that higher orders in the perturbation theory lead to further contributions to the effective dispersivity.

The results for the numerically calculated α_{eff} of the three ensembles of the small fields is shown in Fig. 4.12.

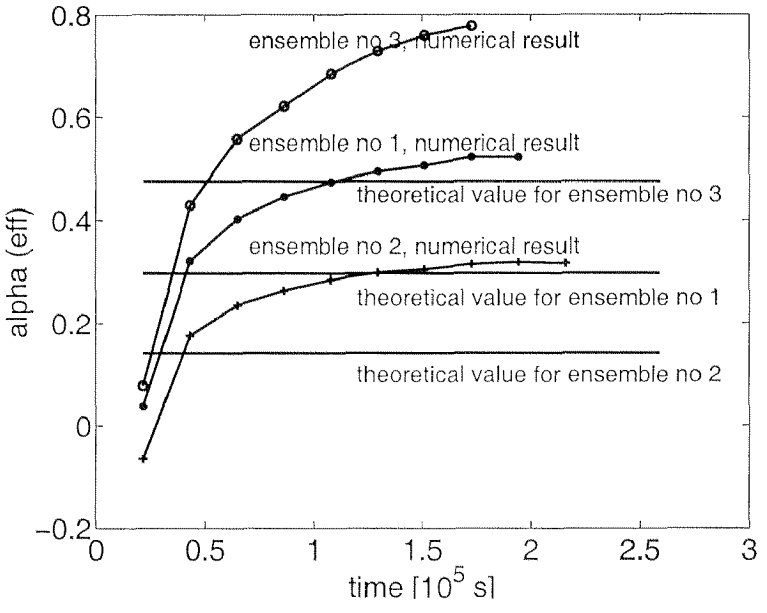

Figure 4.11: α_{eff} calculated from the small fields

The values are also compared to the analytically calculated ones. It can be seen that the fields are not large enough to get the asymptotic time behaviour. This is also due to the larger correlation lengths compared to the correlation length of the large field. As soon as there is breakthrough of the gas front in single realizations the analysis has to be stopped. This time of breakthrough is earlier for the fields with larger correlation lengths. Also the convergence to the asymptotic value becomes slower if the correlation length is larger. From these simulations it can be concluded, that the proportionality of the effective dispersivity to the correlation length could be confirmed very well. The proportionality to the variance of the field does not agree as good in the numerical results. The discrepancy between analytically and numerically obtained α_{eff} gets larger if the variance gets smaller. However, this effect might also be due to the approximation made in the analytical calculations.

4.4 Conclusion of the analytical calculations

In this chapter the mixing effects of the gas saturation due to the fluctuations of the total velocity field have been analyzed analytically with the methods of perturbation theory and homogenization theory. First the problem of solute transport with diffusion and without dispersion in a radially diverging flow field has been considered as a linear analogue to the two-phase flow problem. Ensemble averaged second radial cumulants were calculated to the first order in inverse Peclet number in order to find characteristics of transport properties. The results are valid for intermediate times. Diffusion is enhanced by the variance of the log permeability field due to the fluctuating flow field. For small times and large Peclet numbers the most important effect is a spreading of the second radial cumulant which can be interpreted as a macrodispersion where the dispersion is proportional to the mean flow velocity.

For the radial two-phase flow case the leading time behaviour of appropriately defined effective mixing parameters has been derived within the framework of perturbation theory. The capillary effects were not taken into account here. The analysis of the time behaviour leads to the interpretation, that the fluctuating flow field also causes a "macrodispersion" for the gas saturation which is proportional to the mean flow velocity. There is, however, no microscopic analogue to this effect in the two-phase flow problem. The averaged flow equations were derived by means of homogenization theory. We have also found the macrodispersion coefficient which has been quantified with this method. It can be written as mean radial velocity multiplied by an effective dispersivity $\alpha_{\text{eff}} = \sigma_f^2 l_0 \sqrt{\pi}/2$. The analytical results were compared to results obtained from numerically calculated ensembles of gas saturation fields in heterogeneous media. The existence of an effective macrodispersion could be confirmed qualitatively. The numerically calculated values are in the same order of magnitude as the analytically calculated ones, however they are larger by a factor of about 2. This might be due to the approximations made in the analytical calculations, such as the approximation of the covariance of the total velocity field as that one of a single phase flow problem. An explanation could also be that the higher orders in the perturbation lead to additional effects which are not captured in an analysis up to the second order.

Chapter 5

Conclusions and discussion

In this thesis we have investigated effective properties for two-phase flow in the special case of radial displacement of water by air in a heterogeneous porous medium. The methods which were used are based on the stochastic approach. This averaging procedure enables us to derive effective properties which describe the influence of the heterogeneities on the flow process.

Results

In the first part of the thesis a system was investigated where channeling effects are expected. This is necessary to determine the region of applicability of the ensemble averaging method. Channeling in a heterogeneous porous medium arises if the effects due to the heterogeneously distributed capillary entry pressure dominate the flow behaviour. Channeling develops on the pore scale. However, similar phenomena are also observed on larger scales. Pore scale laboratory experiments were performed in an artificial porous medium with a given heterogeneous aperture field. Two variograms for the aperture fields were taken into account, a fractal one which leads to correlated structures on all scales up to the scale of the measurement, and an exponential one with a finite correlation length. The flow parameters were chosen in a way that the flow process is dominated by the capillary entry pressure effects of the heterogeneous aperture field. The experiments were compared to numerical simulations with an invasion percolation (IP) model. The model proved to be appropriate to reproduce the gas saturation fields. The invasion percolation model is useful to reproduce the flow quantitatively if the porous medium has large scale structures which are known, as was the case in the medium with the fractal variogram. If this is not the case, as in the medium with exponential variogram, where the correlation length is small compared to the medium size, the cluster distribution is sensitive to small changes and can no longer be predicted. If the correlation length of a porous medium is small, the correlated structures can be considered as pixels. It is known from previous work (*Wilkinson and Willemsen* [1983]), that invasion percolation processes on uncorrelated fields produce fractal clusters. Consequently, for capillary dominated flow processes in such media the concept of a REV is not

applicable. Spatial averaging of the saturation depends on the averaging volume if the saturation is distributed in a fractal structure. This has been confirmed by spatial averaging of the gas saturation fields obtained in the laboratory experiments. Averaging over space did not lead to a homogeneously distributed saturation field. It has been tested with numerical IP simulations, that ensemble averages lead to a homogeneous saturation distribution which can be reproduced fairly well within a continuum approach. However, the parameters of such a continuum approach have no predictive power for a single realization. They are useful quantities only for risk assessment considerations in the sense, that the ensemble averaged gas saturation field at location $\vec{x}$ gives the probability that saturation $S = 1$ is measured at this location. We have to keep in mind, that upscaling of the two-phase flow equations for displacement processes in heterogeneous porous media by assigning effective parameters to an equivalent homogeneous system is only justified if channeling effects can be excluded. This is only the case if capillary entry effects are of minor importance. Therefore the channeling flow domain is the limit for the applicability of our method. Heterogeneities have to be handled in a different way if channeling behaviour has to be expected.

For the remainder of the thesis the assumption was made, that entry pressure effects are not important and we are well within the region where the ensemble averaging approach is justified. The two-phase flow was described on the continuum scale and heterogeneities were considered to be due to the permeability and capillary pressure distribution. Entry pressure effects were excluded as it could also be observed in the numerical simulations on the continuum scale, that heterogeneities in the entry pressure lead to channeling phenomena. Numerical simulations of the displacement process were performed for heterogeneous fields using the code TOUGH2. The initial aim was to develop a qualitative understanding of the influence of the heterogeneities on the flow process. The ensemble averaged gas saturation field calculated for an ensemble of heterogeneous media was compared to the saturation calculated on a homogeneous field. The fluctuations lead to an enhancement of the transition zone of the gas front, but do not affect the gas saturation at the injection point. As the enhancement of the transition zone represents a mixing effect we try to capture this effect by varying the capillary pressure, as this is analogous to macrodispersion in an advection-dispersion process. However, an increase of the capillary pressure influences not only the flow behaviour at the front, but also at the injection point. This effect could be compensated by chosing a flatter slope of the capillary pressure curve. However it could be compensated just up to a certain degree. An enhancement of the transition zone was obtained by changing the relative permeability function. The behaviour of the relative permeability is decisive for the development of the transition zone as it causes the selfsharpening effects. Although an intuitive reason for an impact of the heterogeneities on the relative permeability is not given, the averaged gas saturation field can be reproduced more accurately by readjusting the relative permeability function.

From the numerically calculated ensembles of gas saturation two characteristic quantities for the deviations between single realization and averaged field were studied.

Seven ensembles with different values for the variance of logarithmic permeability σ_f^2, inflow rate Q, correlation length l_0, and typical value of capillary pressure P_c were generated.

The variance $\mathcal{D}^\star$ of the ensemble average of the gas saturation was considered. It measures, how much the gas saturation of the single realization deviates from the ensemble mean. The values for $\mathcal{D}^\star$ are maximal at the gas front. At the front the variance $\mathcal{D}^\star$ is determined by the variance of the log permeability σ_f^2. Here the coupling between the heterogeneity of log permeability and capillary pressure is equivalent to the effect of a higher variance of log permeability σ_f^2 for a field with constant capillary pressure. Behind the front the values of $\mathcal{D}^\star$ are determined by the capillary number of the system. Small capillary numbers lead to high values of the variance of gas saturation $\mathcal{D}^\star$. For large capillary numbers, the gas saturation behind the front in the single realization is almost identical to the ensemble average.

Next, the time behaviour of the averaged roughness of an isoline at the front in one single realization was calculated. The growth rate of the isoline roughness determines, whether or not the fluctuations at the front lead to a roughening process. The growth rate of the roughness has to be compared to the growth with $\sqrt{t}$ of the mean radius. The roughness at the front develops due to the fluctuations of the flow field and therefore represents an advective mixing effect. The diffusive mixing effects due to the capillary pressure average out the fluctuations and lead to a smoothing of fluctuations at the front. It was found that initially the roughness grows with the square root of time which indicates a mixing caused by the advective fluctuations when the transversal mixing over different streamlines has not yet occured. The proportionality factor increases with the inflow rate Q. It also increases with the variance of log permeability but not linearly. An enhancement of the capillary pressure also leads to a larger proportionality factor, which can be explained by the coupling of heterogeneous permeability with a heterogeneous capillary pressure field. After a while the roughness grows slower than $\sqrt{t}$ indicating the crossover to the real dispersive mixing. The crossover time where the growth rate slows down is determined by the variance of the log permeability but not systematically. An increase of inflow rate Q leads to an earlier crossover time whereas an increase of correlation length l_0 lead to a delay of the crossover. The crossover time is not sensitive to the capillary pressure.

Ensemble averaged effective parameters have been calculated analytically. The equations were simplified by assuming the capillary pressure to be homogeneous and therefore to be constant. This was justified by the numerical simulations performed before. The coupling of a heterogeneously distributed permeability and a heterogeneously distributed capillary pressure has a similar effect on the flow behaviour at the front as a heterogeneous permeability field where the capillary pressure is set constant but the variance of log permeability is increased. Behind the front the heterogeneously distributed capillary pressure leads to larger fluctuations of gas saturation. Keeping this in mind the neglection of the heterogeneous distribution of capillary pressure is not expected to lead to a loss of important effects. In order to determine the relevant processes the system without nonlinearities is treated first.

It is equivalent to solute tracer transport in a radially diverging flow field with constant flow rate Q, where the transport occurs by advection and constant isotropic diffusion. We used a perturbation theory to second order in the perturbation and to first order in the inverse Peclet number D_0/Q, where D_0 is the microscopic diffusion constant. An assumption was made for the autocovariance function of the fluctuations of the flow, which is consistent with the work of *Indelman and Dagan* [1999]. The large scale mixing behaviour was determined by the ensemble averaged second radial cumulant of the concentration distribution. The results are valid at an intermediate time scale. On the one hand, the solute must have been transported advectively over more than one correlation length. On the other hand the diffusive effects on the local scale have to be small compared to the advective ones. This leads to the restricion

$$\frac{l_0^2}{Q} < t < \frac{Q l_0^2}{D_0^2}. \tag{5.1}$$

In this time regime we obtain two large scale effects. First, we get a macrodispersion, caused by the advective fluctuations of the flow field which is not dependent on the microscopic diffusion. The macrodispersion coefficient can be written as the velocity of a particle moving with the mean flow field multiplied by an effective dispersion length α_{eff}. It therefore decreases with $1/\sqrt{t}$. In the long time limit the macrodispersion coefficient reads

$$D_{\text{disp}}^{\text{eff}} = \alpha_{\text{eff}} \overline{|\vec{u}|} = \alpha_{\text{eff}} \frac{\sqrt{Q}}{\sqrt{\pi t}} \qquad \alpha_{\text{eff}}(t > l_0^2 \pi / Q) = \sigma_f^2 l_0 \sqrt{\pi}/2. \tag{5.2}$$

On short time scales the effective macrodispersion length α_{eff} decreases to zero

$$\alpha_{\text{eff}}(t \to 0) = \sigma_f^2 \sqrt{\pi}/2 \left[l_0 \text{erf}\left(\frac{\sqrt{Qt}}{\sqrt{\pi} l_0} \right) + \frac{\sqrt{Qt}}{\sqrt{\pi}} \exp\left(-\frac{Qt}{\pi l_0^2} \right) \right], \tag{5.3}$$

ensuring that the macrodispersion coefficient does not diverge at the injection point. Secondly we find that in the time domain given by (5.1) the microscopic diffusion is enhanced by the variance of log permeability

$$D_{\text{diff}}^{\text{eff}} = D_0(1 + \sigma_f^2) \tag{5.4}$$

The dispersive effect is dominant on short time scale, but decreasing with $1/\sqrt{t}$ as the solute is transported to larger distances. After long times, the impact of the diffusive effects becomes noticable for measurable quantities such as the second radial cumulant, as diffusion stays constant over time and space.

The flow equation for the fully nonlinear system was also investigated for the problem where capillary effects are negligible, which is the Buckley Leverett problem. This is reasonable as we have seen in the solute transport problem, that on short time scales the main effect of the macroscopic mixing is due to the advective fluctuations. The autocovariance function for the flow was approximated by the one chosen for single phase flow. A scaling function for the homogeneous solution could

be found. It does not depend on the features of the nonlinearities, which is a special property of the configuration with constant inflow. The leading time behaviour of an effective diffusion coefficient and of an effective dispersivity were derived by means of a second order perturbation theory. An effective dispersion length is constant with time, whereas effective diffusion would decrease with $1/\sqrt{t}$. We interpret this in a way similar to the solute transport case. In the two-phase flow problem we have a macrodispersion coefficient which is proportional to the mean velocity and an effective dispersion length.

The time behaviour of the effective dispersivity was also calculated numerically in a simulation with the streamline code of *Batycky* [1997] and our analytical results were confirmed by that.

The ensemble averaged flow equation was calculated up to second order in the perturbations with the method of homogenization theory. A nonlinear effective macrodispersion term was found with an effective dispersion length which depends on the saturation,

$$\partial_t S_0 + \frac{Q}{2\pi r}\vec{e}_r\vec{\nabla}(\psi_1(S_0)) + \vec{\nabla}\left(\frac{Q}{2\pi r}\sigma_f^2 l_0 \frac{\sqrt{\pi}}{2}\left.\frac{d\psi_1}{dS}\right|_{S=S_0}\vec{\nabla}S_0\right) = 0, \qquad (5.5)$$

where S_0 stands for the averaged saturation. The effective time behaviour of the moments cannot be determined from the averaged flow equation as there is no known analytic solution. However it confirms the interpretation of the large scale effect as an effect similar to macrodispersion.

If we include the capillary pressure we would expect something similar to what we obtained in the solute transport problem: the macrodispersion effect dominates on small time scales and after a while the diffusive mixing caused by the capillary pressure becomes dominant. However, there is an important difference between the two-phase flow problem and the solute transport case with respect to the macrodispersion caused by advective mixing. A treatment of dispersion effects, where the dispersion coefficient can be written as the product of the flow velocity and a dispersion length, is known as Scheidegger's approach in the literature and is commonly used for solute transport. For two-phase flow there is no analogue. The capillary pressure is supposed to depend on the saturation only and not on the velocity. In uniform flow configurations this would be of no importance, as the velocity is constant. The macroscopic mixing effect could be described by an effective capillary pressure. In the radial flow configuration the macrodispersion term has to be included in addition to the term of the homogeneous two-phase flow equations.

Taking these considerations into account the numerical simulations of Chapter 3 can be well interpreted. It might be possible to reproduce the larger transition zone caused by the fluctuations of the flow field by an effective capillary pressure term, if it is not considered to be constant. An effective capillary pressure which vanishes at the injection point would not change the gas saturation at the injection point.

The advective mixing is indicated by a growth with the square root of time of the roughness of an isoline at the numerically calculated saturation front at early

times and by a growth with a smaller power at later times. The growth of the roughness is after a while damped out by a diffusive process, in this case by the capillary pressure. The dispersion caused by advective mixing is proportional to the correlation length l_0, to the square root of the inflow rate $\sqrt{Q}$, and to the variance of log permeability σ_f^2 (see Eq. (5.2)). The enhancement of the dispersion effect with increasing σ_f^2 and Q was also found in the numerical simulations. For the solute transport the crossover time where the superdiffusive behaviour changes to a dispersive one has obviously to be related to the correlation length and to the inflow rate. This was also found in the numerical simulations. The crossover time increases with the correlation length and decreases with the inflow rate. The time regime where diffusive processes become important and damp the roughness was not achieved in the simulations. We have seen in the simulations, that due to the coupling between heterogeneous permeability field and heterogeneous capillary pressure field at the front the capillary pressure enhances the effect of the variance of the log permeability. The effect of the enhancement of the crossover time due to the larger variance and of the decrease of crossover time due to the larger capillary pressure might therefore cancel each other. This would explain the insensitivity of the crossover time to the capillary pressure in the numerical simulations.

Outlook

In this work it has been shown, that radial displacement of water by air in a heterogeneous field is subject to a large scale mixing process described by a nonlinear macrodispersion term. A qualitative explanation for this behaviour has been developed, however, the next step would be a validation by numerical simulations. It would be useful to include the macrodispersion function obtained in Eq. (5.5) in the code directly instead of trying to reproduce it by a capillary pressure function which is assumed space dependent in an artificial way. Such a code is not readily available and it would have to be developed from scratch.

An experimental confirmation of the effect would also be very useful. The difficulty here is to perform a field experiment which reproduces the conditions under which our analytical and numerical results are valid. On the one hand the exclusion of channeling effects is a strong restriction. Porous media very often are layered which leads to channeling along the layers. The most reasonable approach would be to perform experiments in artificial porous media in the laboratory. The problem here is the implementation of the heterogeneities. For a quantitative validation we would need a small variance of the permeability distribution and a finite correlation length. A medium which is composed of different sand types would be useful to reproduce such properties, however to build such a medium without cracks between the different soil types which would lead to channeling flow is a very difficult task.

The perturbation theory used for the two-phase flow equation is subject to several approximations. Some of them are due to the radial flow configuration. It would therefore be interesting to study effective mixing parameters in a uniform flow configuration with a line source. This configuration is much easier to handle and some

of the approximations made here could be avoided. The hope is that the results would allow similar interpretation as in the case of the radial flow configuration so that our approximation would be further justified.

One of our basic assumptions is the description of the autocovariance of the flow by the same expression as in single phase flow. However, clearly the relative permeabilities lead to deviations especially in the vicinity of the saturation front. The next step would therefore be to study the autocovariance with numerical simulations. It might be possible to choose a slightly more complicated autocovariance function which incorporates all the most important features.

It would also be an interesting question to develop further analytical approximations for the Buckley Leverett solutions. If approximations for the homogeneous solution can be found, the nonlinearity in time and space in the differential equation for the Green's function is explicit and the Green's functions can be analysed in more detail.

Appendix A

Single realizations of the radial IP calculation

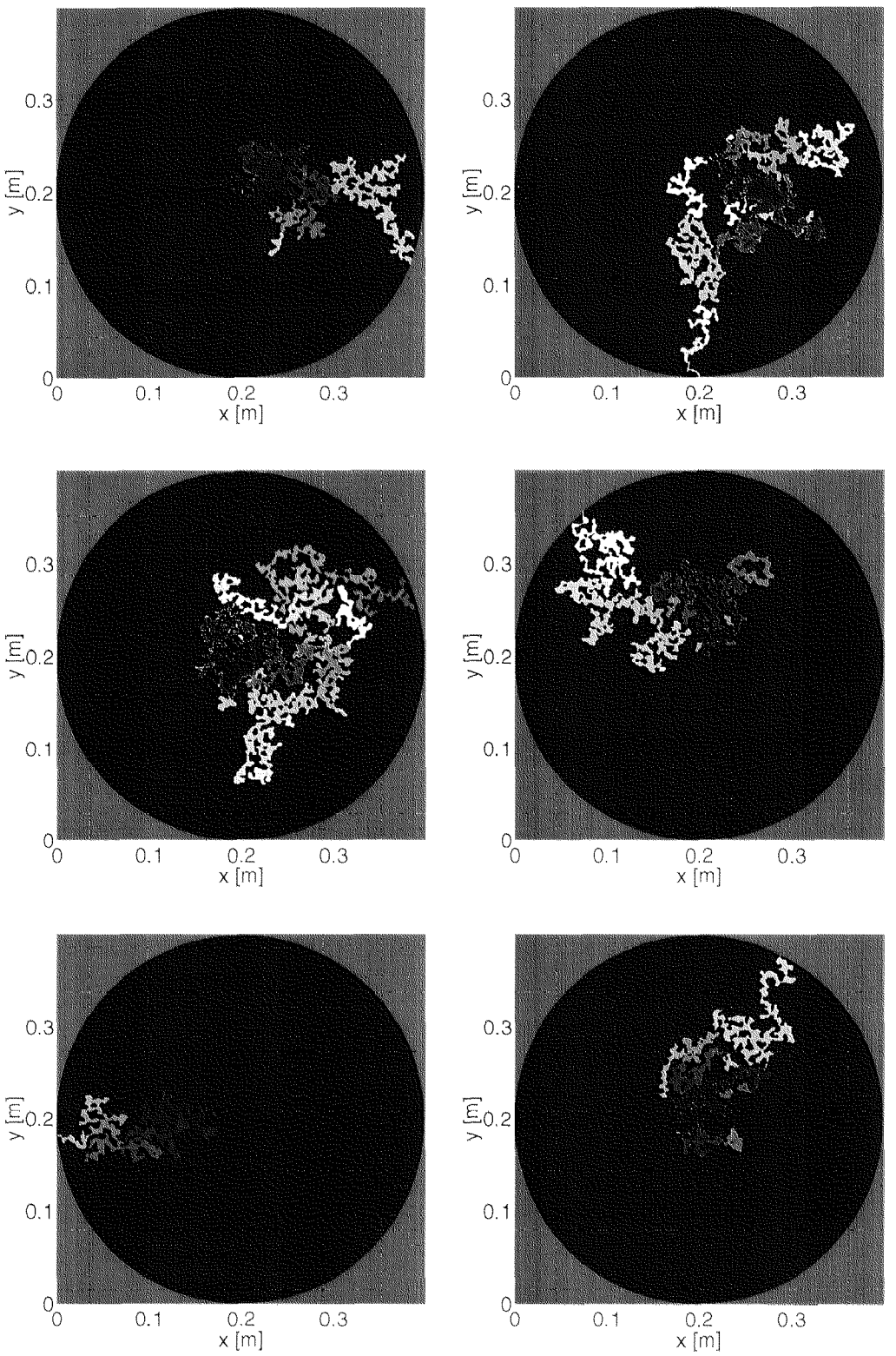

Blue pixels: earlier times, red pixels: later times.

Appendix B

Ensemble averaged and single realization gas saturation fields

Numerically calculated gas saturations fields (TOUGH2) with parameters from Table 3.2.

Case no 1: Norm

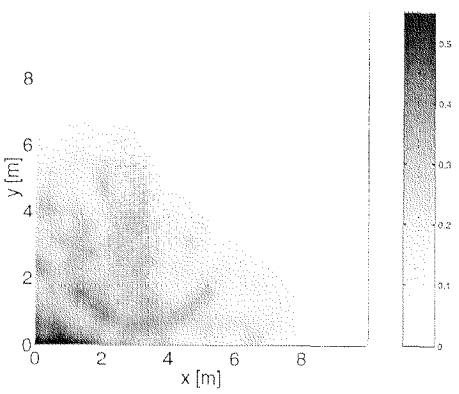

Figure B.1: Single realization

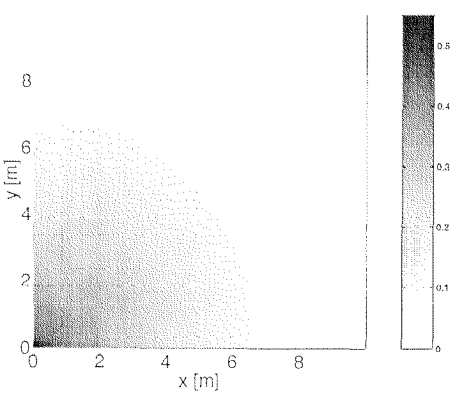

Figure B.2: Ensemble average

Case no 2: High variance

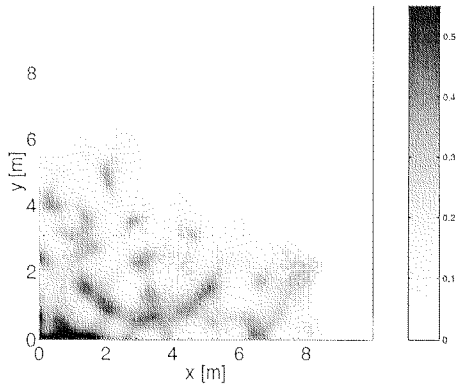

Figure B.3: Single realization

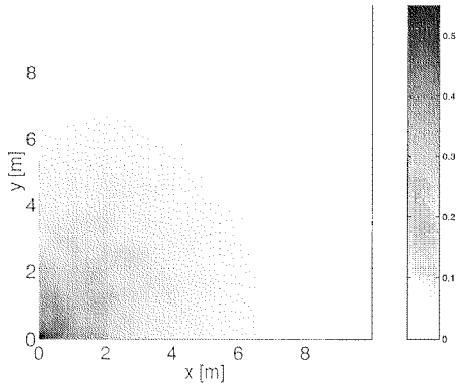

Figure B.4: Ensemble average

Case no 3: Large capillary pressure

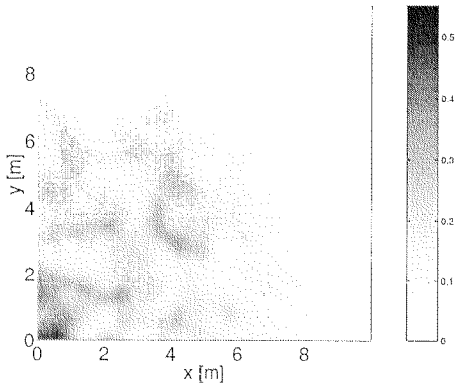

Figure B.5: Single realization

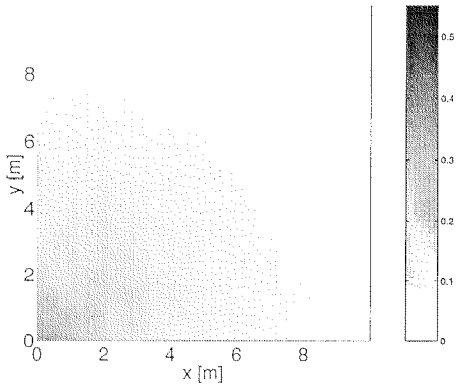

Figure B.6: Ensemble average

Case no 4: Large capillary pressure and high variance

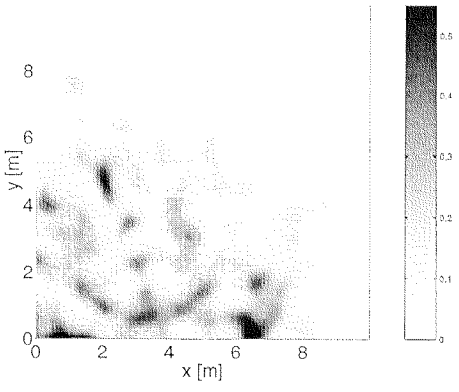

Figure B.7: Single realization

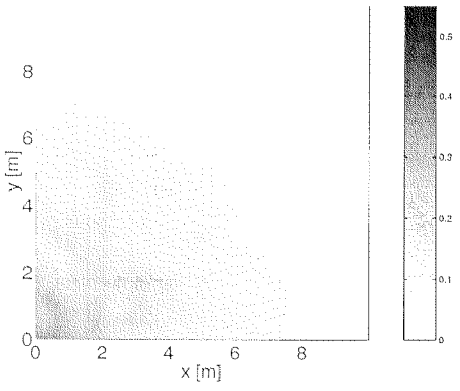

Figure B.8: Ensemble average

Case no 5: Very high variance

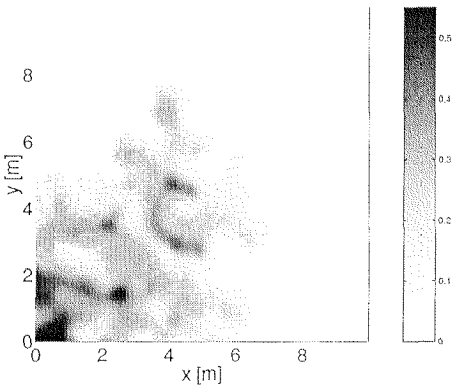

Figure B.9: Single realization

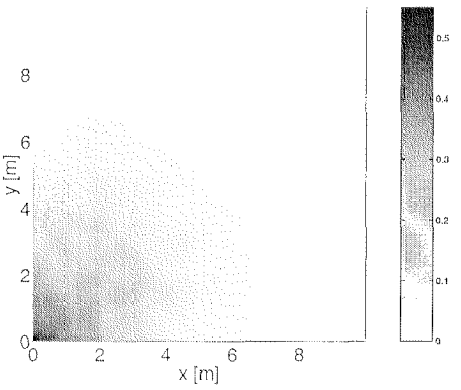

Figure B.10: Ensemble average

Case no 6: Small correlation length

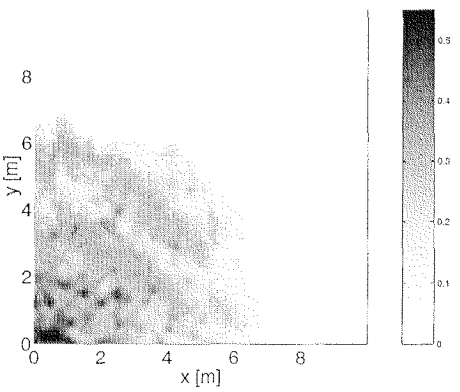

Figure B.11: Single realization

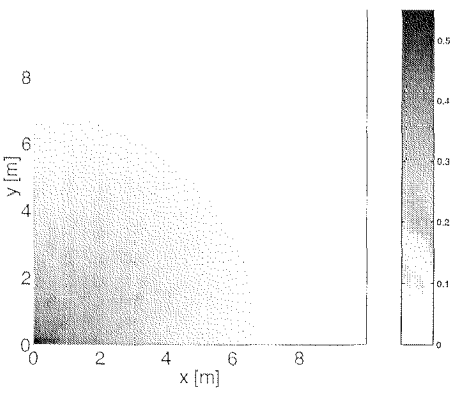

Figure B.12: Ensemble average

Case no 7: High inflow rage

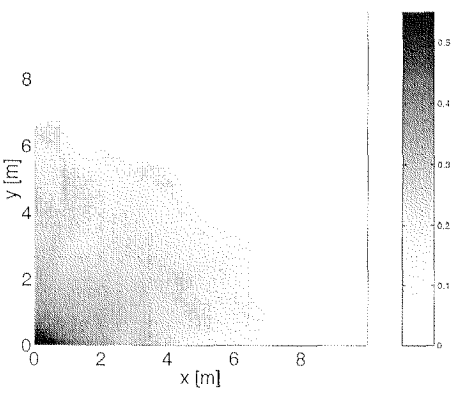

Figure B.13: Single realization

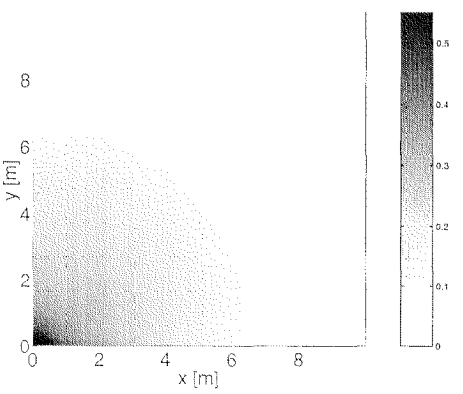

Figure B.14: Ensemble average

Appendix C

Derivation of the solution of the homogenoues transport equation with diffusion

The homogeneous transport equation with constant solute inflow rate $Q = \text{const.}$ in cylindrical coordinates writes

$$\partial_t c_Q(r,t) + \frac{Q}{2\pi r}\partial_r c_Q(r,t) - D_0\left(\frac{1}{r}\partial_r + \partial_r^2\right) c_Q(r,t) = 0 \tag{C.1}$$

with boundary conditions

$$c_Q(0,t) = 1 \quad \text{for } t \text{ finite}, \quad c_Q(r \to \infty, t) \to 0, \quad c_Q(r, t \to \infty) \to 1 \quad \text{for } r \text{ finite} \tag{C.2}$$

and a source term

$$s(r,t) = Q_M \delta(r^2)\Theta(t). \tag{C.3}$$

The variables can be transformed to

$$\eta = \frac{r^2}{4D_0 t} \tag{C.4}$$

This is possible, as in this case the source term and the boundary conditions can be scaled the same way and the conservation of mass is fulfilled. Using this transformation, the transport equation reads

$$\partial_\eta^2 c_Q(\eta) + \left(1 + \frac{1 - Q/(4\pi D_0)}{\eta}\right)\partial_\eta c_Q(\eta) = 0 \tag{C.5}$$

with the boundary condition

$$c_Q(0) = 1, \qquad c_Q(\eta \to \infty) \to 0. \tag{C.6}$$

Inserting

$$g(\eta) = dc_Q(\eta)/d\eta \tag{C.7}$$

leads to

$$\partial_\eta g + \left(1 + \frac{1 - Q/(4\pi D_0)}{\eta}\right) g = 0. \tag{C.8}$$

This differential equation is solved by

$$g(\eta) = \exp(-\eta)\eta^{Q/(4\pi D_0)-1}. \tag{C.9}$$

The general solution for $c_Q(\eta')$ reads therefore

$$c_Q(\eta) = c_1 \int_0^\eta d\eta' g(\eta') + c_2 = c_1 \int_0^\eta d\eta' \exp(-\eta')\eta'^{Q/(4\pi D_0)-1} + c_2 \tag{C.10}$$

which leads to a gamma function (see *Abramowitz and Stegun* [1970]). The boundary conditions are fulfilled by choosing c_1 and c_2 as

$$c_1 = \frac{-1}{\Gamma(Q/(4\pi D_0))} \quad \text{and} \quad c_2 = 1. \tag{C.11}$$

This leads to the solution for the concentration distribution for constant solute injection

$$c_Q(r,t) = \frac{\Gamma\left(Q/(4\pi D_0), r^2/(4D_0 t)\right)}{\Gamma\left(Q/(4\pi D_0)\right)}. \tag{C.12}$$

The solution for constant inflow is obtained from the solution for an instantaneous injection of one unit mass c_δ over the convolution of the solution c_δ with the mass source per unit mass $\mathcal{Q}_{\text{sol}}$ over time and space

$$c_Q(r,t) = \int dr'^2 \int dt' c_\delta(r',t') s(r',t') = \int_0^t dt' c_\delta(r,t') \mathcal{Q}_{\text{sol}}. \tag{C.13}$$

The backward transformation is also possible and the solution c_δ can be obtained from the solution for constant inflow c_Q

$$c_\delta(r,t) = \frac{1}{\mathcal{Q}_{\text{sol}}} \partial_t c_Q(r,t). \tag{C.14}$$

This leads to the solution for instantaneous injection at the injection point

$$c_\delta(r,t) = \frac{\exp\left(-\dfrac{r^2}{4D_0 t}\right)\left(\dfrac{r^2}{4D_0 t}\right)^{\frac{Q}{4\pi D_0}}}{\mathcal{Q}_{\text{sol}} t \Gamma\left(\dfrac{Q}{4\pi D_0}\right)}. \tag{C.15}$$

Appendix D

Radial moments for solute transport with dispersion

The transport equation in cylindrical coordinates for transport with dispersion reads

$$\partial_t c(r,t) + \frac{Q}{2\pi r}\partial_r c(r,t) - \frac{Q}{2\pi r}\alpha\partial_r^2 c(r,t) = 0. \tag{D.1}$$

It is assumed that the solution $c(\vec{x},t)$ does not depend on the angle. The dispersion term can then be treated like a perturbation and the method of Green's functions can be applied to transform the differential equation into an integral equation.

$$c(r,t) = c_0(r,t) - \int_0^\infty dr'^2 \int_0^t dt' G(r,r',t,t')\frac{Q}{2\pi r'}\alpha\partial_{r'}^2 c(r',t') \tag{D.2}$$

where the Green's function G solves

$$\partial_t G + \frac{Q}{2\pi r}\partial_r G = \delta(r^2 - r'^2)\delta(t-t'). \tag{D.3}$$

The Green's fuction is given by

$$G(r,r',t,t') = 2\delta\left(r^2 - r'^2 - \frac{Q}{\pi}(t-t')\right). \tag{D.4}$$

The solution c_0 is given by

$$c_0(r,t) = \frac{1}{\pi}\delta\left(r^2 - \frac{Q}{\pi}t\right) \tag{D.5}$$

Inserting the right hand side of (D.2) as solution for $c(r,t)$ iteratively leads to an infinite sum of terms c_n which contain α n times as a factor. Considering only the zeroth and first order and inserting (D.4) and (D.5) yields

$$c(r,t) = c_0(r,t) - \int_0^\infty dr'^2 \int_0^t dt' \delta\left(r^2 - r'^2 - \frac{Q}{\pi}(t-t')\right)\frac{Q}{2\pi r'}\alpha\partial_{r'}^2\delta\left(r'^2 - \frac{Q}{\pi}t'\right) + \ldots \tag{D.6}$$

If we perform the integrations we obtain

$$c(r,t) = \frac{1}{\pi}\delta\left(r^2 - \frac{Q}{\pi}t\right) - \frac{2\alpha}{\pi}\partial_{r^2}\delta\left(r^2 - \frac{Q}{\pi}t\right)\left(\sqrt{r^2} - \sqrt{r^2 - \frac{Q}{\pi}t}\right)$$
$$+ \frac{2\alpha}{\pi}\partial_{r^2}^2\delta\left(r^2 - \frac{Q}{\pi}t\right)\left(\frac{2}{3}\sqrt{r^2}^3 - \frac{2}{3}\sqrt{r^2 - \frac{Q}{\pi}t}^3\right) + \dots . \tag{D.7}$$

The n-th (not normalized) moment reads

$$m_r^{(n)} = \int_0^{2\pi} d\varphi \int_0^{\infty} r dr\, r^n c(r,t). \tag{D.8}$$

Inserting (D.7) leads to

$$m_r^{(0)} = 1 \tag{D.9}$$
$$m_r^{(1)} = \sqrt{Qt/\pi} + \frac{2}{3}\alpha \tag{D.10}$$
$$m_r^{(2)} = \frac{Q}{\pi}t + 2\alpha\sqrt{Qt/\pi}. \tag{D.11}$$

We obtain therefore for the second radial cumulant

$$\mu_r^{(2)} = \frac{2}{3}\alpha\sqrt{Qt/\pi}. \tag{D.12}$$

Appendix E

Full solution of the second radial cumulant with finite Peclet number

The full solution in leading time order to first order in Peclet number reads

$$\kappa_r^{2,\mathrm{ens}} = D_0 t + \sigma_f^2 D_0 t + \frac{1}{3}\sigma_f^2 l_0 \sqrt{\frac{Qt}{\pi}}\mathrm{erf}\left(\frac{\sqrt{Qt}}{\sqrt{\pi l_0^2}}\right) + \sigma_f^2\left(-\frac{1}{2}l_0^2 + \frac{1}{6}l_0^4\left(\frac{Qt}{\pi}\right)^{-1}\right)\left(1 - \exp\left(-\frac{Qt}{\pi l_0^2}\right)\right) + \dots . \tag{E.1}$$

The effective diffusion coefficient derived from this expression using (4.32) writes

$$D_{\mathrm{eff}} = D_0 + \sigma_f^2 D_0 + \frac{1}{6}\sigma_f^2 l_0 \sqrt{\frac{Q}{\pi t}}\mathrm{erf}\left(\frac{\sqrt{Qt}}{\sqrt{\pi l_0^2}}\right) + \frac{1}{6}\sigma_f^2 l_0^2 (t)^{-1}\exp\left(-\frac{Qt}{\pi l_0^2}\right) - \frac{1}{6}\sigma_f^2 l_0^4\left(\frac{Q}{\pi t^2}\right)^{-1}\left(1 - \exp\left(-\frac{Qt}{\pi l_0^2}\right)\right) + \dots . \tag{E.2}$$

If we derive an effective dispersion length using (4.35) we would obtain

$$\alpha_{\mathrm{eff}} = 3D_0\left(1 + \sigma_f^2\right)\frac{\sqrt{\pi t}}{\sqrt{Q}} + \frac{1}{2}\sigma_f^2 l_0 \mathrm{erf}\left(\frac{\sqrt{Qt}}{\sqrt{\pi l_0^2}}\right) + \frac{1}{2}\sigma_f^2 l_0^2 \frac{\sqrt{\pi}}{\sqrt{Qt}}\exp\left(-\frac{Qt}{\pi l_0^2}\right) - \frac{1}{2}\sigma_f^2 l_0^4\left(\frac{\sqrt{\pi}}{\sqrt{Qt^3}}\right)\left(1 - \exp\left(-\frac{Qt}{\pi l_0^2}\right)\right) + \dots . \tag{E.3}$$

Appendix F

Derivation of the effective dispersion coefficient for the Buckley Leverett problem

The effective dispersion terms are given by the expressions (4.96) and (4.97).

Effective diffusion coefficient

The effective diffusion (4.96) reads

$$D_{\text{eff}} = \frac{\int_0^\infty r dr \int_0^\infty r' dr' \int_0^t dt'\ r\ \left.\frac{d\psi_1}{dS}\right|_{S_0(r,t)} G(r,r',t,t')\ \left.\frac{d\psi_1}{dS}\right|_{S_0(r',t')} \partial_{r'} S_0(r',t') \overline{\tilde{q}(\vec{x})\tilde{q}(\vec{x}')}}{2\int_0^\infty r\ dr\ \ \psi_3|_{S_0}} \tag{F.1}$$

It can be evaluated making the approximations

$$S_0(r/t^{1/2}) = \Theta\left(\frac{r^2\pi}{Qt} - 1\right) \rightarrow \partial_{r^2} S_0 = \delta\left(r^2 - \frac{Qt}{\pi}\right). \tag{F.2}$$

and

$$\lim_{l_0 \to 0} \overline{\tilde{q}(\vec{x})\tilde{q}(\vec{x}')} = \sigma_f^2 \frac{Q^2}{4\pi^2 r r'} l_0 \sqrt{\pi}\delta(r - r'). \tag{F.3}$$

Evaluating the integrations over space leads to

$$D_{\text{eff}} = \frac{\sigma_f^2 \frac{Q^2}{8\pi^2} \int_0^t dt'\ \left.\frac{d\psi_1}{dS}\right|_{S_0(Qt/\pi,t')} G(Qt'/\pi, Qt'/\pi, t, t')\ \left.\frac{d\psi_1}{dS}\right|_{S_0(1)} l_0\sqrt{Qt'}}{2\int_0^\infty r\ dr\ \ \psi_3|_{S_0}} \tag{F.4}$$

It is obvious that the Green's function $G(\frac{Qt'}{\pi}, \frac{Qt'}{\pi}, t, t')$ leads only to a contribution if $t = t'$ and reads

$$G(\frac{Qt'}{\pi}, \frac{Qt'}{\pi}, t, t') = \frac{\pi}{Q}\delta(t - t'). \tag{F.5}$$

With this we can perform the integration over time t'. Writing the denominator in terms of the scaling variable $\eta = r^2/t$ we obtain

$$D_{\text{eff}} = \frac{\sigma_f^2 \frac{Q}{8\pi} \left(\left. \frac{d\psi_1}{dS} \right|_{S_0(1)} \right)^2 l_0 \sqrt{Qt}}{t \int_0^\infty d\eta \ \psi_3|_{S_0(\eta)}} \propto \sigma_f^2 \frac{l_0\sqrt{Q}}{\sqrt{t}}. \tag{F.6}$$

With this we obtain for the effecitve diffusion coefficient (4.96) the leading time behaviour:

$$D_{\text{eff}} \propto \sigma_f^2 \frac{l_0\sqrt{Q}}{\sqrt{t}}. \tag{F.7}$$

Effective dispersivity

The effective dispersivity (4.97) reads

$$\alpha_{\text{eff}} = \frac{\int_0^\infty r dr \int_0^\infty r' dr' \int_0^t dt' \ r^2 \left. \frac{d\psi_1}{dS} \right|_{S_0(r,t)} G(r, r', t, t') \left. \frac{d\psi_1}{dS} \right|_{S_0(r',t')} \partial_{r'} S_0(r', t') \overline{\tilde{q}(\vec{x})\tilde{q}(\vec{x}')}}{2Q \int_0^\infty r \ dr \ \psi_3|_{S_0}}. \tag{F.8}$$

Performing the same approximations as for the effective diffusion coefficient we obtain

$$\alpha_{\text{eff}} = \frac{\sigma_f^2 \frac{Q}{8\sqrt{\pi}} \left(\left. \frac{d\psi_1}{dS} \right|_{S_0(1)} \right)^2 l_0 Qt}{Qt \int_0^\infty d\eta \ \psi_3|_{S_0(\eta)}} \propto \sigma_f^2 \, l_0. \tag{F.9}$$

This leads for the effective dispersivity to the leading time behaviour

$$\alpha_{\text{eff}} \propto \sigma_f^2 \, l_0. \tag{F.10}$$

Bibliography

Abdin, A. and J. J. Kaluarachchi, Stochastic analysis of three-phase flow in heterogeneous porous media: 1. Spectral/perturbation approach, *Water Resources Research 33(7)*, 1549-1558, 1997.

Abdin, A., J. J. Kaluarachchi, C. Chang and M. W. Kemblowski, Stochastic analysis of two-phase flow in porous media: II. Comparison between perturbation and Monte-Carlo results, *Transport in Porous Media 19*, 261-280, 1995.

Abramovitz, M. and I. A. Stegun, *Handbook of Mathematical Functions*, Dover, 1972.

Abu-El-Sha'r, W. and L. Abriola, Experimental assessment of gas transport mechanisms in natural porous media: Parameter evaluation, *Water Resour. Res., 33(4)*, 505-516, 1997.

Amaziane, B., A. Bourgeat and J. Koebbe, Numerical Simulation and Homogenization of Two-phase Flow in Heterogeneous Porous Media, *Transport in Porous Media*, 519-547, 1991.

Attinger, S. and W. Kinzelbach, Nonlinear transport through heterogeneous porous media - an analytical approach, presented at AGU 1999 Spring Meeting, to be published, 1999.

Attinger, S., M. Denz, H. Kinzelbach and W. Kinzelbach, Temporal behaviour of a solute cloud in a chemically heterogeneous porous medium, *J. Fluid Mech., 386*, 77-104, 1999.

Avellaneda, M. and A. J. Majda, An integral representation and bounds on the effective diffusivity in passive advection by laminar and turbulent flows, *Commun. Math. Phys. 138*, 339-391, 1991.

Bastian, P. and R. Helmig: Efficient fully-coupled solution techniques for two-phase flow in porous media. Parallel multigrid solution and large scale computations. *Advances in Water Resources, 23*, 199-216, 1999.

Batycky, R. P., A three-dimensional two-phase field scale streamline simulator, dissertation at Stanford University, Stanford, California, 1997.

Batycky, R. P., M. J. Blunt and M. R. Thiele, A 3d field scale streamline simulator with gravity and changing well conditions, *SPE Reservoir Engineering*, 246-254, 1997.

Bear, J., *Dynamics of Fluids in Porous Media*, Dover Publications Inc., New York, 1972.

Berkowitz, B. and R. P. Ewing, Percolation theory and network modeling applications in soil physics, *Surveys in Geophysics (19)*, 23-72, 1998.

Bensoussau, A., J.L. Lious and G.C. Papanicolauo, *Asymptotic analysis for periodic structures*, North Holland, Amsterdam, 1978.

Bourgeat, A., Two-phase flow, in: Homogenization and Porous Media, ed. U. Hornung, 95-127, Springer, 1997.

Bourgeat, A. and A. Hidani, Effective Model of Two-phase Flow in a Porous Medium Made of Different Rock Types, *Applicable Analysis 58*, 1-29, 1995

Brooks, R. H. and A. T. Corey, Properties of porous media affecting fluid flow, *Journal of the Irrigation and Drainage Division, ASCE, 29 (2)*, 61-88, 1966.

Chang, C., M. W. Kemblowski, J. J. Kaluarachchi and A. Abdin, Stochastic analysis of two-phase flow in porous media: I. Spectral/Perturbation approach, *Transport in Porous Media 19*, 233-259, 1995.

Chouke, R. L., P. van Meurs and C. and der Poel, The stability of slow, immiscible, viscous liquid-liquid displacement in permeable media, *Petrolium Transactions of AIME, 216*, 188-194, 1959.

Dagan, G., *Flow and Transport in Prorus Formations*, Springer, 1989.

Dagan, G., Time-dependent macrodispersion for solute transport in anisotropic heterogeneous aquifers, *Water Resour. Res. 24*, 1391-1500, 1988.

Dale, M., S. Ekrann, J. Mykkeltveit and G. Virnovsky, Effective relative permeabilities and capillary pressure for one-dimensional heterogeneous media, *Transport in Porous Media 26*, 229-260, 1997.

Dentz, M., Zeitverhalten von Transportkoeffizienten in heterogenen poroesen Medien, Diploma thesis, University of Heidelberg, 1997.

Dentz, M., S. Attinger, H. Kinzelbach and W. Kinzelbach, Temporal behaviour of a solute cloud in a heterogeneous porous medium, submitted to: *Water Resour. Res.*, 1999.

Desbarats, A. J., Spatial averaging of transmissivity in heterogeneous fields with flow towards a well, *Water Resour. Res., 28(3)*, 757-767, 1992.

Dias, M. M. and D. Wilkinson, Percolation with trapping, *Journal of Physics A (19)*, 3131-3146, 1986.

Fiori, A., P. Indelman and G. Dagan, Correlation structure of flow variables for steady flow toward a well with application to highly anisotropic heterogeneous formations, *Water Resour. Res., 34(4)*, 699-708, 1998.

Fischer, U., *Experimental and Numerical Investigation of Soil Vapor Extraction*, Diss.ETH No. 11277, 1995.

Flury, M. and H. Fluehler, Modeling solute leaching in soils by diffusion-limited aggregation: Basic concepts and application to conservative solutes , *Water Resour. Res. 31(10)*, 2443-2452, 1995.

Foussereau, X., W. Graham and S. Rao, Stochastic analysis of field scale solute transport in heterogeneous variably saturated soils under transient flow regimes, presented at AGU 1999 Spring Meeting, submitted to Water Resources Research, 1999.

Furuberg, L., K. J. Maloy and J. Feder, Intermittend behaviour in slow drainage, *Physical Review E (53)*,966-977,1996.

Furuberg, L., J. Feder, A. Aharony and T. Jossnag, Dynamics of invasion percolation, *Physical Review Letters, 61(18)*, 2117-2120, 1988.

Gelhar, L. W., *Stochastic Subsurface Hydrology*, Prentice Hall, 1993.

Gelhar, L.W. and M.A. Collins, General analysis of longitudinal dispersion in nonuniform flow, *Water Resour. Res., 7(6)*, 1511-1521, 1971.

Gelhar, L. W. and C. L. Axness, Three-dimensional analysis of macrodispersion in aquifers, *Water Resour. Res., 19(1)*, 161-180, 1983.

Gimmi, T. and H. Fluehler, Flux and resident injection in gaseous advection experiments, *Water Resour. Res., 32(1)*, 1-7, 1996.

Glass, R. J. and L. Yarrington, Simulation of gravity fingering in porous media using a modified invasion percolation model, *Geoderma 70.* 231-252, 1996.

Golden, K. M., Percolation models for porous media, in *Homogenization and porous media*, ed.: U. Hornung, Springer, 1997.

Hansen, A., S. Roux, A. Aharony, J. Feder, T. Jossnag and H. H. Hardy, Real-space renormalization estimates for two-phase flow in porous media, *Transport in Porous Media 29*, 247-279, 1997.

Helmig, R., *Multiphase Flow and Transport Processes in the Subsurface*, Springer Verlag, Berlin, 1997.

Homsy, G.M., Viscous fingering in porous media, *Ann. Rev. Fluid Mech. (19)*, 271-311, 1987.

Indelman, P. and B. Abramovich, Nonlocal properties of nonuniform averaged flows in heterogeneous media, *Water Resour. Res., 30(12)*, 3385-3393, 1994.

Indelman, P. and G. Dagan, Solute transport in divergent radial flow through heterogeneous porous media, *J. Fluid Mech., 384*, 159-182, 1999.

Indelman, P., A. Fiori and G. Dagan, Steady flow toward wells in heterogeneous formations: Mean head and equivalent conductivity, *Water Resour. Res., 32(7)*, 1975-1983, 1996.

King, P.R., The use of field theoretical methods for the study of flow in a heterogeneous porous medium, *J. Phys. A 20*, 3935-3947, 1987.

King, P. R., A. H. Muggeridge and W. G. Price, Renormalization calculations of immiscible flow, *Transport in Porous Media 12*, 237-260, 1993.

Kobus, H., The role of large-scale experiments in groundwater and subsurface remediation research: The VEGAS concept and approach. In: K. Kobus, B, Barczewski and H. Koschitzky (Eds.), *Groundwater and Subsurface Remediation*, 1-18, Springer Verlag Heidelberg, 1996.

Kueper B. H. and E. O. Frind, An overview of immiscible fingering in porous media, *Journal of Contaminant Hydrology 2*, 95-110, 1988.

Lehmann, P., F. Stauffer, C. Hinz, O. Dury and H. Fluehler, Effect of hysteresis on water flow in a sand column with a fluctuating capillary fringe, *Journal of Contaminant Hydrology 33*, 81-100, 1998.

Lenormand, R. and C. Zarcone, Capillary fingering: Percolation and fractal dimension, *Transport in Porous Media 4*, 599-612, 1989.

Lenormand, R., E. Touboul and C. Zarone, Numerical models and experiments on immiscible displacement in porous media, *Journal of Fluid Mechanics, 189*, 165-187, 1988.

Mantoglou, A. and L. W. Gelhar, Capillary tension head variation, mean soil content, and effective specific moisture capacity of transient unsaturated flow in stratified soils, *Water Resources Research 23(1)*, 37-46, 1987.

Marle, C. M., *Multiphase Flow in Porous Media*, 1. edition, Institut Francais du Petrole, Paris, 1981.

Meakin, P., The growth of rough surfaces and interfaces, *Physics Reports 235(4/5)*, 189-289, 1993.

Meakin, P, A. Birovljev, V. Frette, J. Feder and T. Jossang, Gradient stabilized and destabilized invasion percolation, *Physica A (191)*, 227-239,1992.

Metzger, D, H. Kinzelbach, I. Neuweiler and W. Kinzelbach, Asymptotic transport parameters in a heterogeneous porous medium, Comparisoon of two ensemble-averaging procedures, *Stochastic Environmental Research and Risk Assessmen* (13), 396-415, 1999.

Neuman, S. P., Eulerian-Lagrangian theory of transport in space-time nonstationary velocity fields: exact nonlocal formalism by conditional moments and weak approximation, *Water Resour. Res., 29(3)*, 633-645, 1993.

Neuman, S. P. and S. Orr, Prediction of steady state flow in nonuniform geologic media by conditional moments: Exact nonlocal formalism, effective conductivities and weak approximation, *Water Resour. Res., 29(2)*, 341-364, 1993.

Ng, C.-O. and C. C. Mei, Aggregate diffusion model applied to soil vapor extraction in unidirectional and radial flows, *Water Resour. Res., 32(5)*, 1289-1297, 1996.

Oswald, S., Dichtestroemung in poroesen Medien, dreidimensionale Experimente und Modellierung, Schriftenreihe des Instituts fuer Hydromechanik und Wassersirtschaft Band 2, 1999.

Paterson, L., Radial fingering in a Hele Shaw cell, *J. Fluid Mech. 113*, 513-529, 1981.

Philip, J. R., Some exact solutions of convection-diffusion and diffusion equations, *Water Resour. Res., 30(12)*, 3545-3551, 1994.

Popovicova, J. and M. Brusseau, Dispersion and transport of gas-phase contaminants in dry porous media: effect of heterogeneity and gas velocity, *J. Contam Hydrol., 28*, 157-169, 1997.

Pruess, K., Grid orientation and capillary pressure effects in the simulation of water injection into depleted vapor zones, *Geothermics 20(5/6)*, 257-277, 1991a

.

Pruess, K. TOUGH2 A general-purpose numerical simulator ofr multiphase fluid and heat flow, Lawrence Berkeley Laboratory, University of California, Berkeley, 1991b

.

Pruess, K., TOUGH2 Usergs Guide, Lawrence Berkeley Laboratory, University of California, Berkeley, 1987.

Quintard, M. and S. Whittaker, Two-phase flow in heterogeneous porous media: The method of large-scale averaging, *Transport in Porous Media 3*, 357-413, 1988.

Rajaram, H. and L. W. Gelhar, Plume scale-dependent dispersion in heterogeneous aquifers, *Water Resourc. Res. 29(9)*, 3249-3276, 1993.

Robin, M. J. L., A. L. Gutjahr, E. A. Sudicky and J. L. Wilson, Cross-correlated random field generator with the direct Fourier transform method, *Water Resources Research 29 (7)*, 2383ff, 1993.

Rothman, D. H., Cellular-automaton fluids: A model for flow in porous media, *Geophysics 53(4)*, 509-518, 1988.

Sanchez-Vila, X., Radially convergent flow in heterogeneous porous media, *Water Resour. Res., 33(7)*, 1633-1641, 1997.

Schwarz, C., Dichteabhaengige Stroemungen in homogenen und heterogenen poroesen Medien, Dissertation ETH-Nr. 13028, 1999.

Shaw, T. M., Movement of a drying front in a porous material, in: *Mat. Res. Soc. Symposium Proc. (73)*, ed.: C. J. Brinker, D. E. Clark and D. R. Ulrich, 215-223,1986

Shvidler, M. I., Filtration flows in heterogeneous media (in Russian), *Izv. Akad. Nauk SSSR Mech., 3,*, 185-190, 1962.

Sorensen, I., Solute Transport and Immiscible Displacement in Single Fractures, Master Thesis C938719, Technical University of Denmark, 1999.

Stauffer, D., *Introduction to percolation theory*, Taylor & Francis, London, 1992.

Stauffer, F., Hysteretic unsaturated flow in porous meda cuased by periodic movement of the phreatic surface: Model and experiment, to be presented at: International Symposium 2000 on Groundwater, IAHR, Sonic City Omiya, Japan, 1999.

Stauffer, F. and T. Dracos, Experimental and Numerical Study of Water and Solute Infiltration in Layered Porous Media, *Journal of Hydrology, 9-34*, 1986.

Su H. and W. Kinzelbach, Application of 2D random generators to the study of solute transport in fractures, to be published, 1999.

Trantham H., and D. Durnford, Stochastic aggregation model (SAM) for DNAPL-sater displacement in porous media, *Journal of Contaminant Hydrology 36*, 377-400, 1999.

Ustohal, P., F. Stauffer and T. Dracos, Measurment and modeling of hydraulic characteristics of unsaturated porous media with mixed wettability, *Journal of Contaminant Hydrology 33*, 5-37, 1998.

van Genuchten, M. Th., A closed-form equation for predicting the hydraulic conductivity of unsaturated soils, *Soil Sci. Soc. Am. J. 44*, 892-898, 1980.

Van Kampen, N. G., *Stochastic Processes in Physics and Chemistry*, North-Holland, 1981.

Wilkinson, D. and J. F. Willemsen, Invasion percolation: a new form of percolation theory, *Journal of Physics A (16)*, 3365-3376, 1983.

Witherspoon, P. A., J. S. Y. Yang, K. Iwai and J. E. Gale, Validity of the cubic law for fluid flow in a deformable rock fracture, *Water Resources Research 16(6)*, 1016-1024, 1980.

Witten, T. A. and L. M. Sander, Diffusion limited aggregation, *Physical Review B, 27*, 5686-5697, 1983.

Yeh, T.C., L.W. Gelhar and A.L. Gutjahr, Stochastic analysis of unsaturated flow in heterogeneous soils, 2: Statistically anisotropic media with variable alpha, *Water Resources Research 21(4)*, 457-464, 1985.

Yortsos, Y. C., Stability of displacement processes in porous media in radial flow geometries, *Physic of Fluids 30(10)*, 2928-2935, 1987.

Yortsos, Y. C., C. Satik, J.-C. Bacri and D. Salin, Large-scale percolation theory of drainage, *Transport in porous media (10)*, 171-195, 1993.

Zhang, D., Nonstationary stochastic analysis of transient unsaturated flow in randomly heterogeneous media, *Water Resources Research 35(4)*, 1127-1141, 1999.

Danksagung

An dieser Stelle möchte ich all denen danken, die mir beim Entstehen dieser Arbeit geholfen haben.

Ganz besonders möchte ich Wolfgang Kinzelbach danken, zum einen für die Themenstellung, für die Betreuung dieser Arbeit und die Diskussionsbereitschaft bei etlichen schwierigen Fragen. Vor allem aber auch dafür, dass er mich in meinen Plänen und Ideen immer unterstützt, ermutigt und nach allen Möglichkeiten gefördert hat.

Ich möchte mich auch bei Hannes Flühler für die Uebernahme des Koreferats, für sein Interesse an der Arbeit und seine Hilfsbereitschaft bedanken.

Sabine Attinger will ich ganz herzlich danken für alle ihre Unterstützung, ihre Gesprächs- und Diskussionsbereitschaft und die hilfreichen Ideen und Vorschläge. Die Zusammenarbeit war nicht nur produktiv sondern hat vor allen Dingen auch grossen Spass gemacht.

Ivan Soerensen möchte ich auch für die Zusammenarbeit danken. Seine Arbeit war für mich sehr wertvoll.

Für das Korrekturlesen dieser Arbeit möchte ich Kai Zoellmann, Sabine Attinger, Carsten Schwarz und Wolfgang Kinzelbach, danken, und vor allem, für grosse Heldentaten, Margit Steiner.

An dieser Stelle möchte ich mich auch bei Stefan Finsterle und Karsten Pruess vom LBNL Berkeley bedanken für ihre Gastfreundschaft und für ihre Hilfe und Unterstützung mit dem Programm TOUGH2. Ebenfalls möchte ich Roland Lenormand vom IFP in Paris für seine Gastfreundschaft und die nützlichen Ratschläge und Gespräche danken.

Danken möchte ich auch den Kolleginnen und Kollegen am IHW, mit denen ich eine gute Zeit hatte und die für eine nette Arbeitsatmosphäre gesorgt haben.